SAPIENZA
UNIVERSITÀ DI ROMA

DOTTORATO DI RICERCA IN BIOCHIMICA
CICLO XIX (A.A. 2003-2006)

The structure of the NO-sensing domain of the transcription factor DNR from *Pseudomonas aeruginosa*

Dottorando
Giorgio Giardina

Docente guida
Prof. Maurizio Brunori

Coordinatore
Prof. Paolo Sarti

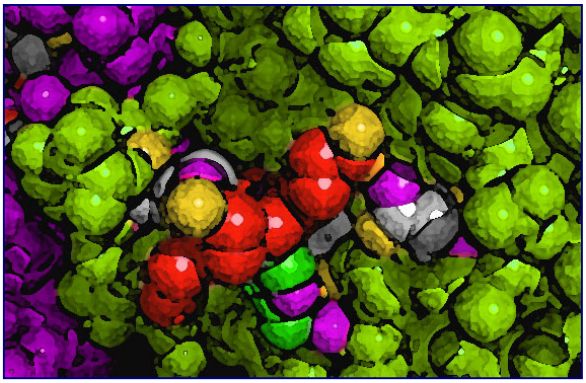

Dicembre 2006

ACKNOWLEDGEMENTS

The work I describe in this thesis was performed at the Department of Biochemical Sciences “A. Rossi Fanelli”, University of Rome “La Sapienza”, under the supervision of Prof. Maurizio Brunori.

First of all I want to thank Prof. Brunori for giving me the opportunity to step into the fascinating world of protein crystallography, as well as for his support.

I am grateful to Prof. Francesca Cutruzzolà who supervised my bench work and was extremely patient with me in the last three years and during the revisions of my manuscript.

I am grateful to Dr. Adele Di Matteo who spent a lot of time teaching me the basic crystallographic techniques.
Thanks to Dr. Serena Rinaldo with whom I shared the every day purification and characterization work on DNR, and who patiently introduced a chemist to the common biochemical techniques.
Thanks to Dr. Kenneth Allan Johnson who helped my to obtain the first set of phases when I was starting to despair.
Thanks to Dr. Veronica Morea for precious advise and help during the modelling.

Thanks to the ‘Soppalco’ people: Francesca ‘Chop’ Cutruzzolà, Serena ‘Sora Mirella-Chip’ Rinaldo, Fabio ‘Mad Sliver’ Centola, Nicoletta ‘Blond Sweety’ Calosci, Nicoletta ‘Brunette’ Castiglione, Manuela ‘Download’ Caruso, Gianna ‘Peace and Love’ Panetta, Alessandro ‘Rocky’ Borgia, Stefano ‘Lazy’ Gianni, Sir Carlo Travaglini Allocatelli.

Thanks to the crystallographers: Adele ‘Sellerona’ Di Matteo, Daniele ‘Nut Cracker’ Bonivento, Adriana ‘EnergErica’ Miele (always there), Stefano ‘Tribalista’ Franceschini, Andrea ‘Very Bold’ Ilari, Lord Tommaso Moschetti, Linda ‘Chat’ Savino, Paola ‘Kir’ Baiocco, Luca ‘Antico Toscano’ Federici, Louise ‘La Peppa’ Gourlay, Fabiana ‘Always happy’ Renzi, Giuliano ‘The Dancer’ Sciara, Beatrice ‘Roller-Blade’ Vallone, Giuseppe ‘Tipo Latino’ Nativio.

But over and above all: Grazie Francesco!!!

And thanks to all the other people I meet every day at the department for nice discussions as well as for sharing lunch in the roman sun, coffee and cigarettes.

TABLE OF CONTENTS

INTRODUCTION

DNR was discovered in the context of investigating the expression of the anaerobic respiratory system of nitrate denitrification. The name is derived either from *D*issimilatory *N*itrate respiration *R*egulator, or from the acronym of its exact role in bacterial denitrification. The denitrification respiratory chain is active in the absence of oxygen or at low oxygen tensions, and in the simultaneous presence of N-oxide(s). Nitrate (NO_3^-), nitrite (NO_2^-), nitric oxide (NO) or nitrous oxide (N_2O) all serve as alternative respiratory substrates. The gene encoding the DNR transcription factor was revealed on sequencing the regions downstream of the *nor* operons encoding NO reductase of *Pseudomonas aeruginosa* (Arai *et al.,* 1995).
By sequence comparison the *DNR* gene encodes a putative transcription factor belonging to the CRP-FNR superfamily of regulators. This superfamily has been named after the first two identified members. CRP, Cyclic adenosine monophosphate (cAMP) Receptor Protein from *E. coli* (McKay and Steitz, 1981) also referred as Catabolite gene Activator Protein (CAP), and FNR, Fumarate and Nitrate reduction Regulator, that is an oxygen sensing iron-sulfur cluster containing a protein which acts as global regulator of anaerobiosis in *E. coli* (see below) (Green *et al.*, 2001).

1.1 Denitrification and nitric oxide homeostasis

Nitrogen cycle

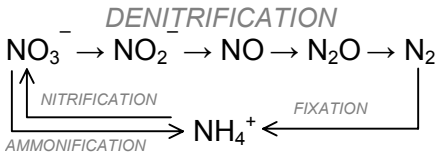

Denitrification represents one of the major processes involved in the nitrogen cycle, which is entirely carried out by bacteria.
In this pathway nitrogen oxides like nitrates and nitrites can be used as the only nitrogen source and as terminal electron acceptors under anaerobic growth conditions (Zumft, 1997), through their progressive reduction to molecular nitrogen.
Four reductases are involved in this process: nitrate, nitrite, nitric oxide and nitrous oxide reductases encoded by the *nar, nir, nor* and *nos* genes respectively. The process is carried out, in Gram negative bacteria, both in the periplasmic space and in the inner membrane and small proteins like azurins and various cytochromes c are also involved as electron donors (Figure 1.1). Denitrification is a facultative process induced by the presence of nitrates/nitrites and low oxygen tension and the

activity of the four enzymes is regulated both kinetically and transcriptionally to avoid accumulation of toxic intermediate (i.e. nitric oxide).

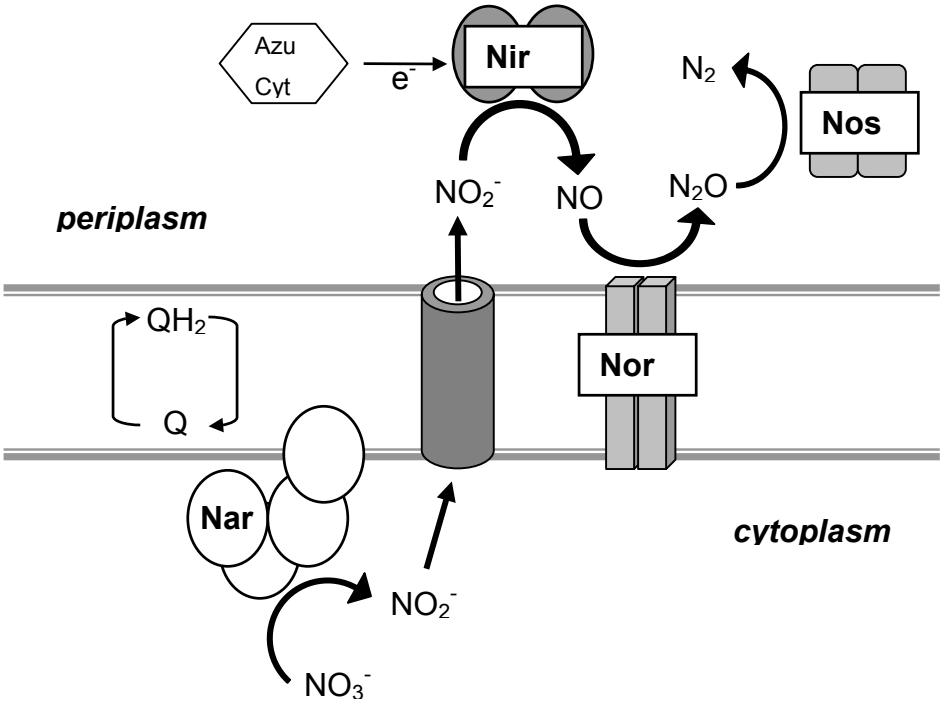

Figure 1.1 *Schematic representation of the denitrification in Gram negative bacteria. Q/QH_2 indicates the quinol mediated electron transfer; Azu and cyt are azurin and cytochromes respectively*.

The expression of the denitrification gene clusters is tightly controlled by redox signalling through a cascade of oxygen-responsive regulators activating the N-oxides-responsive ones.
These regulators control the nitric oxide (NO) homeostasis maintaining the steady-state concentration of nitrite and NO below cytotoxic levels; as a consequence, free NO concentration is in the nanomolar range. These conserved NO-sensors, which belong to the CRP-FNR superfamily of bacterial regulators, play a crucial role as NO is a highly reactive species.

NO reactivity - At low concentration, NO functions as a signalling molecule, whereas at high concentration, NO can be a general poison due to its capability to

alter biological macromolecules both directly or indirectly through NO-derived species.
At high levels, the gas reacts mainly with heme centres and labile 4Fe–4S clusters and thus inhibits terminal oxidases and aerobic respiration (Poole and Hughes, 2000; Wink and Mitchell, 1998). NO can also react both with molecular oxygen or superoxide (O_2^-) to produce nitration/nitrosation modifications or peroxynitrite ($OONO^-$, Huie and Padmaja, 1993) respectively.
Peroxynitrite acts as a strong oxidant by reacting with other molecules and can decompose to the highly reactive hydroxyl ($HO^\cdot$) and nitrogen dioxide ($NO_2^\cdot$) radicals. It was proposed that most of the damages produced by the presence of NO is mediated by peroxynitrite (Packer, 1996), which causes, if present at 1 mM concentration, cell death in *E. coli* in 5 seconds upon exposure (Brunelli et al., 1995).
In addition, NO-derived species can react with thiols present in small molecules and proteins, thereby disrupting protein activity as well as depleting the reduced glutathione pool to generate nitrosylated glutathione (GSNO), which in turn can modify proteins.
Eukaryotic cells use high concentrations of NO to fight invading prokaryotic pathogens and parasites (Bastian and Hibbs, 1994; Nathan and Hibbs, 1991).
The NO released by macrophages is not the only source of NO that microbes need to deal with, because this compound is also produced abiotically (*e.g.* by decomposition of nitrite) and biotically by denitrifiers (Zumft, 1997) and as a product of side reactions in ammonification and nitrate assimilation/respiration (Corker and Poole, 2003).

1.2 Nitric Oxide: a key regulator in *Pseudomonas aeruginosa*

P. aeruginosa is one of the most important opportunistic pathogens. This Gram negative bacterium grows in inflamed tissues forming multicellular, matrix-enclosed assemblies (biofilms). These surface-associated microbial communities are frequently associated with the emergence of antibiotic-resistant subpopulations of bacteria (Singh *et al.*, 2000). Using cooperative traits such as cell-cell signalling (quorum sensing), bacteria in biofilms often develop three-dimensional structures known as microcolonies, in which cells become highly differentiated from free-living, planktonic bacteria (Webb *et al.*, 2003). Cells within a biofilm have a number of advantages over their planktonic counterparts, including protection against the immune system and predation by protozoa, enhanced ability to transfer genetic information, and, most important, microcolonies that are generally highly tolerant to standard antimicrobial agents; it has been shown that bacteria embedded within

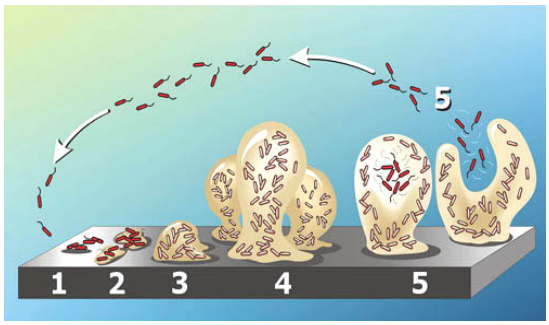

Figure 1.2 *biofilm developmental cycle*

such structures can be 1,000-fold more resistant than are planktonic cells (Brooun *et al.,* 2000; Costerton *et al.,* 1999). Therefore these surface-associated microbial communities are frequently associated with the emergence of antibiotic- resistant subpopulations of bacteria (Singh *et al*., 2000). Thus, biofilm formation complicates a variety of chronic infections, including the devastating pulmonary infections that are caused by *P. aeruginosa* in cystic fibrosis patients and other opportunistic infections by this organism (Yoon *et al.,* 2006). On the other hand, the biofilm environment is restrictive for bacterial growth (Waite *et al.,* 2005). Entrapment in the biofilm matrix also precludes the ability of a cell to flee hostile conditions or migrate to a more propitious site when opportunities arise. Not surprisingly, microbes actively form, as well as exit or disperse, from biofilm. The resulting developmental cycle (Figure 1.2) is characterized by a succession of changes in gene expression and phenotype (Southey-Pillig *et al.,* 2005).

Strategies to induce biofilm dispersal would have broad medical applications.

In one commonly observed process of dispersal in *P. aeruginosa* named seed dispersal, organisms evacuate the interior of the microcolonies, leaving behind hollow, shell-like structures, a little like plant seeds (Hunt *et al.,* 2004; Purevdorj-Gage *et al.,* 2005; Sauer *et al.,* 2002). The mechanisms underlying these events are poorly understood but have been shown to involve quorum sensing (Purevdorj-Gage *et al.,* 2005) and complex processes of differentiation, including the lysis of a subpopulation of cells within microcolonies (Mai-Prochnow *et al.,* 2004; Webb, Thompson *et al.,* 2003). In *P. aeruginosa*, cell lysis and dispersal were recently linked to the generation of oxidative or nitrosative stress inside microcolonies (Webb, Thompson *et al.,* 2003). Specifically, Yoon et al. (2002) have shown that organisms housed in anaerobic biofilms and lacking the *rhl* quorum-sensing circuit commit a metabolic suicide via NO intoxication. Furthermore it has been recently demonstrated that in *P. aeruginosa* NO is able to induce biofilm dispersal at concentrations that are non toxic (in the nanomolar range) (Barraud, *et al.,* 2006). These findings suggest that in *P. aeruginosa* regulation of NO levels is crucial for the formation of persistent biofilms.

P. aeruginosa, which is a facultative anaerobe, can use denitrification as the anaerobic energy producing pathway (Hassett *et al*., 2002). Low oxygen tension and the presence of N-oxides produced by the host defence mechanism induce high levels of expression of *nir-nor* operons (Hassett *et al*., 2002). Under anaerobic

conditions, the denitrification pathway not only works as a source of electrons and as NO scavenger given that the classical flavohemoglobin-mediated detoxification pathway is not active (Arai *et al.*, 2005), but may also be related with the biofilm developmental cycle as it is now evident that low concentrations of NO directly or indirectly induce biofilm dispersal and inhibit biofilm formation in *P. aeruginosa.*
Pathogenesis, NO regulation and denitrification are therefore strictly related.
The molecular basis of these complex regulation system is yet to be unrevealed.

NO sensing in Pseudomonas aeruginosa - The induction of denitrification by oxygen depletion in *P. aeruginosa* requires ANR (*A*naerobic regulation of arginine deaminase and *N*itrate *R*eduction), a FNR-like global regulator for anaerobic gene expression (Galimand *et al.*, 1991). ANR induces the expression of the DNR protein, which activates, in the presence of N-oxide(s), the *nirS*, *norCB*, *nosR* promoters (Arai *et al.*, 1997, 1995, 2003) (Figure 1.3).

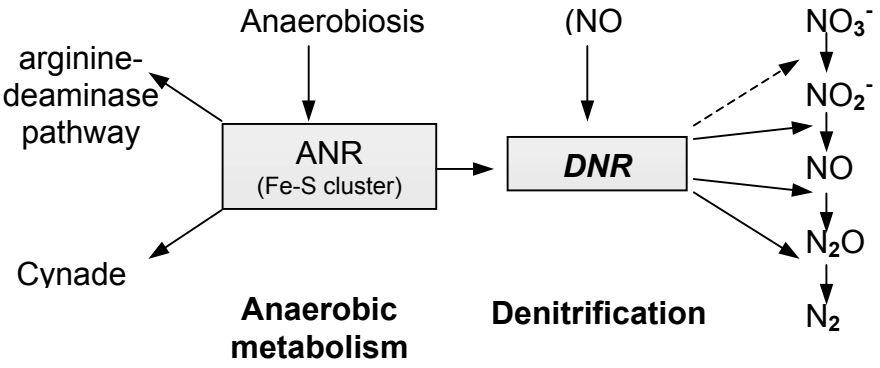

Figura 1.3 *Signaling and components of the regulation of the denitrification in P. aeruginosa. ANR represents the global regulator of anaerobiosis, which activates the regulators of denitrification, arginine deaminase and cyanide production pathway. The DNR protein in the presence of N-oxides (presumably NO) activates the transcription of the enzymes involved in the denitrification. The substrates and products of each N oxide-reducing system are shown.*

Mutants without the *anr* or *dnr* genes are not able to induce *nirS* and *norCB* promoters under growth conditions where denitrification should be active (Arai *et al.*, 1995). *anr* defective strains are not able to activate the transcription of the *dnr* gene but denitrification can be induced after transformation with a plasmid carrying the *dnr* gene (Arai *et al.*, 1997). DNR-mediated transcriptional activation of denitrification depends on endogenous NO concentration (Arai *et al.*, 1999, 2003); the transcriptional activation analysis is summarized in Table 1.1.

As already mentioned DNR is a member of a large superfamily of regulators, the CRP-FNR superfamily of transcription factors.

strains	***dnr***	***nirS***	***norB***
anr-	-	-	-
dnr-		-	-
anr-pDNR		+	+

Table 1.1 *Transcriptional activation analysis of the dnr, nirS and norB promoters carried out by using reporter gene systems (Arai et al., 1995, 1997, 1999). P. aeruginosa mutants lacking the anr (anr-) or dnr (dnr-) genes are not able to activate these promoters. The anr- strain transformed with a plasmid carrying the dnr gene (anr-pDNR) recovers the nirS and norB promoters activation.*

1.3 The CRP-FNR superfamily of transcription factors

The CRP-FNR regulators are DNA-binding proteins that mainly function as positive transcription factors, even if an additional role as repressors can not be ruled out. Two distinctive features characterize these regulators: an N-terminal effector binding domain, similar to the nucleotide-binding domain of CRP and a C-terminal helix-turn-helix (HTH) motif involved in DNA binding (Figure 1.4).

Figure 1.4 *BLAST search result for Conserved Domains of DNR from P.aeruginosa.*

CRP-FNR superfamily classification based on a phylogenetic relationship results in the assembly of the regulators in the following distinct clusters or subgroups: ArcR, CooA, CprK, Crp, Dnr, FixK, Flp, Fnr, FnrN, MalR, NnrR, NtcA, PrfA, and YeiL (Figure 1.5, A). Several other groups consist of sequence-derived proteins of unknown physiological roles; some of them are tight clusters of highly similar members (Körner *et al.*, 2003).
The CRP-FNR regulators are involved in the regulation of many enzymatic pathways including oxygen respiration, denitrification, nitrogen fixation, methanogenesis, CO-respiration, halo-respiration and virulence activation.

Therefore they respond to a broad spectrum of intracellular and exogenous signals such as cAMP, anoxia, the redox state, oxidative and nitrosative stress, nitric oxide, carbon monoxide, 2-oxoglutarate, or temperature (Figure 1.5, B) (Aono, 2003; Eiting *et al.*, 2005; Joyce *et al.*, 2006).

To accomplish their roles, CRP-FNR members have intrinsic sensory modules allowing direct binding of allosteric effector molecules, or have prosthetic groups which interact with the signalling molecule(s). The regulatory adaptability and structural flexibility represented in the CRP-FNR scaffold has led to the evolution of an important group of physiologically versatile transcription factors (Körner *et al.*, 2003) which owns its name to the two best characterized proteins among this class of regulators; CRP and FNR from *E. coli.*

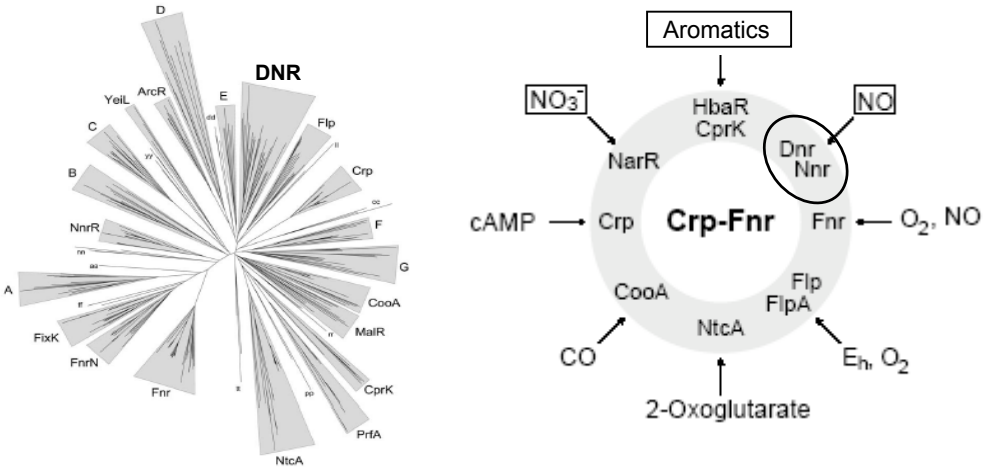

A **B**

Figure 1.5 *A) The main branches of the CRP-FNR superfamily of transcription factors (modified from Körner et al., 2003). B) Signals processed by regulators of the Crp-Fnr family. Boxed signals have not been proven to interact directly with the cognate regulator. Eh, midpoint potential (Körner et al., 2003; Joyce et al., 2006).*

CRP or CAP (Catabolite Activator Protein) is very well known as it was the first transcription activator to be discovered and to have its X-ray structure solved. The relatively simple activation mechanism of a target gene, requiring in the basic case besides CRP and RNA polymerase no additional protein factor, has made CRP a prime object of structural, biochemical, and genetic research (Schultz *et al.,* 1991; Botsford *et al.,* 1992; Busby *et al.,* 1999). CRP regulates the expression of over 150 proteins, thus controlling a wide spectrum of physiological processes, comprising the metabolism of sugars or amino acids, transport processes, protein folding, as well as toxin production or pilus synthesis (Kolb *et al.,* 1993). Being CRP the first

member of the superfamily, all the proteins which share the same domain organization (see below) are classified as CRP-FNR regulators.
FNR contains an iron-sulphur cluster, and can be considered as the paradigm of an oxygen responsive transcription regulator (Green and Scott, 2001; Spiro, 1994; Guest *et al.,* 1996; Unden, 1998; Kiley and Beinert, 1999). FNR binds to a partially palindromic sequence termed the Fnr box or, occasionally, the anaerobox. The FNR scaffold must have a high degree of adaptability and flexibility to accommodate interaction with several chemically distinct sensor molecules, and to allow for different DNA-binding and RNA polymerase contacts. The spectrum of regulated functions in which FNR is involved is considerable. Among them are genes coding for alcohol dehydrogenase, aconitase, asparaginase, C4-dicarboxylate transporter, cytochrome *d*- and *o*-type oxidases, dimethylsulfoxide reductase, fumarate reductase, molybdenum cofactor biosynthesis, hydrogenase, nickel transport, and NADH and succinate dehydrogenases (Körner *et al.,* 2003).

Structure organization of CRP-FNR regulators - Transcription factors belonging to the CRP-FNR superfamily share the same tertiary structure as well as the domain organization although the sequence identity can be very low (below 20%). The size is constant with approximately 230-250 amino acid residues. They are physiologically active as homodimers, each monomer being constituted by three distinct domains: an N-terminal β-barrel as the effector or sensing domain (first 120-150 residues); a long dimerization α-helix (30 residues, usually referred as C-helix); and a C-terminal helix-turn-helix DNA binding domain (HTH) (Figure 1.6).

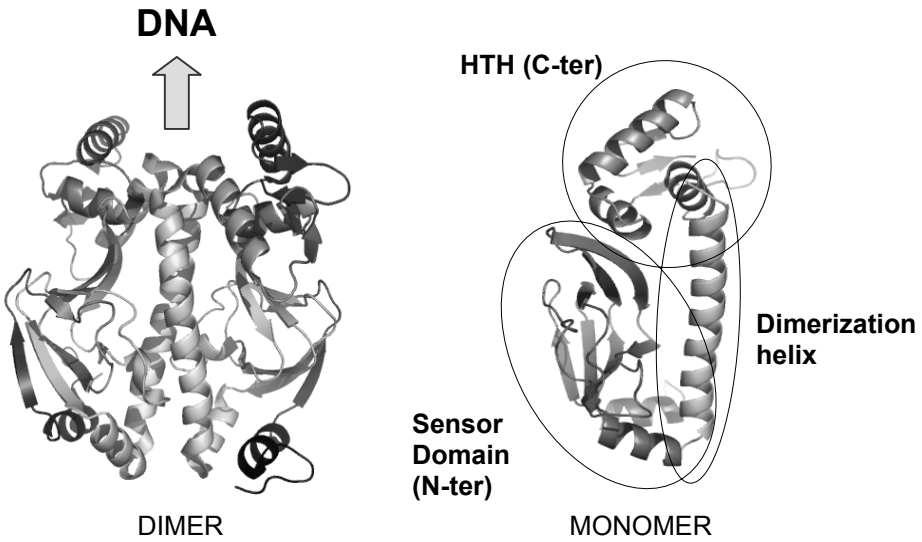

Figure 1.6 *Structural organization of the CRP-FNR regulators. On the left the active dimer, on the right domain organization of the monomer. Structure are of CRP protein of E.coli (pdb code 1g6n; Passner* et al., *2000).*

Upon binding of the allosteric effector molecule the sensing domain undergoes a conformational change that is transmitted through the C-helix to the HTH motif and results in an overall reciprocal repositioning of the sensing and DNA-binding domains. These adjustments promote surface-patch interaction with RNA polymerase and allow the two recognition helices of the HTH-motif to interact with the major groove of target DNA sequence, the FNR box ($TTGATN_4ATCAA$, Körner *et al.*, 2003).

This is thought to be the allosteric mechanism that switches the CRP-FNR superfamily proteins from the OFF-state (inactive / not able to bind DNA) to the ON-state (active / DNA binding) (Harman, 2001; Passner *et al.,* 2000; Yu *et al.,* 2004). In the last two years a major contribution to the understanding of the structural basis of the allosteric control in CRP-FNR structural homologs has come from the crystal structures of CprK (halorespiration regulator of *Desulfitobacterium dehalogenans*) in the OFF and ON like conformation (oxidized CprK in presence of the ligand *ortho*chlorophenolacetic acid and of reduced CprK in absence of this ligand) (Joyce *et al.,* 2006), and of PrfA (a key virulence regulator of *Listeria monicytogenes*) wild type (OFF-state) together with PrfA-G145S that is a constitutively active mutant (ON-state) (Eiting *et al.,* 2005). Before these two papers the only known structures of this class of transcription factors were several structures of CRP always in presence of cAMP, thus in its active state (McKay *et al.,* 1981; Passner *et al.,* 1997 and 2000), and CooA, a heme containing CO binding protein, in the inactive state (Lanzillotta *et al.,* 2000) (Figure 1.7).

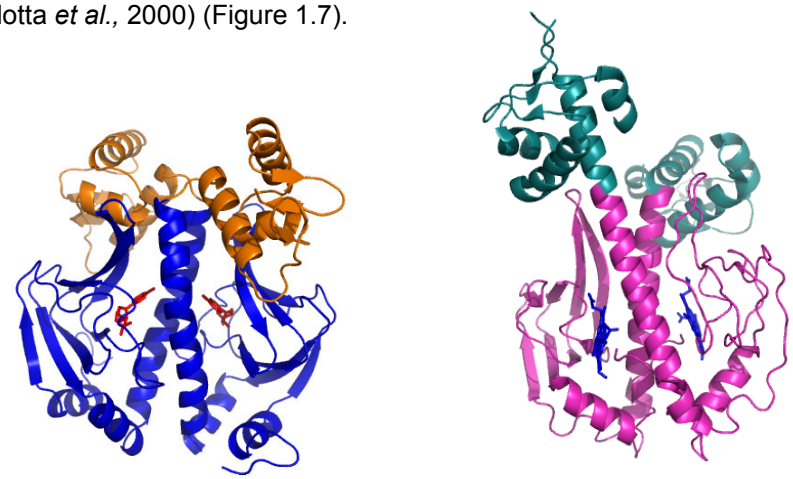

CRP - **ON conformation** *CooA* – **OFF conformation**

Figure 1.7 *CRP in the active (ON) conformation in complex with cAMP (red) (pdb code 1g6n; Passner et al., 2000) and CooA in the inactive (OFF) conformation binding ferric heme (blue) (pdb code 1ft9; Lanzillotta et al., 2000). In both proteins the HTH domain is colored differently. Notice the striking difference in the relative orientation of the HTH domain with respect to the dimerization helix in the two conformations.*

CooA (CO-oxidation activator protein) regulates the expression of genes involved in the oxidation of carbon monoxide (CO) in the bacterium *Rhodospirillum rubrum* (Aono *et al.,* 1996). CooA senses the presence of CO, in the highly reducing environment of the cytoplasm, by mean of a heme group and responds inducing the transcription of operons encoding proteins involved in the oxidation of CO to CO_2 and reduction of protons to H_2 (Roberts *et al*., 2005).
To date, in this class of regulators, CooA is the only gas sensor containing a heme moiety that as been characterized both functionally and structurally (Lanzillotta *et al.,* 2000; Aono, 2003; Reynolds *et al.,* 2000).

NO-responsive components of the CRP-FNR superfamily - Multiple members of these regulators, belonging to different subgroups, can either co-exist in the same host or regulate the same metabolic pathway in different organisms (Körner *et al*., 2003). This is the case for the regulators of denitrification and in general for NO-responsive components which belong to the FNR, DNR and NnrR subgroups of the CRP-FNR superfamily and can control N-oxide homeostasis both under anaerobic and aerobic conditions (Körner *et al*., 2003).
FNR proteins, which are general oxygen sensors, under anaerobic conditions and in the presence of NO are also able to activate detoxification by promoting expression of flavohemoglobin (encoded in the *hmp*-gene) and other associated detoxifying entities such as the NO dioxygenase, NO denitrosylase, and NO reductase. In *E.coli* under aerobic conditions FNR is a dimer and acts as an *hmp* repressor; in the presence of NO the $[4Fe\text{-}4S]^{2+}$ centre, which controls protein dimerization and DNA binding activity, is converted into the $[2Fe\text{-}2S]^{2+}$ state inducing monomer formation in the FNR protein. This NO-modified FNR form binds the *hmp* promoter with lower affinity, inducing flavohemoglobin expression (Cruz-Ramos *et al.*, 2002).
Recently a different activation mechanism has been reported for FNR from *Bacillus subtilis*. *B. subtilis* FNR forms a homodimer independently of the oxygen tension in the environment and the integrity of the $[4Fe\text{-}4S]^{2+}$ cluster. Under oxygen limiting conditions a $[4Fe\text{-}4S]^{2+}$ cluster is formed which is coordinated by three cysteine residues localized, unexpectedly, at the C-terminal and a yet unknown fourth ligand of the regulator. Cluster formation induces a DNA-binding domain conformation which allows promoter recognition and transcriptional activation (Reents *et al.,* 2006).
DNR and NnrR are the other two subgroups of redox sensors regulators belonging to the CRP-FNR superfamily which act as NO responsive factors. Members of these subgroups are involved in the activation of the denitrification respiratory chain in the presence of N-oxide(s) and under low oxygen tension. To date no structural information and limited biochemical data are available on this two groups and the mechanism by which these proteins may sense NO is still unclear (Körner *et al.,* 2003).

The DNR-type of transcription regulators - All members of the DNR subgroup share the same motif (E-SR amino acid residues located in the HTH recognition helix) involved in recognition of the binding site on DNA, while most members of the NnrR subgroup contain an histidine instead of a glutamate residue (Spiro, 1994). Both groups of regulators (DNR and NnrR) do not contain enough cysteines for iron-sulfur cluster formation contrary to FNR, suggesting a different mechanism of N-oxide(s) sensing.

Members of both NnrR and DNR subgroups are found in facultative anaerobic bacteria; the transcriptional regulation is exerted in the presence of N-oxide(s) and under low oxygen tension. In *Rhodobacter sphaeroides* and in *Paracoccus denitrificans* for example, it was shown, by genetic approach, that the transcriptional regulators designated respectively NnrR (belonging to the NnrR-type) and Nnr (belonging to the DNR subgroup) can both activate the expression of the nitrite and NO reductase genes in response to NO (Kwiatkowski and Shapleigh, 1996 and Van Spanning *et al.,* 1999).

The members of DNR-type class of regulators found in the *Pseudomonas* sp. (Arai *et al.*, 1997 and Vollack and Zumft, 2001) share an high sequence identity (Figure 1.8) but may not fulfil an identical physiological role.

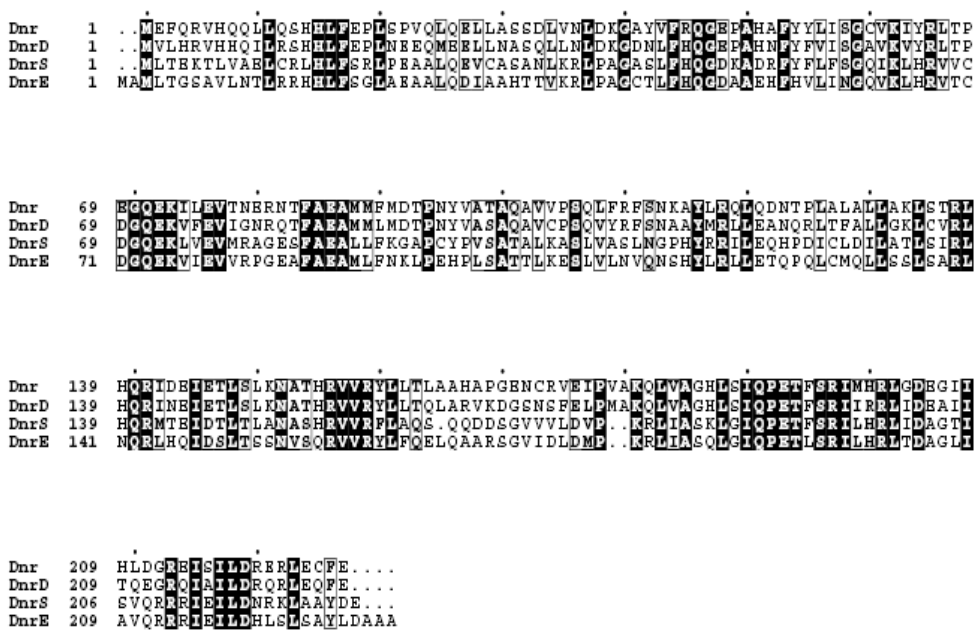

Figure 1.8 *Multiple alignment of DNR protein sequences from Pseudomonas aeruginosa (DNR) and Pseudomonas stutzeri (DnrD, DnrS and DnrE). Invariant positions are boxed in black; alignment columns displaying amino acid with the same physico-chemical properties are boxed in white with the conserved residues shown in bold.*

This is not surprising given that *Pseudomonads* are well known for their metabolic flexibility which reflects the capability of the different species to survive as free living organisms in soil, water and animals, where are often responsible for diseases.
In *Pseudomonas stutzeri* there are at least three regulators (DnrD, DnrS, DnrE) involved in the NO-sensing (DnrD), activation of the nitrate pathway (DnrE) and possibly in redox sensing (DnrS) under anaerobic conditions (Körner *et al.*, 2003).
The DnrD transcription factor induces the expression of *nirSTB*, *norCB*, *nosZ* operons (encoding respectively nitrite, nitric oxide and nitrous oxide reductases) in the presence of NO but not nitrite (the *nos* gene is activated also in presence of high concentration of nitrous oxide). The NO concentration required for the *nir-nor* operons activation is in the range of 5-50 nM (Vollack and Zumft, 2001). DnrD overexpression *per se* is not sufficient for the transcription of the *nir-nor* operons, indicating that additional factors may be required (Vollack and Zumft, 2001).

As previously discussed Nitric oxide (NO) is a highly diffusible free radical that has, at high concentrations, a well-characterized reactivity with various cellular components such as dioxygen (O_2), metal ions, thiols and is a potent weapon used by the immune system to kill infectious organisms and tumor cells. Nonetheless, it is now clear, that at low nanomolar concentrations, NO is an effective and physio-pathologically important signalling molecule controlling processes such as blood vessel relaxation, myocardial function, cerebral blood flow, synaptic plasticity in the brain, platelet aggregation, and egg fertilization (Denninger *et al.*, 1999; Toda *et al.*, 2003) and also seed dispersal of *P. aeruginosa* biofilms (Barraud, *et al.,* 2006). To function in this important signalling role, NO requires highly sensitive and selective receptors. DNR from *P. aeruginosa* is part of the growing complex network of NO/redox sensors which can activate different scavenging mechanisms and metabolic pathways depending on the balance between N-oxide and oxygen in the medium.
Given the large amount of processes controlled by this gas, understanding the fate of nitric oxide (NO) inside the cell has become a major issue in biology and medicine.

AIM OF THE PROJECT

All denitrifiers can keep the steady-state concentration of nitrite and nitric oxide (NO) below cytotoxic levels controlling the expression of denitrification gene clusters by redox signalling through transcriptional regulators belonging to the FNR-CRP superfamily.
NO-responsive regulators belong to three different subgroups of the CRP-FNR superfamily (FNR, DNR and NnrR) and can control N-oxide homeostasis both under anaerobic and aerobic conditions. The FNR-type share a cystein rich motif involved in the formation of an iron-sulfur cluster as a redox centre which is not present in the other two subgroups.
Most of the regulators involved in the regulation of denitrification, belonging either to the DNR and NnnR subgroups, regulate nitrite reductase (*nir*), nitric oxide reductase (*nor*) and nitrous oxide reductase (*nos*) gene expression. The NO dependence of the transcriptional activity of promoters regulated by these transcription factors suggested that these factors may act as NO sensors *in vivo*.
Despite the growing interest in the regulation of denitrification, functional and structural characterization of these NO sensors is still lacking.

Controlling the denitrification pathway could be a powerful tool in the control of the nitrate contents in wastewater and of the greenhouse gas production. In fact, nitrate, irrespective of its role as an essential plant nutrient, has become a pollutant of groundwater and surface water, causing a major problem for the supply of drinking water and N_2O is next to CO_2 and CH_4 in its importance as a potent greenhouse gas.
Moreover, recent studies indicate that the denitrification (Hassett et al., 2002) and in general anaerobiosis (Sarti et al., 2004) are responsible of the NO-resistance of pathogens. Among denitrifier, *P. aeruginosa* is one of the most studied organism due to its capability to colonize different environments also as opportunistic pathogen, mainly in cystic fibrosis patients. The lung epithelium of these patients shows a mucus layer, due to an altered ion transport, which blocks the normal mucociliary clearance; the mucus adheres to the epithelium, and this layer imposes an oxygen gradient. *P. aeruginosa* can penetrate this layer and chronically colonize the epithelium by using denitrification as the energy source and resistance mechanism towards the NO, released by the defence host systems; during this chronic infections, the *nir* and *nor* genes are overexpressed. During colonization of the inflamed tissues this pathogen forms stable biofilms. Cells within a biofilm have a number of advantages over their planktonic counterparts, including protection against antimicrobial agents and other stresses (Fux *et al.,* 2005). The mechanisms that permit bacteria to make the transition from an unattached or planktonic cell to a

surface-associated multicellular biofilm and back have become a subject of intense interest to microbiologists over the past several years (Romeo, 2006). Recent studies (Barraud *et al.,* 2006) have identified nitric oxide (NO), at concentrations (nM) far below the toxic levels for this bacteria, as an elicitor of biofilm dispersal or detachment by *Pseudomonas aeruginosa*. Furthermore, low levels of NO were sufficient to sensitise the cells to at least some bactericidal agents. How these effects of NO are mediated is yet to be determined.
Indeed a deeper insight onto NO sensing in *P. aeruginosa* could lead to a new therapeutical approach in the treatment of chronic infections based on antipathogenic drugs and/or antibiotic compounds by attenuation of bacterial virulence and inhibition of biofilm formation such that the organism would fail to colonize (Hentzer and Givskov, 2003). One of these new targets could be the inhibition of the DNR-mediated denitrification pathway.
DNR protein was recently expressed in *E. coli* and partially characterized in its DNA binding activity to understand which environmental signals can control the DNR-mediated denitrification activation (Rinaldo *et al*., 2005).

My PhD work was focused on the determination of the 3D structure of DNR from *P. aeruginosa* by X-ray crystallography in order to better clarify the structure-function relationships of these transcription factors.
X-ray Crystallography is a complex technique that requires a number of steps, starting with protein expression-purification and ending with a refined 3D model of the protein of interest, going trough crystallization, data collection and phasing. Given that each of these steps is part of a pipeline, the final result is never guaranteed.
Full length DNR from *P. aeruginosa* was expressed and purified but unfortunately all trials to obtain crystals of this protein were unsuccessful. Given that the function of DNR is embedded in the N-terminal sensor domain, we decided to express a C-terminal deletion mutant constituted by the dimerization helix and the sensor domain (DNR-N152stop hereafter ΔDNR or truncated DNR). This truncated DNR mutant was purified and crystallized, its structure has been solved and is described in this work.
This work will have to be completed with the determination of the 3D structure of the full length protein, still in progress. Nevertheless the structure of the truncated DNR provides interesting new insights into the effector-mediated allosteric switch and the chemistry of NO sensing and will hopefully help to shed light on the global regulation mechanism of denitrification.

RESULTS

3.1 His-tagged and native DNR from *P.aeruginosa*: expression, purification and characterization

The *dnr* gene from *P. aeruginosa* genomic DNA had been already isolated by our group using PCR and inserted it in the expression vector PET28b (Novagen). The pET-DNR vector was transformed in BL21 (DE3) *E. coli* strain, the protein was expressed, purified to homogeneity and concentrated as reported in Rinaldo et al. (2005).

To facilitate the purification of high quantities of protein suitable for crystallization the DNR protein was engineered by introducing a tag. The *dnr* gene was amplified by PCR and cloned into the pET28b vector in frame with a 6xHistidine tail at the N-terminal of the protein. The plasmid (pET-DNR-HIS) was then transformed into BL21(DE3) *E. coli* strain and the protein was expressed both in presence of 1 mM IPTG or in the absence of inducers (Figure 3.1 A, lane 1 and 2). The DNR-HIS protein was detected by western blot, using commercial anti-histag antibodies (Figure 3.1 A, lane 3). High yields of purified DNR-HIS (50 mg/l of cell culture) was easily obtained as described in the experimental section. The his-tag tail was then removed by thrombin proteolysis (Figure 3.1 B).

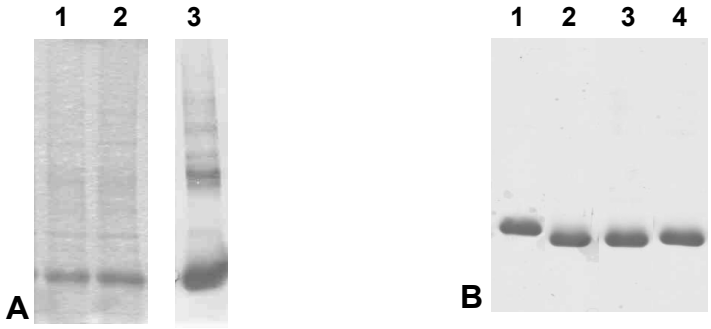

Figure 3.1 *Expression and purification of the DNR-HIS protein, SDS/PAGE. A) Lane 1: overnight cell extract without IPTG. Lane 2: overnight cell extract after induction with 1 mM IPTG. Lane 3: western blot analysis of overnight cell extract after induction with 1 mM IPTG using anti his-tag antibodies (Santa Cruz Biotechnology, Inc.). B) Lane 1: purified DNR-HIS protein. Lane 2-4: room temperature incubation of DNR-HIS with 20 units of thrombin at different times (2h, 4h and 15 h, respectively).*

Gel filtration on DNR-HIS revealed that the protein was mainly aggregated also in the presence of high salt concentration (NaCl 150-300 mM), while the purified protein digested with trombin was found mainly in the dimeric physiological state (not shown). This protein, however, also populates high molecular weight aggregates, more then the native protein, as also assayed by native poly-acrylamide gel (Figure 3.2).

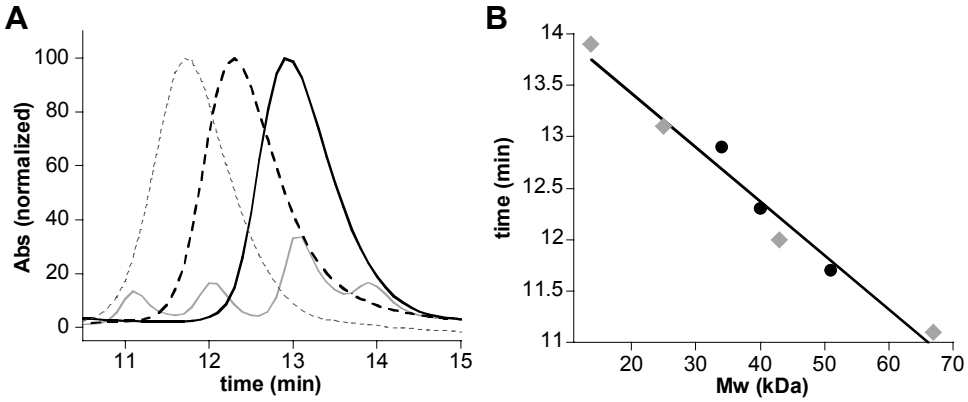

Figure 3.2 *A) Aggregation state of the purified proteins run on a gel filtration column in comparison with molecular mass markers. The elution profiles of the samples (from left to right; DNR-wt, DNR-N152stop-HIS, DNR-N152stop) are normalized to 100 and superimposed on that of the markers; grey trace - from left to right: BSA 67 kDa, ovalbumin 43 kDa, chymotrypsinogen 25 kDa and RNase A 13.7 kDa. B) Linear dependence of the elution times of the markers on their molecular weight (squares), and of the samples (dots) plotted against the expected Mw (DNR-wt 52kda, DNR-N152stop-HIS 40kDa, ΔDNR35kDa).*

Despite the difficulty to purify the dimer, the native protein was chosen for further crystallization trials; however, the pET-DNR-HIS vector was used as template for the mutagenesis.

3.2 *DNR* and *DNR-HIS* crystallization trials

Both DNR and DNR-HIS were concentrated up to 3.3 mg/ml in 20 mM Tris/HCl pH 7.2, 150 mM NaCl after the PCT (Per Crystallization Test, Hampton Research).
Initial crystallization trials were performed with the hanging/sitting-drop vapour-diffusion techniques (Ducruix and Geigè, 1992), previously described, using crystal

screening reagents supplied by Hampton Research (Crystal Screen 1-2 and Index Screen) and by Emerald Bioscience (Wizard Screens 1-2). Drops were set up both at 21°C and 4°C by mixing equal volumes of protein solution and reservoir solution on siliconized cover slips. Drops were allowed to equilibrate against 1.0 ml or 0.5 ml of the same reservoir solutions. More than 2500 different condition were tested but on crystals were observed.

3.3 Mutagenesis: *N152stop-HIS* and *T124stop-HIS* mutants

As described in literature for other DNA binding proteins (Wisén *et al.,* 2004; Tomita *et al.,* 2003) the difficulty to get crystals could be due to the extreme mobility of the DNA binding domain of the non-active form of the protein; thus we decided to express a C-ter deletion mutant.
Using pET-DNR-HIS vector as template for mutagenesis the nucleotides coding for residues asparagine 152 and threonine 124, located respectively at the end and at the beginning of the dimerization α-helix in the sequence, were mutated into a stop codon.
The two mutants N152stop, composed by the sensing domain plus the dimerization helix, and T124stop, composed only by the sensing domain(Figure 3.3), were expressed and purified as described previously for DNR-HIS protein.

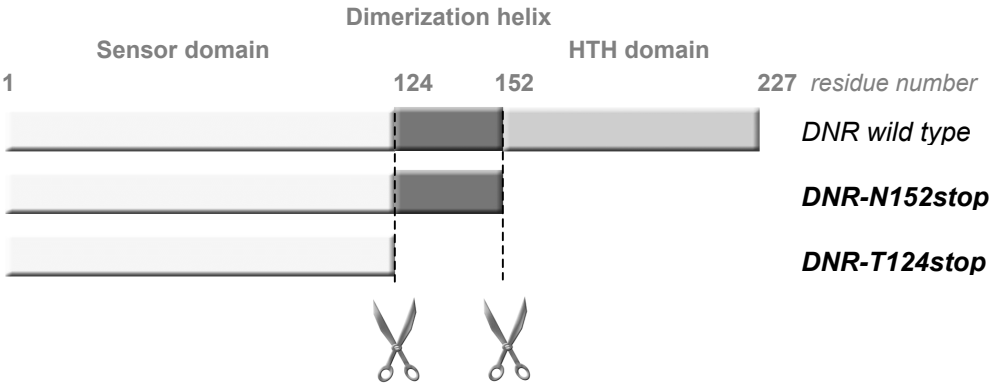

Figure 3.3 *Domain composition of the two DNR deletion mutants.*

Only the DNR-N152stop his-tagged mutant (DNR-N152stop hereafter ΔDNR or truncated DNR) resulted soluble and stable as a dimer (Figure 3.2); it could be purified to homogeneity in high yields (60 mg/l). The protein was subsequently

digested with trombin resulting in a 154 aa protein of 17.5 kDa (as confirmed by LC-ESI Mass-spectrometry) and with a theoretical pI of 6.2. The aa sequence, including the first three residues belonging to the removed his-tag, is reported below.

```
GSH 1 MEFQRVHQQLLQSHHLFEPLSPVQLQELLASSDLVNLDKGAYVFRQGEPAHAFYYL
ISGCVKIYRLTPEGQEKILEVTNERNTFAEAMMFMDTPNYVATAQAVVPSQLFRFSNKAYLR
QLQDNTPLALALLAKLSTRLHQRIDEIETLSLK 151
```

3.4 Biochemical characterization of DNR and DNR-N152stop

The CD spectrum showed that both the wild type and the truncated protein have a secondary structure content (%beta-%alfa) which suggest that the purified proteins are correctly folded in solution (see below).
DNR wt and are mainly dimers in solution, as shown by gel filtration of the proteins in 20 mM Tris-HCl and 150 mM NaCl (Figure 3.2). Higher aggregation states are populated at lower salt concentration (not shown), and thus all experiments and crystallization trials have been carried out with salt concentrations $\geq$ 150 mM NaCl.
No difference in the aggregation state was observed in presence of reducing agents such as β-mercaptoethanol, neither by gel filtration nor by SDS-PAGE (not shown).

Heme titration – in order to investigate the nature of a possible prosthetic group of DNR, and considering that DNR is an NO sensing protein we performed a heme titration on both DNR wt or ΔDNR.
Titrations were carried out with by increasing amounts of a hemin (Fe^{3+}-protoporphirin IX) solution to the protein samples (Figure 3.4, A-B). As a negative control the same titration was performed also on CRP.
For each heme/protein mixture a spectrum was recorded in the 260-700 nm range. In these spectra, the absorbance at 412 nm correlates with the concentration of the heme bound to the protein, while the absorbance at 380 nm correlates with the concentration of the free heme. Absolute spectra show that a spectral shift consistent with heme iron coordination is observed for DNR, but not for CRP, where only aspecific binding could be observed (Figure 3.4, C), strongly suggesting that heme is binding to both DNR proteins.
The difference between the absorbance at 412 nm and at 380 nm (A_{412}-A_{380}) was plotted as a function of the mole fraction of added hemin; formation of the complex is maximized when the monomer of wt protein and heme are present in a 0.85 to 1 ratio, while for the mutant this ratio is 1 (Figure 3.5, A-B). The stoichiometry of binding is assumed to be one heme per monomer in both cases.

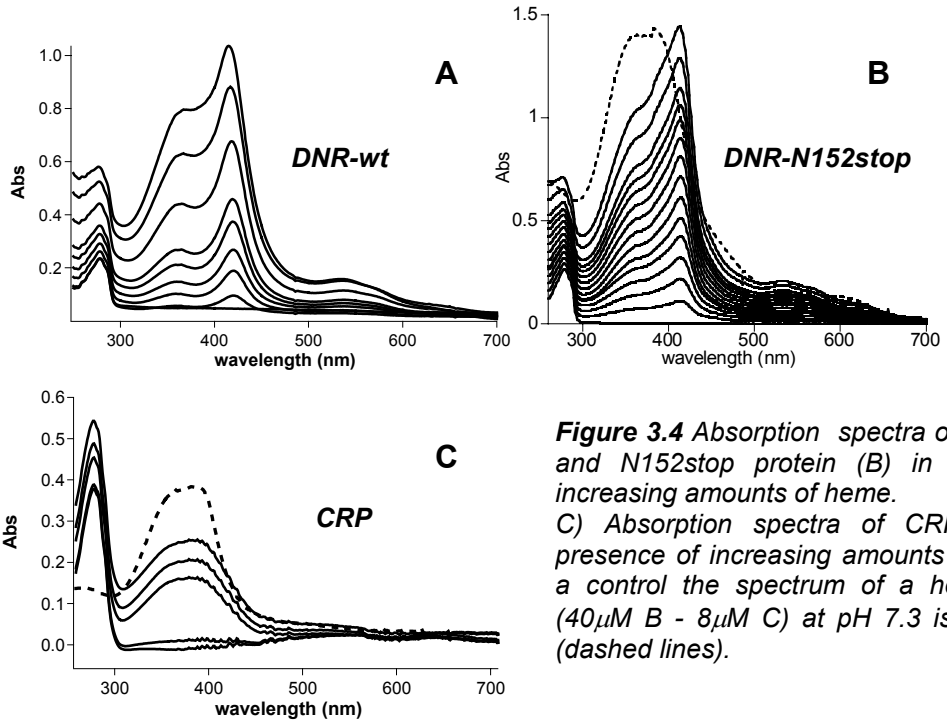

Figure 3.4 *Absorption spectra of DNR and N152stop protein (B) in prese increasing amounts of heme.*
C) Absorption spectra of CRP pro presence of increasing amounts of he a control the spectrum of a heme s (40μM B - 8μM C) at pH 7.3 is also (dashed lines).

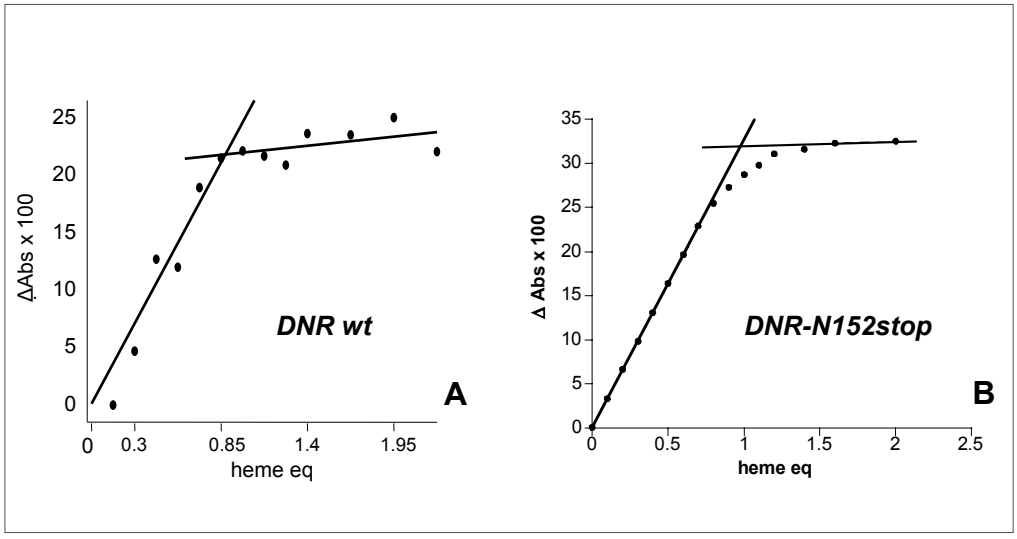

Figure 3.5 *Binding of heme. Plot of delta absorbance value (A_{412}-A_{380}) of DNRwt (A) and ΔDNR(B) heme solutions as a function of heme equivalents.*

Heme reconstitution and spectroscopic properties of DNR wt and ΔDNR-The absorbance peaks for the heme-reconstituted proteins at 412 nm and 530 nm suggest a ferric state of the coordinated iron (Figure 3.6, A-C, black line). In anaerobiosis and in presence of an excess of dithionite, the ferrous derivatives formation was confirmed by spectroscopic changes in the Soret band, shifted from 412 nm to 426 nm (Figure 3.6 A,C grey line). The reduced proteins were also incubated with carbon monoxide (CO) and nitric oxide (NO) and the corresponding derivatives spectra are shown in the Figure 3.6 B,D. The spectroscopic transition of the reduced form to the NO-bound derivative is characterized by an isosbestic point at 408 nm; the NO-bound derivative showed a peak at 398 nm, which resembles a five-coordinated state of the iron (Figure 3.6 B, inset). NO binding was observed also in absence of reducing agents, under anaerobic conditions (Figure 3.6 D, inset), suggesting that NO is able to reduce and subsequently bind to the ferrous iron of the heme-protein complex.

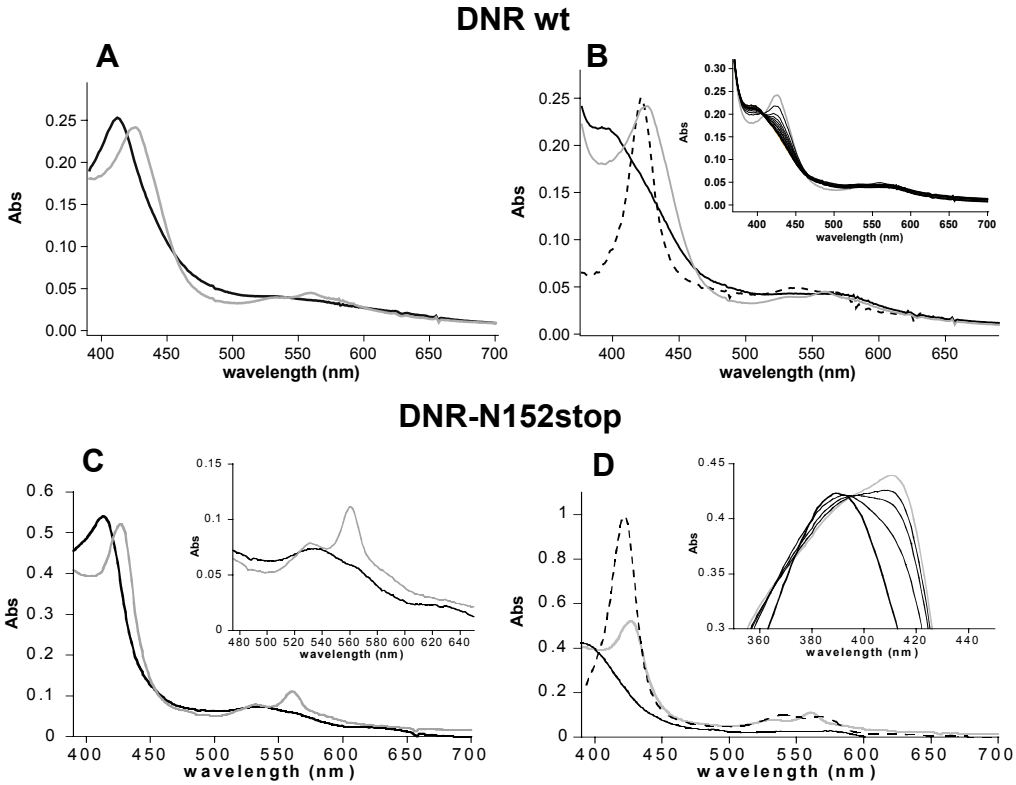

Figure 3.6. *DNR-heme and DNR-N152stop-heme complexes. (A,C) Absorbance spectra of the oxidized (black line) and reduced (grey line) forms. (B,D) Absorbance spectra of reduced protein-heme complex (grey line) bound to NO (black line) or CO (dashed line). NO-bound complex formation from the reduced form (B) and from the oxidized form (D) is also shown (inset).*

Binding of ANS - To get some insights on the DNR structural organization, titration with ANS (8-anilino-1-naphthalenesulfonic acid; Heyduk and Lee, 1989) was performed on both DNR wt and on DNR-N152stop.
When ANS binds to the protein in an hydrophobic environment its fluorescence emission is significantly increased and the emission maximum is shifted from about 530 nm to below 500 nm. The DNR and ΔDNR samples (2 μM) in presence of increasing ANS amounts (2-35 μM) showed a maximum fluorescence emission at 460 nm (Figure 3.7, A-B), which indicates complex formation between the protein and the ANS ligand.

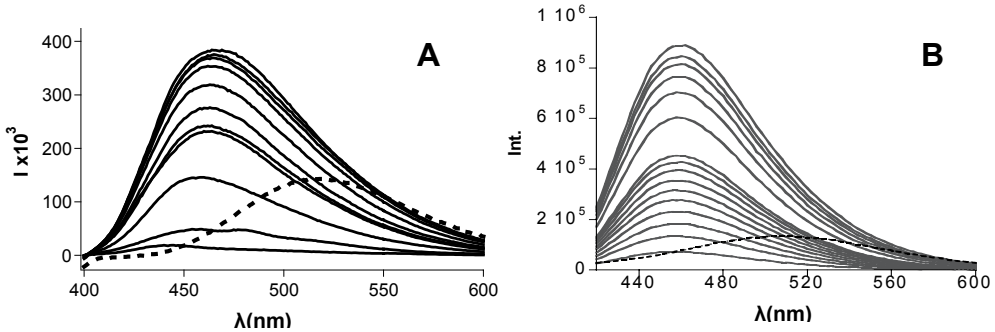

Figure 3.7 *Fluorescence emission spectra of DNR-ANS (A) and DNR-N152stop-ANS (B) complex at different ANS concentration (2-35 μM range). As a control the intrinsic fluorescence emission spectra of 35 μM ANS is also shown (dashed line).*

To determine the dissociation constant (K_D) for the ANS ligand, different concentrations of the DNR (2, 4 and 7μM monomer) and ΔDNR(1,2, and 4μM monomer) were titrated with increasing amounts of ANS (2-35 μM) (Figure 4A-C). The stoichiometry of the wt and mutant protein complexes with ANS was determined by titrating different ANS concentrations (1,2 and 4 μM) with increasing amounts of the two proteins (1-10 equivalents with respect to the starting ANS concentration) under the same experimental conditions (Figure 4B-D).
Data, analysed as described in Horowitz and Criscimagna (1985), showed that DNR wt and ΔDNR bind the ANS molecule with a K_D of 6.2 ± 0.6 μM and of 6.9 ± 0.5 μM respectively. The stoichiometry is also similar: 0.40 ± 0.05 mol of ANS per monomer of protein for DNR wt and 0.35 ± 0.05 mol of ANS for DNR-N152stop.

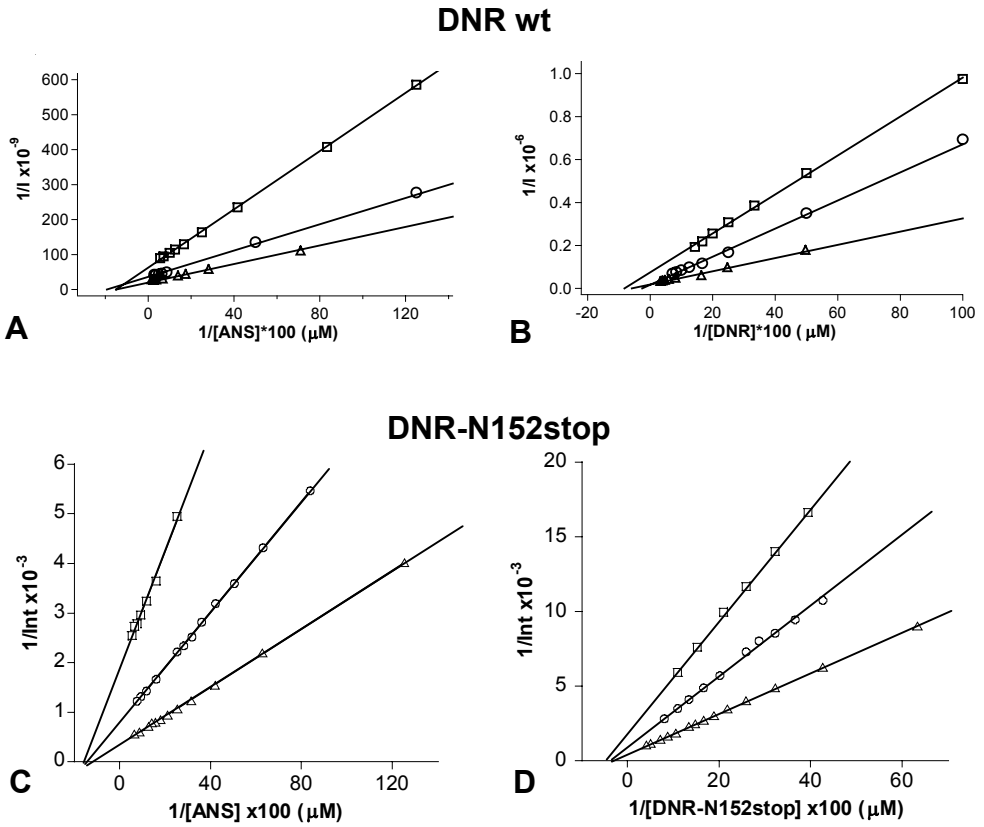

Figure 3.8. *Characterization of the binding of ANS to DNR wt and N152stop. (A,C) The dissociation constants for the ANS–Protein complexes were obtained from the abscissa intercept as described in the Materials and Methods section. Protein concentrations used: A) 2 μM (□), 4 μM (○) and 7 μM (△); C) 1 μM (□), 2 μM (○) and 4 μM (△). (B,D) The number of binding site(s) for the ANS to the wt and mutant protein were calculated from the abscissa intercept as described in the Materials and Methods section. ANS concentrations used: B,D) 1 μM (□), 2 μM (○) and 4 μM (△).*

Displacement of ANS - In order to determine whether heme is able to displace the bound ANS, a competition experiment was carried out by titrating both ANS-saturated proteins with increasing amounts of heme, and following the changes in fluorescence emission of ANS (Figure 3.9, A-D).

In the sample of DNR-ANS, we have observed, upon the addition of hemin, a stepwise reduction in the fluorescence enhancement together with a shift of the emission maximum from 460 nm to 530 nm, indicative of the absence of specific binding of ANS at the end of the experiment (Figure 3.9, A).

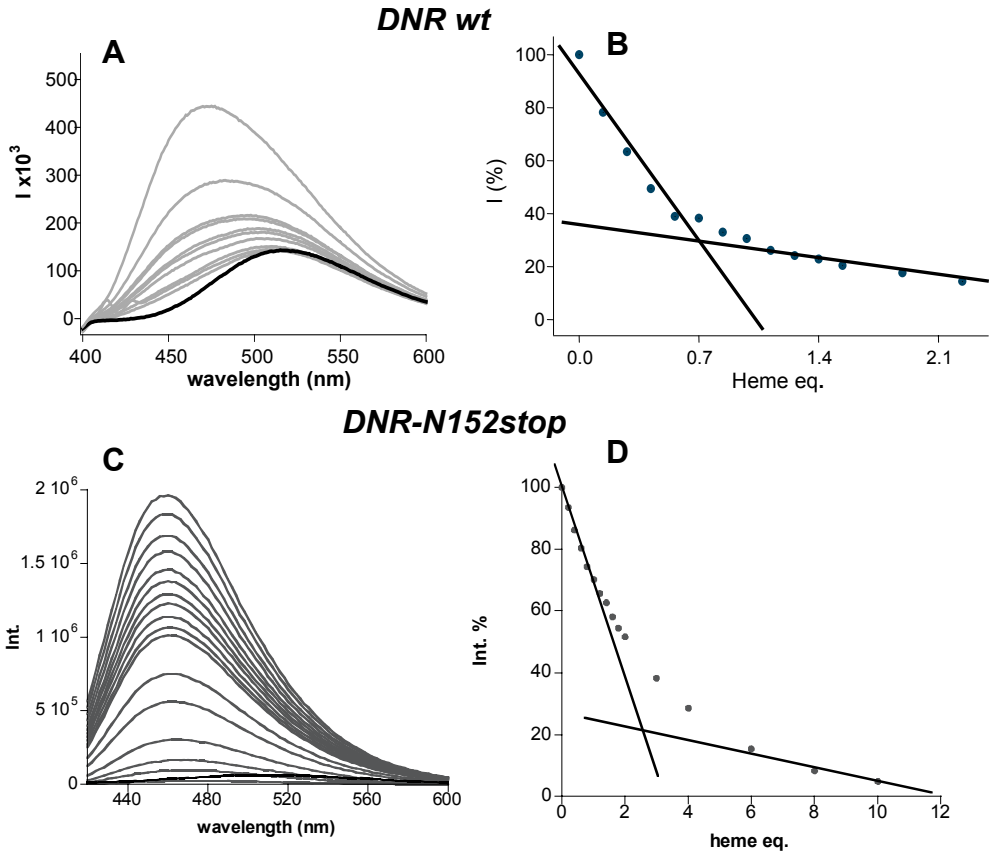

Figure 3.9 *Displacement of ANS from its complex with DNR by the addition of hemin. (A,C) Fluorescence spectra showing the reduction in fluorescence intensity of ANS bound to protein (grey line) upon the addition of aliquots of hemin solution. The black lines show the spectrum of ANS alone. The samples contained 35 μM ANS and 3.5 μM protein. (B,D) Fraction of fluorescence enhancement in the spectra shown in A,C (normalized for the signal in the absence of hemin) is plotted as a function of the equivalents of hemin added to the sample of ANS-protein complex.*

Full ligand displacement is obtained at 0.7 to 1 stoichiometric ratio (heme: DNR monomer, Figure 3.9, B). For the mutant protein ΔDNR only quenching of the ANS fluorescence intensity with no shift of the emission maximum is observed, indicating that the ligand is not displaced but is still bound within a distance of less than 20 Å from the bound heme(s) (Figure 3.9, C-D).

These results suggest that heme and ANS have different binding sites with different stochiometry, 1 heme per monomer and 1 ANS per dimer. Furthermore while in the wt protein ANS is released upon heme binding, this is not true for ΔDNR indicating that the HTH domain, lacking in the truncated protein, might undergo a conformational change upon heme binding that results in ANS displacement.

CD spectra and thermal melting experiments -Circular dichroism spectra were collected to determine the secondary structure content of the proteins in solution; the experiment was carried out either with the purified proteins or with the heme reconstituted proteins (Figure 3.10).

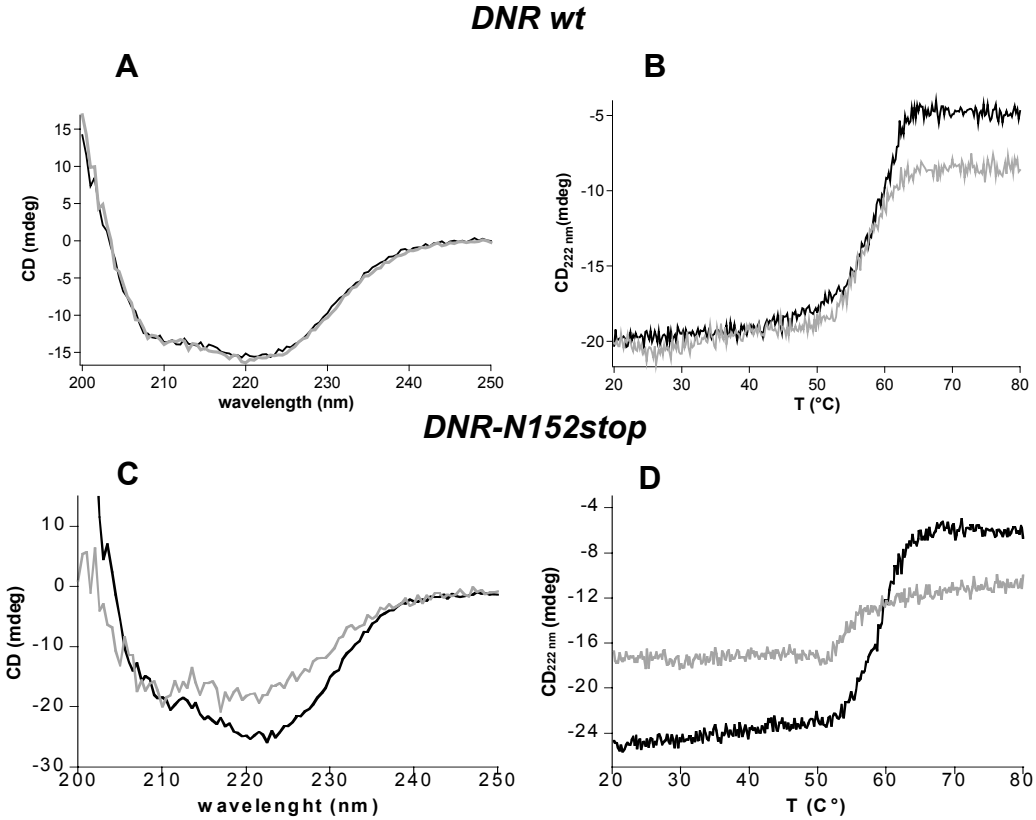

Figure 3.10 *A) Circular dichroism (CD) analysis of 8 μM purified DNR (black line) and heme reconstituted (grey line) protein. CD spectra carried out at 20°C; the wavelength used reports on the α-helix and β secondary structure contents. (C) CD analysis of 18 μM purified ΔDNR (black line) and heme reconstituted (grey line) protein. (B,D) The. Equilibrium thermal denaturation experiments as a function of temperature in the range 20-80°C in 20 mM Tris-HCl pH 7.2, 300 mM NaCl; the graph shows the CD data at 222 nm recorded at 1 degree intervals. The T_m was calculated as described in Materials and Methods. The different end point indicates a different residual in the secondary structure content at 80°C.*

DNR wt - No significant variations in the CD spectra of the *apo* and reconstituted protein was observed for DNR wt (Figure 3.10, A). To determine the stability of both *apo* and reconstituted proteins , equilibrium thermal denaturation, followed at 222 nm, was performed; for wt protein the calculated temperature of melting was 55 °C

in both cases (Figure 3.10, B)

ΔDNR- for ΔDNR the reconstituted protein displays a lower stability with respect to the apo-ΔDNR (Figure 3.10, C) as qualitatively reflected by a decreased cooperativity in the thermal melting profiles (Figure 3.10, D); such a behaviour reflects a decreased ΔH upon denaturation. A quantitative analysis is however complicated by precipitation events. The calculated temperature of melting was 55 °C for the *apo* protein and 50°C for the reconstituted mutant.

3.5 DNR-N152stop: Crystallization and cryoprotection

DNR-N152stop native crystal - As for DNR and DNR-HIS, ΔDNR was concentrated up to 3.3 mg/ml in 20 mM Tris/HCl pH 7.2, 150 mM NaCl after the PCT (Per Crystallization Test, Hampton Research) and initial crystallization trials were performed with the hanging drop technique, using reagents supplied by Hampton Research (Crystal Screen 1-2).
Crystals appeared in 4 different conditions at 21°C with drops made mixing equal volumes (1µl) of protein solution and reservoir solution and allowed to equilibrate against 0.5 ml of the same reservoir.
The best crystals were observed in 0.1 M HEPES pH 7.5, 8% v/v ethylen glycol, 10% w/v PEG 8000 solution (n.37 Crystal Screen 2, Hampton). The pH was optimised to 7.2 but unfortunately crystals grown in this conditions were very small (Figure 3.11, A) and didn't diffract further than 7 Å resolution.
To obtain crystals suitable for X-ray analysis all the initial conditions in which we found crystals in the first screen were optimised by screening different combination of the following variables: protein concentration, PEG 1000/10000 at various concentrations, temperature, nature and pH of the buffers, volumes of the droplet components and of the reservoir. Many known techniques to improve crystal size and quality as *microdialisys, macro/micro seeding and crystallization under oil* were also applied to the samples (these methods are described in Appendix A).
The best crystals were grown by using seeding technique at 21°C in the following conditions: 17% w/v PEG 4000, 0.1 M sodium citrate pH 7.4, 0.2 M ammonium phosphate. The droplets were made by mixing 1.5 µl of protein solution (2.3 mg/ml in 20 mM Tris/HCl pH 7.2, 150 mM NaCl) and 1.5 µl of a solution of reservoir containing crystalline seeds (10^{-4} dilution) of DNR-N152stop. Crystals reached the final dimensions of 50x40x40 µm in 3-4 days and diffracted up to 2.3 Å resolution (Figure 3.11, B).

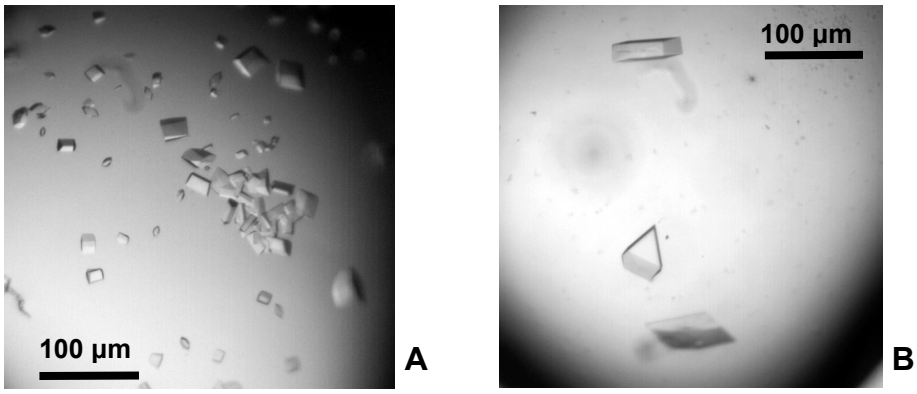

Figure 3.11 *A) crystals of ΔDNR obtained in the initial screen, solution n.37 Crystal Screen 2 (Hampton). B) optimised crystal after micro seeding, grown at 21°C in: 17% w/v PEG 4000, 0.1 M sodium citrate pH 7.4, 0.2 M ammonium phosphate.*

In order to preserve crystals from radiation damage during X-ray exposure the sample is kept at 100° K by a dry air stream cooled with liquid nitrogen (*cryo-crystallography*). For this reason, before exposure, single crystals were flash-freezed in liquid nitrogen. To prevent disruption of the crystal due to ice forming in the *mother liquor* (solution in witch the crystal has grown) crystals are usually cryoprotected using compound like glycerol, MPD, ethylene glycol.
After testing different cryoprotectants ΔDNR crystals were transferred is a droplet containing 10% glycerol, 20% w/v PEG 4000, 0.1 M sodium citrate pH 7.4, 0.2 M ammonium phosphate.

DNR-N152stop Selenomethionine derivative - The derivatized protein was expressed and purified as described in the experimental section. 100 % Selenium incorporation (4 methionines per monomer) was assessed by LC-ESI mass spectrometry. Since it was not easy to obtain crystals using the conditions mentioned before, many attempts were necessary to grow useful Selenomethionine crystals. Finally, crystals were obtained in 16% w/v PEG 4000, 0.1M Tris/HCl pH 8.0, 75mM ammonium sulfate, 3% v/v ethylen glycol as described in the experimental section, and diffracted up to 3.1 Å resolution.

3.6 Data collection and processing

ΔDNR crystals often diffracted poorly, and only after many attempts, both with our in-house source and with synchrotron radiation, using crystals grown in different conditions and various cryoprotectants, we were able to collect a complete data-set for native crystal at 2.3 Å resolution, one MAD data-set for an Iridium derivative at 4.0 Å resolution and a MAD data-set for a Se-methionine derivative crystal at 3.1 Å resolution (see experimental section and appendix B).

DNR-N152stop native crystal 2.3 Å resolution - The best data set was collected at the ID14-3 beamline of ESRF Synchrotron (Grenoble, France). The radiation wavelength was set to 0.931 Å, and the crystal to detector distance was set at 145 mm. Diffraction images were collected with an oscillation range corresponding to a $\Delta\varphi$ = 0.5°. A typical diffraction image of ΔDNR crystal is shown in Figure 3.12.

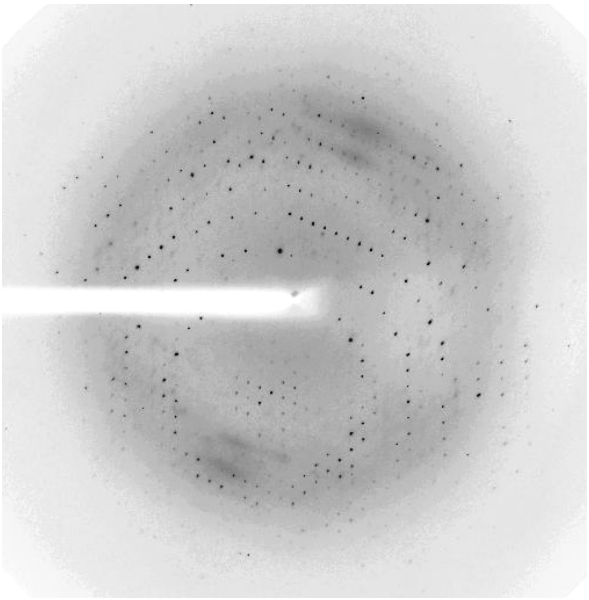

Figure 3.12 *Diffraction image, visualized with the program XDISP (Otwinowski, 1993), of ΔDNR crystal collected at ESRF Synchrotron ID-14-3 (Grenoble, France).*

A total of 445,739 spots were collected corresponding to 18,512 independent reflections. The overall completeness of data is 99.0% between 30.0 and 2.3 Å resolution (last resolution shell 99.0%). The average I/σ is 18.4. Data were indexed with DENZO, scaled and reduced with SCALEPACK (Otwinowski, 1993). The analysis of diffraction data shows that ΔDNR native crystal belongs to the monoclinic space group C2 with the following unit cell dimensions (Å, deg.): a=55.76, b=105.77, c=74.86, β=98.21. The statistical analysis of the intensities of

symmetry related reflections are summarized in the values of the R_{merge} = 0.041 and the value of χ^2 = 0.939.
Another important value that must be estimated during data processing is the mosaicity. Most crystals cannot be considered as ideal single crystals, because the regular repetition of the unit cells is interrupted by lattice defects. The diffraction pattern of such crystals can be regarded as the sum of the diffraction patterns originating from mosaic blocks with slightly different orientations. The mosaicity for ΔDNR native crystal is 0.85, indicating that the crystal has an intrinsic high disorder.

Data collection statistics are summarized in Table 3.1.

Table 3.1

DNR-N152stop native data collection and statistics parameters.

Beamline	ID14-3 ESRF
Wavelength (Å)	0.931
Resolution (Å)	30.0-2.3
Reflections	
Total (N)	445,739
Unique (N)	18,512
Completeness (last shell)	99.0 (99.0)
Average I/σ	18.4
Mosaicity	0.85
R_{merge} (last shell)	0.041 (0.131)
χ^2 (last shell)	0.939 (0.712)

A first estimate of the number of molecules per asymmetric unit can be performed using a method proposed by Matthews (Matthews, 1968). Based on an average molecular weight of 17500 (monomer) for the protein in the crystal we first assumed the presence of two molecules (one physiological dimer) in the asymmetric unit obtaining a V_m value of 3.1 $Å^3$/Da (Matthews, 1968) and a solvent content of 60.3%. percentage that is in the range generally encountered for protein crystals. This assumption was later demonstrated to be incorrect by the structure determination. In fact we found that the asymmetric unit contained a third monomer with the dimerization axis lying along the 2 fold symmetry crystallographic b axis, thus forming the physiological dimer with a symmetry related molecule; the V_m value changed to 2.1 $Å^3$/Da. and the solvent content to 40.5 %. This finding complicates the final structure determination by confusing the crystallographic and non-crystallographic symmetries (NCS) during calculation.
Main parameters for ΔDNR native crystal are summarized in Table 3.2.

Table 3.2
Main parameters of DNR-N152stop native crystal.

Bravais lattice	monoclinic
Space group	C2
Unit cell parameters (Å, deg.)	a = 54.76
	b = 105.77
	c = 74.86
	β = 98.21
Unit cell volume ($Å^3$)	437463
Asymmetric unit per cell	4
Wilson average B factor	45.6
N. of molecules per AU	3
Solvent content (%)	40.5

Data collection and processing for the Selenomethionine derivative at 3.1 Å resolution is described in the next paragraph.

3.7 Phasing and refinement

Molecular replacement trials - Despite intensive effort, phases could not be obtained by molecular replacement procedure (see Appendix B for method description) based on the available structures of CRP (pdb code 1hw5 - 1gn6; Chu *et al.,* 2001; Passner *et al.,* 2000) and CooA (pdb code 1ft9; Lanzillotta *et al.,* 2000). Polyalanine models, homology models and models representing the whole monomer or individual domains were used as templates, but no solution was found. It must be said that the sequence identity of the templates was never higher than 24%, that is the lower limit in general cases (Taylor, 2003).

Heavy atom derivatives - We tried to obtain heavy atom (HA) isomorphus derivative to solve the phase problem. more than 40 crystals obtained with different HA species, both with soaking and co-crystallization techniques, were tested at the synchrotrons and in our in-house source, but only one iridium derivative was obtained at 4.0 Å resolution. The HA sites were found using SOLVE (Terwilliger and Berendzen, 1999) and initial phases were obtained, but the corresponding electron density maps were uninterpretable even after density improvement with both RESOLVE (Terwilliger and Berendzen, 1999) and DM (Cowtan & Zhang, 1999) procedures.

Selenomethionine derivative 3.1 Å resolution - Meanwhile we expressed, purified and crystallized with great effort the selenomethionine derivatized DNR-N152stop. Finally we were able to collect a complete MAD data set at the ESRF synchrotron (Grenoble, France) on ID14-4 beamline. The radiation wavelength was set to 0.9795, 0.9797 and 0.9724 Å respectively for the peak, inflection and remote data collections; the crystal to detector distance was set at 285 mm; 300 diffraction images were collected with an oscillation range corresponding to a $\Delta\varphi$ = 1° for each wavelength. Unfortunately the MAD experiment was unsuccessful because crystal had suffered of serious radiation damage, we obtained however good data at the peak wavelength that was used for phasing using a SAD procedure (Figure 3.13) (see Appendix B for MAD and SAD techniques).

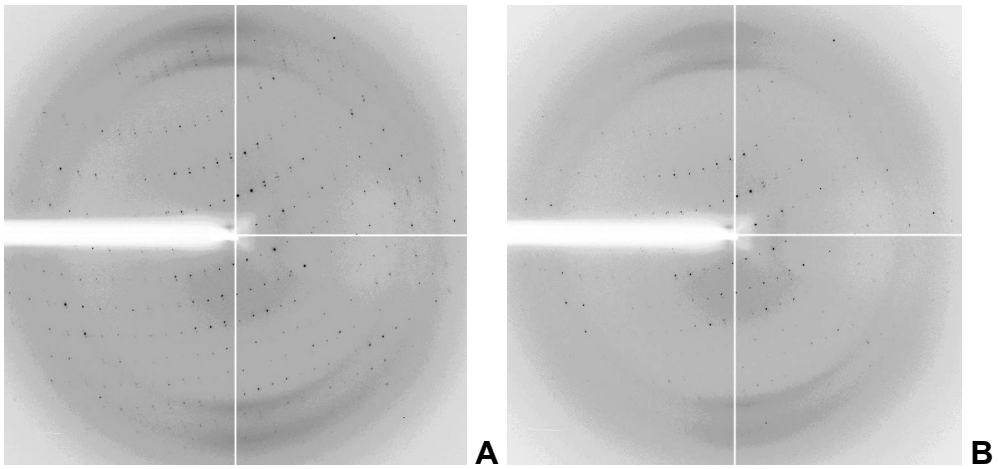

Figure 3.13 *Diffraction images, visualized with the program XDISP (Otwinowski, 1993), of DNR-N152stop-Se-methionine crystal collected at ESRF Synchrotron ID-14-4 (Grenoble). A) first frame of the data-set collected at the peak wavelength. B) first frame of the data-set collected at the inflection wavelength. The crystal is in the same orientation as in A, but 300 frames have already been collected. The loss in the intensity of the reflections is evident.*

Data were indexed with DENZO and scaled with SCALEPACK (Otwinowski, 1993). ΔDNR Se-methionine derivative crystallized in the monoclinic space group $P2_1$ with the following unit cell dimensions (Å, deg.): a=57.05, b=167.73, c=59.10, β=116.93. Data collection statistics and crystal parameters are summarized in Tables 3.3 and 3.4.

Table 3.3
DNR-N152stop Se-methionine derivative data collection and statistics parameters.

Beamline	ID14-4 ESRF
Wavelenght (Å)	0.9795
Resolution (Å)	84.0-3.1
Reflections	
Total (N)	172,679
Unique (N)	18,154
Completeness (last shell)	99.4 (98.9)
Average I/σ	12.4
Mosaicity	0.51
R_{merge} (last shell)	0.086 (0.369)
χ^2 (last shell)	0.992 (0.863)

Table 3.4
Main parameters of DNR-N152stop Se-met. derivative crystal

Bravais lattice	monoclinic
Space group	$P2_1$
Unit cell parameters (Å, deg.)	a = 57.05
	b = 167.73
	c = 59.10
	β = 116.93
Unit cell volume ($Å^3$)	504271
Asymmetric unit per cell	4
Matthews coef. ($Å^3$/Da)	2.4
N. of molecules (monomers) per AU	6
Solvent content (%)	48.4

The HA sites were detected using the program SOLVE (with the kind help of Dr. Kenneth Allan Johnson; Dep. of Medical Biochemistry and Biophysics “Karolinska Institutet” - Stockholm, Sweden), 15 selenium atom site coordinates were refined to an overall figure of merit (FOM) of 0.23 in the 30.0 to 3.1 Å shell, producing a first set of phases. A density modification procedure based on solvent flattening and histogram matching was then applied using the program RESOLVE (Terwilliger and Berendzen, 1999), yielding a FOM of 0.43 at 3.1 Å resolution. Heavy metal coordinates and relative statistic parameters are summarize in Table 3.5.

Table 3.5

SAD analysis for DNR-N152stop Se-met. derivative crystal

Site	x	y	z	occupancy	B_{factor}	Height/sigma
1	0.701	0.998	0.274	0.428	60.0	10.8
2	0.557	0.990	0.326	0.317	41.9	11.5
3	0.317	0.527	0.350	0.265	60.0	6.4
4	0.908	0.496	0.130	0.221	60.0	6.6
5	0.180	0.316	0.362	0.373	60.0	9.4
6	0.380	0.541	0.318	0.352	60.0	9.1
7	0.002	0.720	0.044	0.260	60.0	7.6
8	0.092	0.268	0.364	0.299	60.0	7.4
9	0.978	0.774	0.122	0.258	60.0	6.5
10	0.294	0.593	0.342	0.228	60.0	6.4
11	0.705	0.973	0.262	0.278	60.0	5.2
12	0.408	0.852	0.064	0.196	60.0	3.8
13	0.008	0.505	0.135	0.190	60.0	3.8

overall FOM before DM	0.23
overall FOM after DM	0.43

Of the 4 methionine residues present in each monomer one is the N-terminal residue and is not visible because of the high mobility, the other three are very close one to another and specifically are the residues 88, 89 and 91 respectively (see end of paragraph 3.3). These three selenomethionine residues cluster all in a very mobile loop (loop 7, see below), and this could explain the low occupancy values of the detected Se atoms sites, as well as the low FOM. On the other hand this cluster turned out extremely useful for maps interpretation. In fact, visual inspection of the detected Se atoms revealed that they were positioned in groups of three, as we expected from the sequence (Figure 3.14, A). Therefore by looking at the position and orientation of the heavy atom substructure made by clusters of three atoms we could detect the position of each monomer. We detected 13 sites out of the 18 expected (6 monomers in the AU, three visible Se atoms per monomer).

Visual inspection of the electron density maps obtained with the refined phases (Figure 3.14, B) revealed good connectivity and it was possible to fit with the program COOT (Emsley & Cowtan, 2004) 6 monomers of a starting homology model of ΔDNR obtained with bioinformatic methods from CRP structure (pdb code - 1gn6; Passner *et al.,* 2000).

Although we could dock the position of each monomer in the map, to facilitate and speed up the building work we performed a density modification and phase extension to 2.8 Å resolution using PIRATE (Cowtan, 2000). PIRATE performs

statistical phase improvement by classifying the electron density map by sparseness/denseness and order/disorder and often gives better results than conventional methods based on solvent flattening.

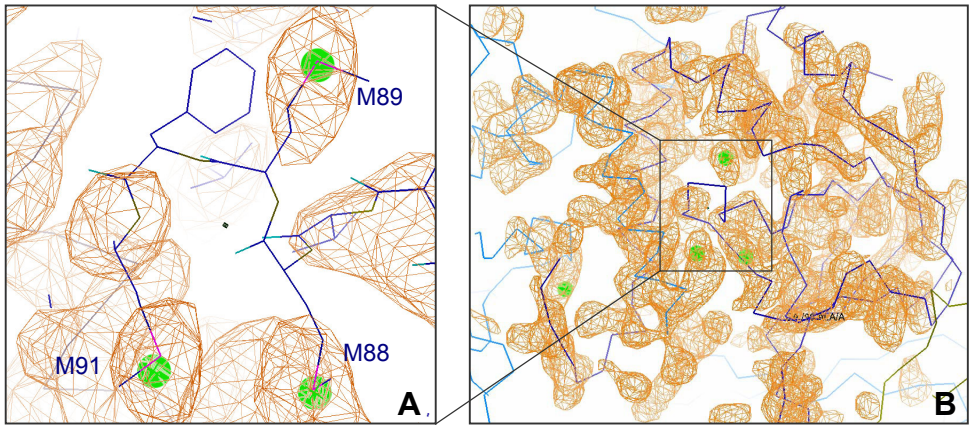

Figure 3.14 *First maps at 3.1 Å resolution (contoured at 1.0 σ) obtained from the set of initial phases coming from RESOLVE. Se atoms are shown as green spheres. The protein model is the final one. A) Se atoms cluster resulting from the close methionine residues 88,89 and 91. B) larger view of the same map revealing good connectivity. By looking at these characteristic clusters it was possible to deduce the position of each monomer.*

At this stage the N and C-terminal were not visible, but it was possible to build the backbone atoms of the residue range 32 - 135 and all the visible side chains. The Se atoms cluster and a group of three aromatic residues (F53,Y54,Y55) were used to dock the sequence in the map and start the building-refinement cycles routine using COOT (Emsley & Cowtan, 2004) and REFMAC5 (Murshudov *et al*., 1997).

We then moved to the higher resolution native data set and used the partial model of the monomer as template for molecular replacement. A complete solution (3 monomers in the AU) was found by merging the results obtained using both MOLREP (Vagin *et al*., 1997) and PHASER (McCoy *et al.,* 2005).
The resulting maps allowed to build a model for the three monomers in the AU chains A, B and C. Chain A forms the physiological dimer with chain B, while monomer C, that has the dimerization axis coincident with the two fold rotation axis of the cell, forms the dimer with a symmetry related molecule (Figure 3.15).

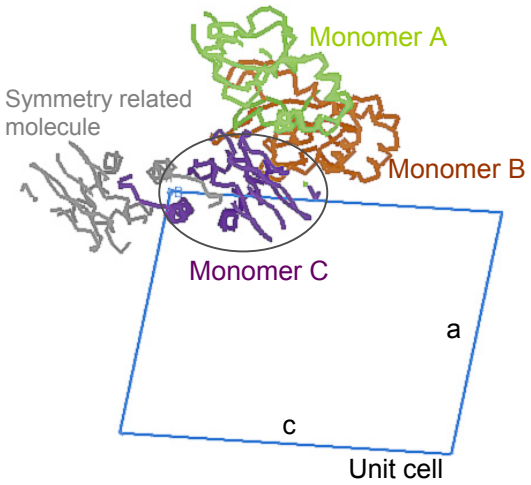

Figure 3.15 *the three monomers in the AU of ΔDNR native crystal. Subunit A and B (in brown and green respectively) are forming the physiological dimer. Monomer C (purple) is forming the dimer with the symmetry related molecule (grey) resulting from a 180° rotation around the two fold rotation axis of space group C2 (B axis) which is perpendicular to the picture.*

Electron density of monomer C results very poor and building the model was very difficult (only 117 residues out of 154 are visible), this is not true for monomers A and B which fit very well the electron density map. Therefore all the discussion in this work is based on the structure of chain A and B, which, as discussed, form the physiological dimer. Concerning these two subunits, It was possible to build the backbone atoms of all the residues (res. -2 to 150) and 91% of the side chains of monomer A, while the backbone of monomer B is 91% complete (res. 8 to 148) and 85% of the side chains are visible.

Refinement was carried out with REFMAC5 (Murshudov *et al.*, 1997), and water residues were added into the *Fo-Fc* density map, contoured at 3.5 σ, with the *find-waters* tool of COOT (Emsley & Cowtan, 2004). Several cycles of refinement, visual inspection, manual rebuilding, and addition of solvent molecules were performed.

Superimposition of the two monomers forming the dimer, A and B, results in a rms deviation of 1.16 Å. Indicating that the

Table 3.6 summarizes all the statistics relative to refinement for the ΔDNR structure and Figure 3.16 shows a portion of the final model and the final map contoured at 1.5σ.

Table 3.6 *Refinement statistic and geometrical parameters*	
Resolution (Å)	30 – 2.3
Average B factor	49.8
$R_{cryst.}$ (%)	27.6
R_{free} (%)	31.3
R.m.s.d. bonds lenghts (Å)	0.012
R.m.s.d. bond angles (deg.)	1.8
Ramachandran plot (%)	
N of residues	462
Allowed	80.7
Additional	15.5
Generous	1.9
Disallowed	1.9

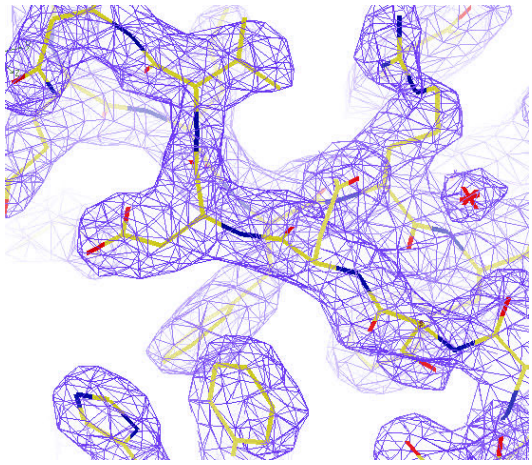

Figure 3.16*. Portion of final map contoured at 1.5σ and of the final model.*

3.8 The crystal structure of DNR-N152stop from *P. aeruginosa*

The structure of ΔDNR from *P. aeruginosa* was determined at 2.3 Å and is illustrated in Figure 3.17, while the secondary structure topology is shown in Figure 3.18. ΔDNRis the first NO-sensing domain belonging to a bacterial transcription factor whose structure has been solved.

DNR belongs to the CRP-FNR superfamily of transcription factors (Arai *et al.,* 1995). The physiological unit of these regulators is constituted by an homodimer. Each monomer constituted by three distinct domains; (i) an N-terminal sensing domain (also referred as large or effector domain) with the typical β-barrel fold of the cAMP binding domains of CRP, (ii) a long dimerization α-helix usually α-C (in ΔDNR corresponding to α-D, see below) recruited to form the dimer interface and (iii) a C-terminal DNA binding domain which contains an helix-turn-helix (HTH) motif (also referred as small domain) (Passner et al., 2000 and references therein). The only known structures of CRP-FNR superfamily of regulators are: CRP from *E. coli,* the CO sensing regulator CooA from *R. rubrum* (Lanzillotta *et al.,* 2000), PrfA that induces virulence in *L. monocytogenes* (Eiting *et al.,* 2005) and CprK which activates halorespiration in *D. dehalogenans* (Joyce *et al.,* 2006).

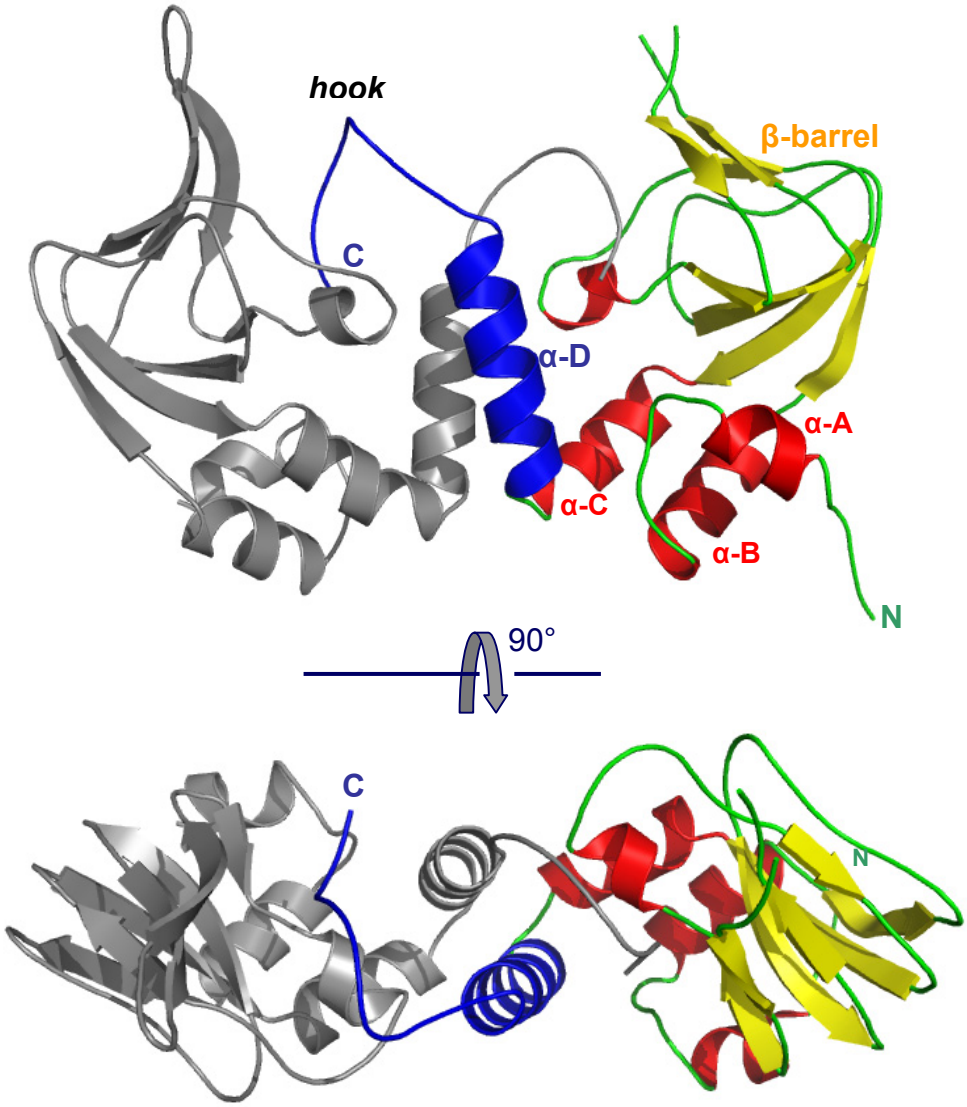

Figure 3.17 *structure of ΔDNR dimer. Side and top view. Subunit A in coloured by secondary structure, subunit B is grey. The dimerization helix of subunit A is coloured in blue.*

The structure organization of the small domain in ΔDNR resembles the β-barrel fold of CRP and of the other structural homologues (apart for an additional α-helix, see below), but in ΔDNR the angle formed by the sensing domain and the dimerization helix appears to be bigger.
This results in the formation of an hydrophobic cleft between the large domain and the D-helix (Figure 3.18). Surprisingly the last fifteen C-terminal residues of each monomer unfold, from the expected helix conformation, forming an domain swapping interaction (that resembles a *hook*) by filling the N-terminal hydrophobic cavity of the other subunit (Figure 3.17, 3.18).

The ΔDNR fold consists of seven β-sheets (β-1 to β-7) and four α helix (α-A to α-D, for simplicity we will consider the one-helix-turn, from residues 86 to 89, as part of loop 7, see table X). The seven β-sheets, forming a β-barrel, and the first three α-helix constitute the sensing domain while the α-D is the dimerization helix. The overall topology is illustrated in Figure 3.18, and the relative residue range of the secondary structure organization is summarized in Table 3.7.
In the proteins belonging to the CRP-FNR superfamily the β-hairpin corresponding to β-sheet 3, loop 5 and β-sheet 4 is usually called the *flap*. As we will see in the next section, among these regulators, the flap plays an important role in transmitting the conformational change to the HTH domain when the effector molecules binds to the sensing domain. In ΔDNR, lacking the small domain, the flap is completely exposed to the solvent and residues in the range 68-71 of subunit A were not visible in the electron density map, as well as many side chains of both subunits in this zone.

It is worthwhile to notice that the secondary structure predicted by PSIPRED (Protein Structure Prediction Server*)* on the basis of the sequence was found to be 100% correct apart for the *hook* residues (Jones *et al.,* 1999).

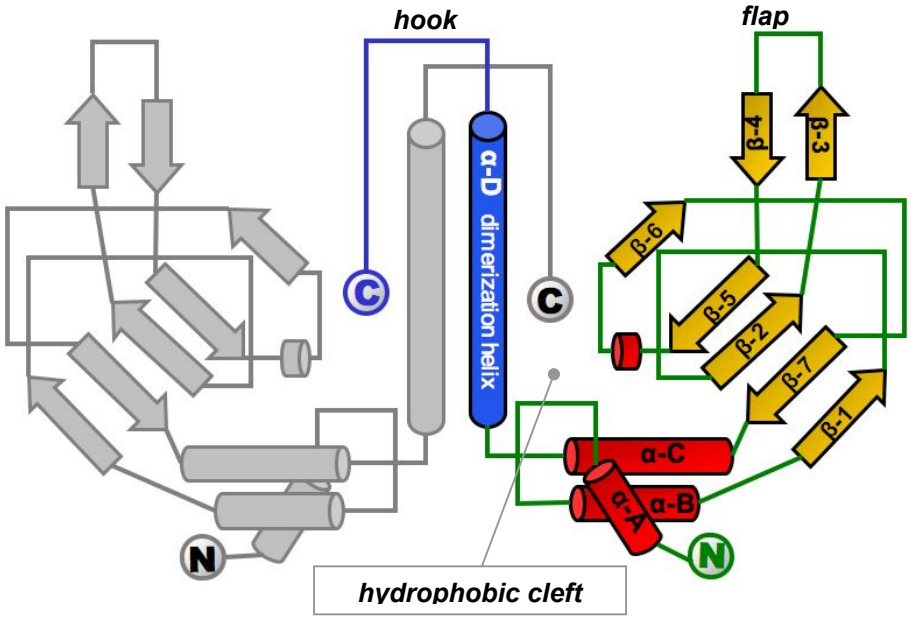

Figure 3.18 *Secondary structure topology of DNR-N152stop. monomer A is coloured, Monomer B is shown in grey. for the sensor domain α-helix are shown in red and β-sheets in yellow, while the dimerization helix is coloured in blue. The C-terminal of one monomer fills the hydrophobic cleft in the other monomer*

Table 3.7

Secondary structure organization of DNR-N152stop

Res. range	secondary struc.		Res. range	secondary struc.		
G(-1) – E2	N-term. (first 3 res. from His-tag)		C60 – T68	**β-3**	9 – sheet	***flap***
F3 – S13	α-A	3 turns– helix	P69 – Q71	**loop 5**		
H14 – P19	loop 1		E72 – T78	**β-4**	7 – sheet	
L20 – S31	α-B	4 turns– helix	79 – 80	loop 6		
S32 – D33	loop 2		R81 – F84	β-5		
L34 – L37	β-1	4 – sheet	A85 – V97	loop 7 (1 helix turn A87 – F90)		
D38 – H51	loop 3		A98 – V103	β-6	6 – sheet	
A52 – I57	β-2	6 – sheet	V104 – P105	loop 8		
S58 - G59	loop 4		S106 – S112	β-7	7 – sheet	
			N113 – D122	α-C	3 turns– helix	
			N123 – L138	α-D	4 turns– helix	
			H139 – K151	***hook***	C-term.	

Dimer interface and the C-terminal loop: the hook – the unfolding of the last fifteen C-terminal residues of each monomer results in the loss of four helix-turns in the α-D helix. This reduces the physiological dimer interface of almost 50%. The residual helices interface is occupied by two leucine residues per monomer (Leu-131 and 134), that are involved in dimerization (Figure 3.19).

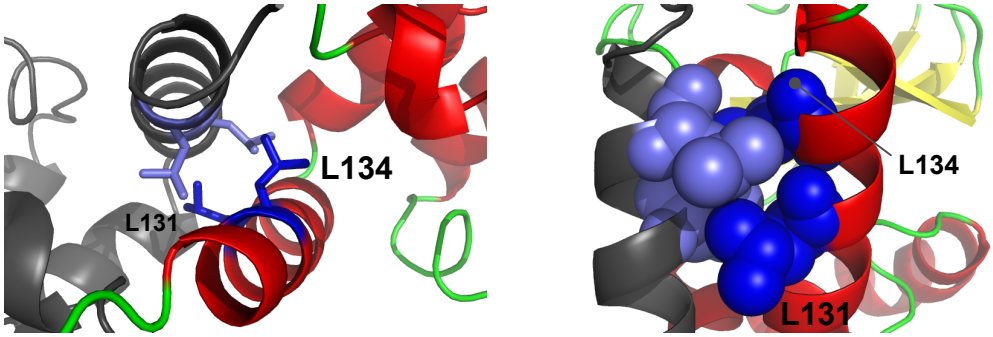

Figure 3.19*. top view (A) and a sphere representation side view (B) of the interaction of Leu-134 and 131 from the two monomers at the dimer interface of DNR-N152stop.*

The final fifteen residues of each monomer dock in the N-terminal hydrophobic cleft of the other monomer resulting in a domain swapping interaction, the *hook* (Figure 3.18), which also contributes to dimerization.
The main interactions of the hook, due to Leu-148, Leu-150 and S-149, are summarized in Table 3.8 and illustrated in Figure 3.20.
Residues in the range 145 - 150 are clearly visible in the electron density map, while the loop ranging from Arg-137 (end of α-D) to Glu-144 only density for the backbone atoms is visible. No electron density is visible for the side chain of the C-terminus Lys-151, which is exposed to the solvent.
The *hook* docks perfectly in a large hydrophobic cleft which is described below (Figure 3.20, C), and contacts all the secondary structure elements that are thought to be involved in the allosteric activation mechanism of the proteins belonging to the CRP-FNR superfamily of transcription factors (see discussion section), which are the dimerization helix, the zone referred as *flap* (β-3 / loop 5 / β-4) and loop-7 (Kim *et al.,* 1992; Passner *et al.,* 2000; Harman *et al.,* 2001; Yu *et al.,* 2004; Eiting *et al.,* 2005; Joyce *et. al.,* 2006).

Table 3.8

Main domain swapping interactions of the C-terminal hook residues (Figure 3.20, B)

hook res	Interacting res. other subunit	Zone	hook res	Interacting res. other subunit	Zone
Leu-148	Phe-44	β-2	**Ser-149**	Glu-76	β-5
	Ile-63	β-4			
	Leu-75	β-5	**Leu-150**	His-15	loop 1
	Met-89	loop 7		Ala-87	loop 7
	Met-91	loop 7		Phe-90	loop 7
	Val-97	loop 7		Leu-130	α-D

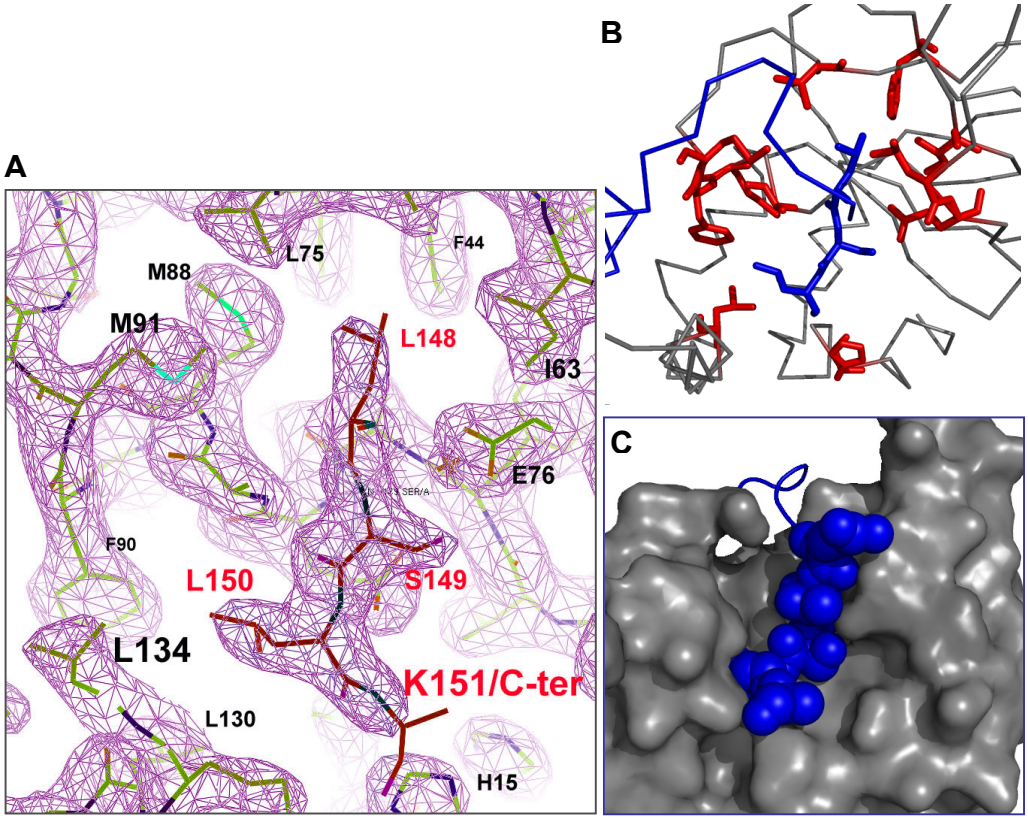

Figure 3.20 *The C-terminal hook residues.*
A) electron density map of the hook zone. Residues from the two monomers are shown in dark red and yellow. Electron density is contoured at σ = 1.0. B) interactions between the hook residues (blue) and the residues belonging to the other monomer (red). C) surface representation of one monomer (grey) and sphere representation of the C-terminal hook (blue) of the other monomer.

DNR-N152stop compared with known structures: a different orientation of the dimerization helix – The superimposition of the Cα trace of the sensing domains of the structure homologues of DNR (CRP code 1g6n – Passner *et al.,* 2000; CooA code 1ft9 – Lanzillotta *et al.,* 2000; CprK code 2h6b – Joyce *et al.,* 2006; PfrA-G145S code 2bgc – Eiting *et al.,* 2005; and a transcription factor with pdb code 2gau, that has not yet been characterized), reveals that the overall reciprocal position of the dimerization helix with respect to the sensing domain is very similar among these structures. On the contrary, in ΔDNR (Figure 3.21 - red structure) the position of the dimerization helix deviates from this common orientation. In fact in ΔDNR the α-D helix is shifted away from the N-terminal domain of 3 Å, and forms an angle of 11° with the direction of the dimerization helices of the other proteins (Figure 3.21, A; ΔDNR in red with respect to the other structures, in blue).
This different relative orientation between the D-helix and the large domain observed in ΔDNR structure results in the presence of a large hydrophobic cleft. This cleft, as we have seen, is filled by the C-terminal residues of the other subunit. Interestingly 11 of the 17 strictly conserved residues, among the DNR subgroup of regulators, cluster around this cleft (Figure 4.4 and 4.5, in the discussion section).
Among this conserved residues there is His-15 which has the imidazole ring pointing towards the centre of the cavity. It is important to notice that His-15 together with Leu-16 and Phe-17 lay in loop 1 (between α-A and α-B). This high percentage of conserved residues suggests that loop 1, among the DNR subgroup of regulators, could be important for the physiological role of NO sensing or for cofactor binding.

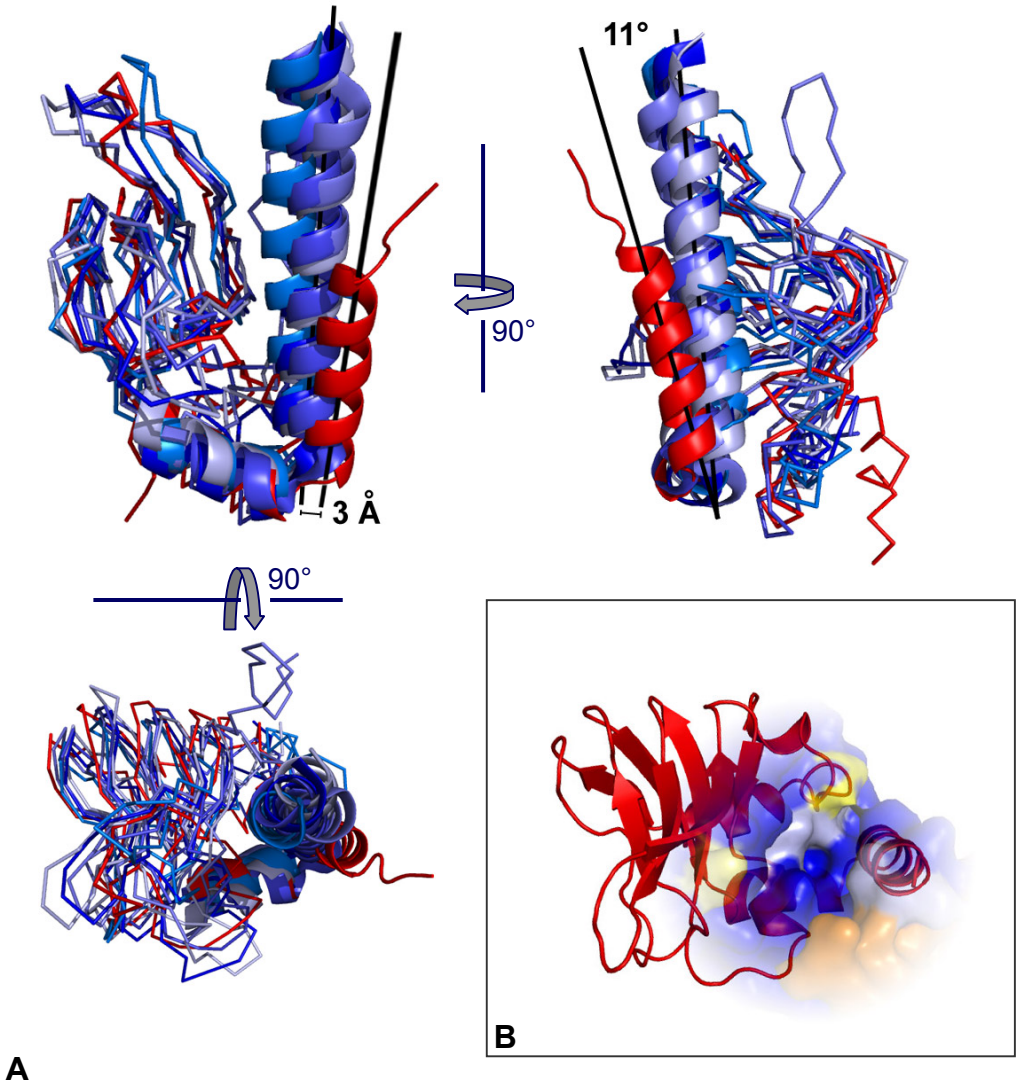

Figure 3.21 *Structural comparison of ΔDNR with the known structures of the CRP-FNR superfamily regulators (CRP code 1g6n; CooA code 1ft9; CprK code 2h6b; PfrA-G145S code 2bgc and a transcription factor with pdb code 2gau)*
A) Cα-s superimposition of the sensing domains. Structures from the CRP-FNR superfamily are blue-coloured. ΔDNR is shown in red, the hook residues have been removed for clarity. Except for ΔDNR all the other share the same relative orientation between the dimerization helix and the sensing domain. B) Cartoon and surface representation of subunit B of DNR-N152stop, top view, showing how the different relative orientation between the D-helix and the large domain results in the presence of a large hydrophobic cleft.

3.9 Modelling

heme ligand - Looking at the structure of ΔDNR and comparing the binding sites of the effector molecules in other transcription factors belonging to the same superfamily, we identified the hydrophobic cleft, described above, as the possible heme binding site. Furthermore all the conserved residues among the DNR family, except two glycine residues, are localized around the cleft (Figure 4.4 and 4.5 in the results section), strongly suggesting a possible role of this cleft in NO sensing.
Thus we decided to manually dock a heme-*b* in the structure of DNR-N152stop, considering His-15 as the proximal ligand. The docking procedure used is described in the experimental section and the result is illustrated in Figure 3.22. Side chains of the residues Leu-16, Glu-86 and Lys-133 had to be moved from the original position to accommodate the heme, as well as Glu-76 that was making unfavourable electrostatic contacts with one of the propionate groups. For these residues side chains we chose alternative conformational rotamers.

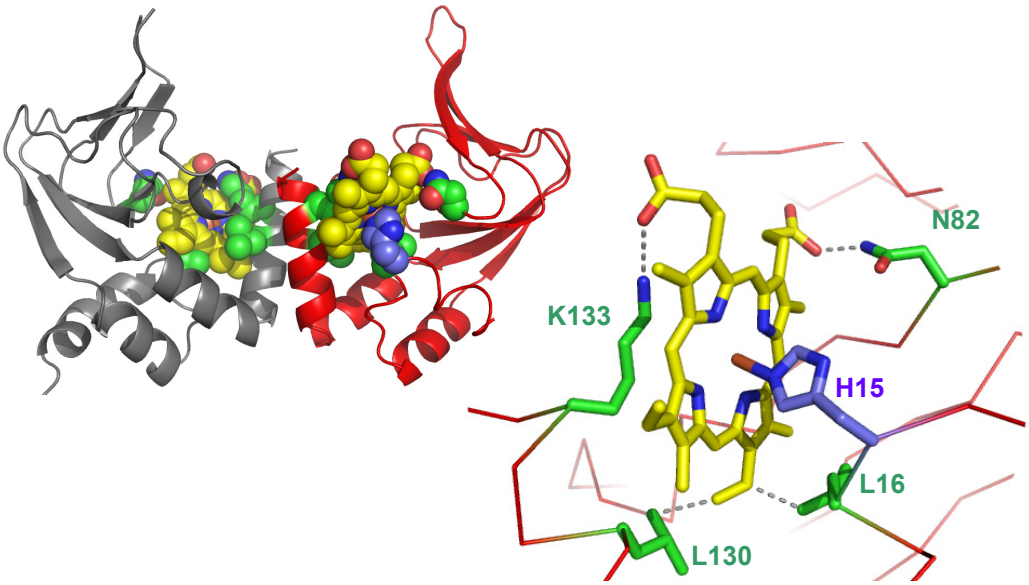

Figure 3.22 *Manual docking of heme-b in the hydrophobic cavity of DNR-N152stop. The C-terminal residues of the hook have been removed to accommodate the heme. The two monomers are red and grey respectively. His-15 is coloured in blue. Lys-133, Asn-82, Leu-130 and Leu-16 side chains are in green.*

The distance between the iron atom and the nitrogen of His-15 was fixed at 1.85 Å, and the plane of the heme was kept perpendicular to the direction of the N-H bond of the histidine far-nitrogen. The two propionate groups of heme were positioned by the solvent interface and are able to make electrostatic interaction one with the amino group of Lys-133 (or alternatively with Arg-137) and the other with the amino group of Asn-82, while the vinyl groups of the heme make hydrophobic interaction with Lue-16 and Leu-130.
The heme fits in the pocket and its chemical environment is coherent with heme binding.

HTH domain - To understand if the peculiar orientation of α-D in ΔDNR structure was compatible with the presence of the C-terminal HTH motif excluded by mutagenesis, we modelled the missing DNA binding domain.
This is a qualitative model, whose importance relies on the possibility to check whether or not the structure of the truncated DNR is compatible with its physiological role.
The position of the missing HTH domain was extrapolated on the basis of the direction of α-D in DNR-N152stop.
The DNR full length model was build by adding a polyalanine backbone of the DNA binding domain extracted from the structure of a putative transcription factor found in the protein data bank (pdb code: 2gau, paper not published) to the structure of DNR-N152stop. The template structure 2gau was chose because, among all the known structures, it is the one whose N-terminal domain fold is the most similar to DNR-N152stop.
The resulting structure is a chimera in which the sensing domain and half of the dimerization helix belong to DNR-N152stop, while the second half of α-D and the HTH motif is a polyalanine model (Figure 3.23). In this model the distance of the two recognition helices is 28 Å and they share the same direction, as expected for CRP-FNR regulators in the active conformation. Each HTH domain can make contacts with the *flap* zone (β- 3 and 4 and loop 5).
These features are similar to what observed in the other known structures (Kim *et al.,* 1992; Passner *et al.,* 2000; Harman *et al.,* 2001; Yu *et al.,* 2004; Eiting *et al.,* 2005; Joyce *et. al.,* 2006), suggesting that the relative position of α-D with respect to the N-terminal domain in ΔDNR is physiologically possible.

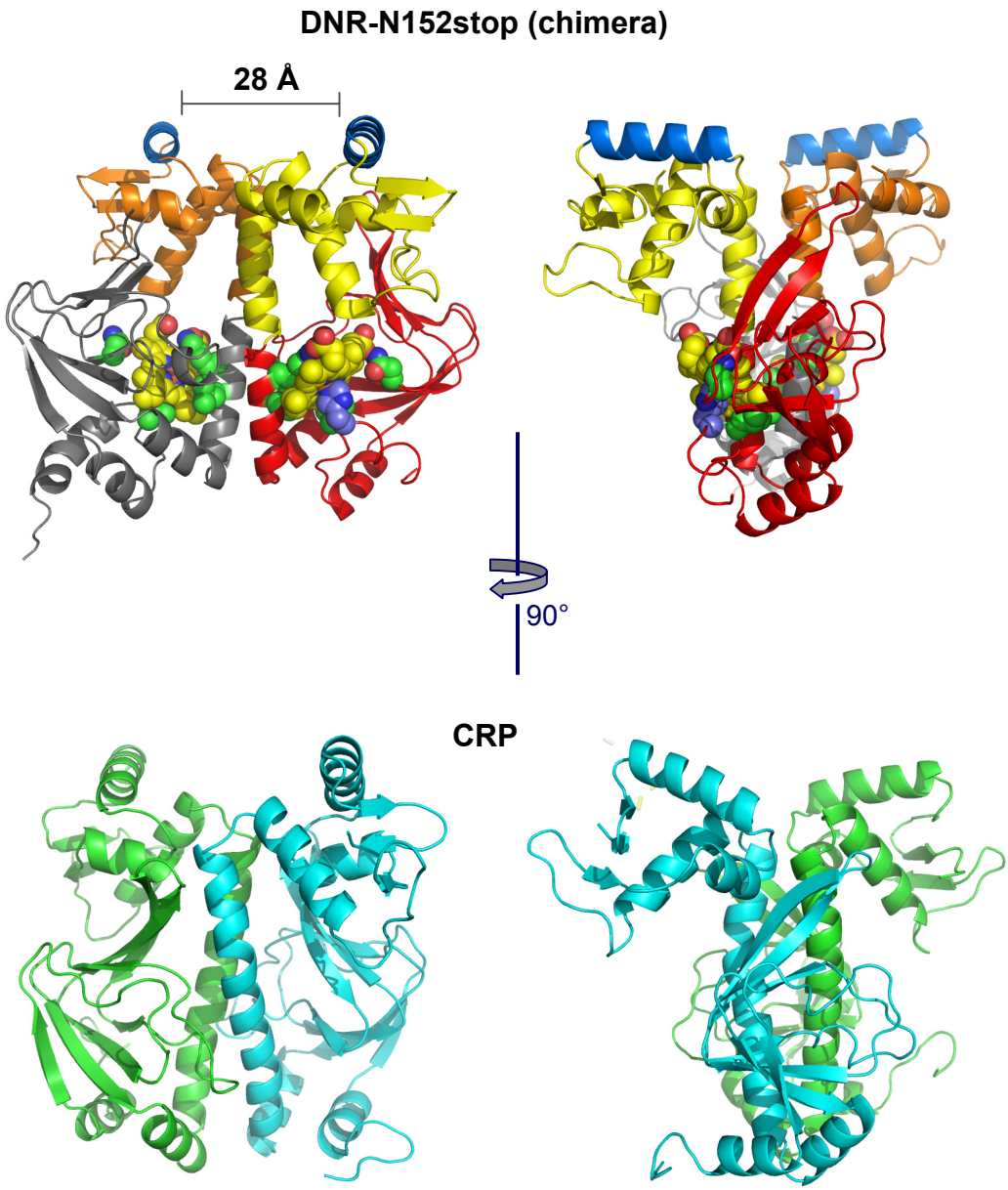

Figure 3.23 *Chimera of ΔDNR(top). The residue in the range 137-150 (hook) have been removed. A polyalanine model of the HTH domain, extrapolated from the structure of a transcription factor with pdb code 2gau, has been added two each monomer. The Chimera is composed as follows. Subunit A and B of ΔDNR (grey and red respectively), models of the HTH domains (yellow and orange) the recognition helices which are involved in DNA binding are shown in blue. The structure of CRP (active form) in the same orientations is shown for comparison (bottom)*

DISCUSSION

Denitrifiers can use nitrate instead of oxygen as the final electron acceptor in the respiratory chain, by reducing it to dinitrogen (Zumft, 1997). The stepwise reduction of nitrate, catalyzed by four reductases (nitrate, nitrite, nitric oxide and nitrous oxide), produces as an obligatory intermediate NO, which may be toxic for cells. Denitrifiers can keep the steady-state concentration of NO below cytotoxic levels by controlling both the expression and the catalytic efficiency of the four reductases involved in the denitrification process.
In *Pseudomonas aeruginosa* the expression of genes of the denitrification pathway is controlled by the NO-responsive regulator DNR (*D*issimilative *N*itrate respiration *R*egulator) which belongs to the CRP-FNR superfamily of transcription factors.
In denitrifiers the NO dependence of the transcriptional activity of promoters regulated by transcription factors of the Dnr and NnrR subgroups has suggested that they may act as NO sensors *in vivo* (Zumft, 2002).
Recent findings indicate that NO is also an important signaling molecule *in vivo*, being able, at concentration far below cytotoxic levels, to induce dispersal of *P. aeruginosa* biofilms.
These results strongly suggest that denitrification, regulation of the NO-homeostasis and pathogenesis are strictly correlated in denitrifying bacteria.

In vitro DNA binding activity of DNR (EMSA assays) with one of the putative target promoters (*nirS* gene promoter) was obtained in our lab by Dr. Serena Rinaldo. A DNR-enriched sample, obtained from the total cell extract of *P. aeruginosa* grown under conditions where denitrification should be active (Arai *et al.*, 1995) (i.e. in presence of nitrates and under low oxygen tension), was able to form two different complexes with the promoter of the *nirS* gene. One of these complexes was shown to be specific. These results show for the first time the direct involvement of a DNR protein in DNA binding *in vitro*, supporting the hypothesis that this class of proteins regulates denitrification *via* direct activation of the target promoters.
EMSA assays were attempted also with the purified recombinant DNR from *E. coli*. No DNA binding activity was detected by using the purified protein expressed in *E. coli*, suggesting that some cofactor(s) or partner component may be required for the DNA binding activity and the NO sensing (Rinaldo *et. al*., manuscript in preparation)

To date structural information on this class of gas sensors is still lacking.
In order to shed light on the structural basis for the putative NO-dependent allosteric regulation of the DNR proteins, I have crystallized and solved the 3D structure of the sensing domain of DNR protein from *P. aeruginosa*: DNR-N152stop.

4.1 The CRP-FNR superfamily of regulators

Transcription factors belonging to the CRP-FNR superfamily are physiologically active as homodimers, each monomer being constituted by three distinct domains: an N-terminal effector or sensing domain (also referred as large domain; first 120-150 residues); a long dimerization α-helix (30 residues, usually referred as C-helix); and a C-terminal DNA binding domain containing an helix-turn-helix (HTH) motif (also referred as small domain; last 50-60 residues) (figure 4.1).
This class of regulators is involved in the control of many enzymatic and metabolic pathways including oxygen respiration, denitrification, nitrogen fixation, methanogenesis, CO-respiration, halo-respiration and virulence activation.
In order to accomplish their role, these transcription factors are able to bind very many different kinds of effector molecules, both directly or by means of cofactors like Iron-sulphur clusters or heme (Aono, 2003; Eiting *et al.*, 2005; Joyce *et al.*, 2006).
To date, among over 400 proteins belonging to the CRP-FNR superfamily, only four have had the structure solved: CRP (Catabolite gene activator from *E. coli*; McKay *et al.,* 1981; Passner *et al.,* 1997 and 2000), CooA (CO-oxidation activator protein in *Rhodospirillum rubrum*; Lanzillotta *et al.,* 2000), PfrA (a key virulence regulator of *L. monocytogenes*; Eiting *et al.,* 2005) and CprK (halorespiration regulator of *Desulfitobacterrium dehalogenans*; Joyce *et al.,* 2006).
The general structural features of these structures are shown in Figure 4.1, the complete structures are shown in Figure 4.2 and the functional properties of the proteins are summarized in Table 4.1.

Considering the similarity in the overall structural organization of these proteins, despite the wide functional diversity, it is possible to point out a few common structural features involved in the effector-mediated allosteric transition of these regulators from the inactive form (OFF conformation, unable to bind DNA) to the active one (ON conformation, able to bind DNA) (Figure 1.6 and 1.7; introduction section).
Due to the considerable distance of the effector binding site from the HTH domain (~10-20 Å), it is unlikely that the conformational rearrangement can occur *via* direct interaction of the effector molecule with the DNA binding domain. Thus the conformational change must be some how transmitted from the large sensing domain to the small HTH domain. Not surprisingly, in all the available structures the effector binding sites are located between the dimerization helix and the sensor domain, making extensive interaction with both.
The first hypothesis of allosteric mechanism reported for CRP-FNR superfamily of transcription factors is described in a paper on the cAMP receptor protein (CRP) of *E. coli* (Kim *et. Al,.* 1992). Kim and co-workers identified, by site directed

mutagenesis, as crucial for allosteric change the hinge region connecting the cAMP-binding domain to the DNA-binding domain. When cAMP binds to the sensor domain, the dimerization helix and the first α-helix of the HTH domain come together and very important electrostatic interactions, among specific polar residues, can occur. As a consequence, the recognition helix can then interact with DNA.

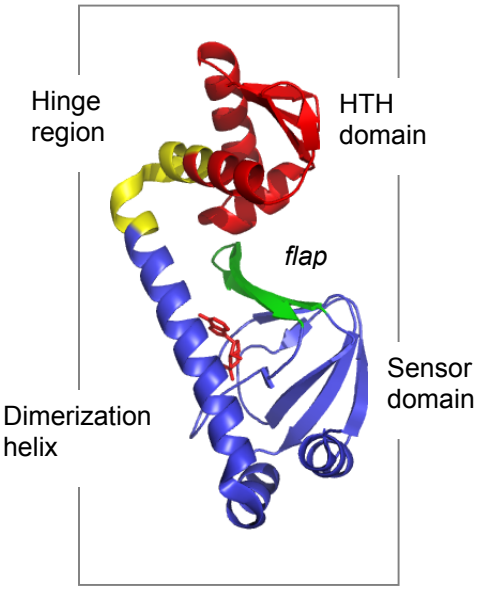

Figure 4.1 *structure of the monomer of CRP (pdb code 1g6n; Passner* et al., *2000) in complex with cAMP, taken as example to illustrate general features of the CRP-FNR regulators. The sensor domain and the dimerization helix are shown in blue. The hinge region, connecting the HTH domain (red) to the dimerization helix is coloured in yellow. The β-hairpin, usually referred as flap, is shown in green. The effector molecule of cAMP is coloured in red.*

Table 4.1

Name and functions of CRP-FNR regulators with known structures

Protein	function	organism	effector	cofactor
CRP	Catabolite regulator	*E.coli*	cAMP	-
CooA	CO-oxidation activator	*R.rubrum*	CO	heme
PrfA	Virulence activator	*L.monocytogenes*	?	?
CrpK	Halo-respiration regulator	*D. dehalogenans*	CHPA	-

Another key element for the activation mechanism is the *β*-hairpin formed by β-sheet 4, β-sheet 5 and the loop interconnecting them (usually referred as the *flap*), which simultaneously provides side chains that contact both the binding site and the HTH, and seems able to stabilize the HTH motif upon effector binding (Yu and Lee, 2004; Harman, 2001; Passner *et al.,* 2000; Schultz *et al.*, 1991).

These results were recently confirmed by the crystal structures of PrfA wild type in the inactive state and of its constitutively active mutant PrfA-G145S (Eiting *et. Al.,* 2005), as well as by the crystal structures of CprK both in the ON state (in complex with its effector CHPA, 3-cloro-4-hydroxyphenylacetate) and in the OFF state (ligand free) (Joyce *et. Al.,* 2006).
It seem now clear that, in these regulators, the effector-binding is able to induce a conformational change of the sensor domain which, via a reorientation in the hinge region, is transmitted through the two dimerization helices to the DNA binding domain. This results in a different relative orientation of the large and small domains and eventually in DNA binding.
Looking at the available structures, it is important to notice that in the inactive state the small domain is found in many different orientations with respect to the large domain and it seem likely that in solution the HTH domain is flexible and highly mobile around the hinge region (Figure 4.2).

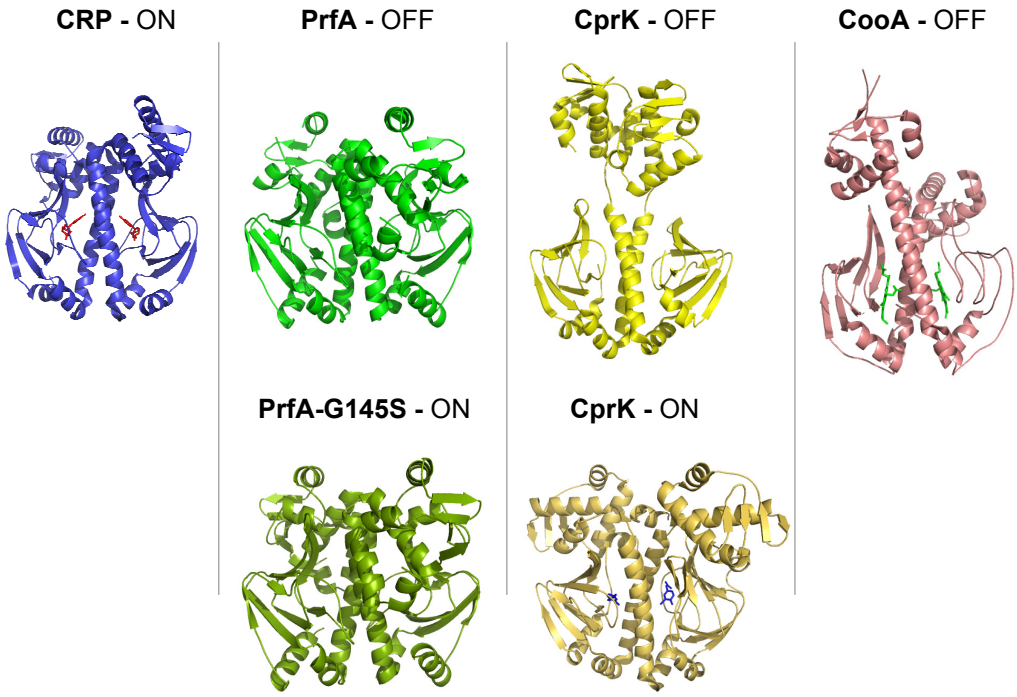

Figure 4.2 *Known structures of CRP-FNR superfamily regulators. ON and OFF refer to the active and inactive conformation respectively. Effector molecules or cofactors when present are coloured differently.*

The mobility of the DNA binding domain could be the reason for the extreme difficulty to obtain diffracting single crystals for this class of regulators, reported in

literature (Wisén *et al.,* 2004; Tomita *et al.,* 2003); This explains why only four structures out of almost 400 known proteins, have been solved among the CRP-FNR superfamily of transcription factors (Körner *et al.,* , 2003).
As described in the results section, despite a very considerable effort, we could not obtain crystals of full length DNR from *P. aeruginosa*. Thus we decided to express a C-terminal deletion mutant comprising the N-terminal sensing domain and the dimerization helix: DNR-N152stop (hereafter ΔDNR or truncated DNR).
The structure of ΔDNR as been solved and is discussed below.

4.2 The crystal structure of DNR-N152stop from *Pseudomonas aeruginosa:* a surprising conformation of the C-terminal residues

ΔDNR is a dimer in solution and has crystallized in the C2 space group with three monomers in the asymmetric unit. The discussion that follows will concern the physiological dimer which is composed by subunit A and B and illustrated in the results section (Figure 3.17;see also experimental section).

In ΔDNR the fold of the sensor domain is similar to the other known structures of CRP-FNR regulators, except for the presence of an additional α-helix at the N-terminal (α-A), which, as we shall see below, is important to keep loop 1 in the correct position. ΔDNR monomer is composed of 7 β-sheets (β-1 to β-7) in a β-barrel conformation plus 3 α-helices (α-A, B and C, for simplicity we will consider the one helix turn in the residue range 87-91 as part of loop 7, see Table 3.7 results). The dimerization helix in ΔDNR corresponds to α-D (Figure 3.17 results).

The hook - The first striking and unexpected feature observed in ΔDNR structure is the unfolding of the last fifteen C-terminal residues. These residues, that where expected in an α-helix conformation, interact with a hydrophobic cleft which is clearly visible at the junction between the N-terminal domain and the dimerization helix of the other subunit. This domain swapping, that can be described as a *hook* of one C-terminal domain docking in the cavity of the other subunit, results in a more compact structure in which the hydrophobic residues of the cavity side wall are buried (Figure 4.3, A and Figure 3.20 results).
By looking in more detail at the interactions of the C-terminal hook of one subunit with the other subunit, which yields the domain swapping, we observe that the core of the hydrophobic interaction is due to two leucine residues of the hook (Leu150 and 148) which are making contacts with several hydrophobic residues of the cavity in the partner subunit (Figure 4.3, B and Figure 3.20, Table 3.8 results).

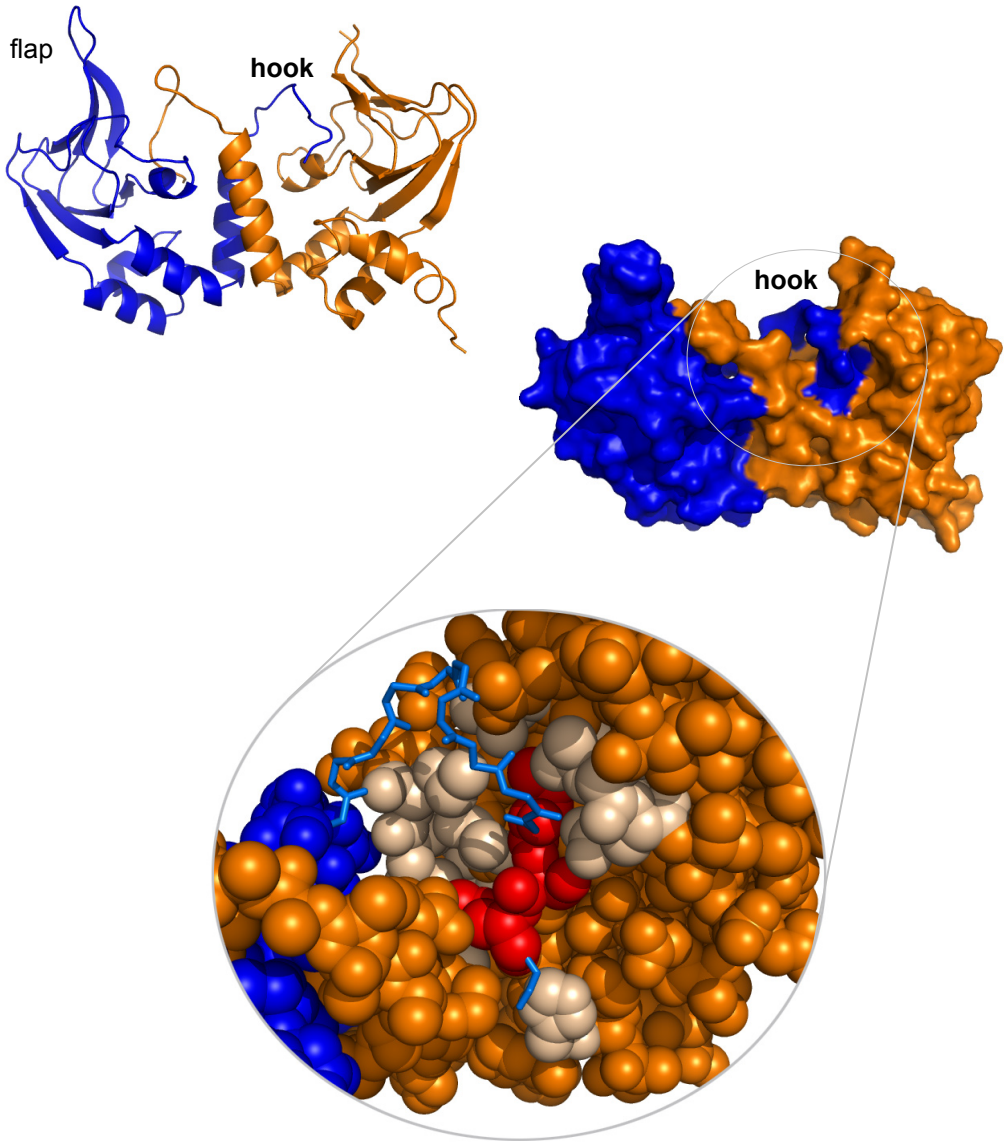

Figure 4.3 *A) Cartoon and surface representation of ΔDNR dimer, the hook conformation results in a more compact structure. B) detail of the interactions between residues Leu-148 Ser-149 and Leu-150 of the hook (red) with hydrophobic and charged residues of the other subunit (light grey). These residues and their interaction are described in more details in the results section (Table 3.8 and Figure 3.20)*

The hydrophobic cavity – The hydrophobic cleft in which the hook residue from the other monomer docks, is a peculiar feature of ΔDNR, and is not observed in the other structures of CRP-FNR regulators.
In ΔDNR, in fact, the dimerization helix α-D is forming an angle with respect to the sensor domain that is 11° larger than that observed in the structural homologues. This particular orientation of the sensor domain relative to the dimerization α-helix, results in the formation of the above mentioned cleft (Figure 3.21, results).
Interestingly, most of the effector mediated conformational changes discussed above, involve secondary structure regions surrounding this hydrophobic cleft suggesting that this could be the binding site for a putative cofactor (probably a heme). This hypothesis is strengthen considering that 11 out of 17 (Figure 4.4) of the strictly conserved residues among the DNR subgroup contribute to form the hydrophobic cleft (Figure 4.5, A).
Three of these conserved residue are positioned in loop 1 (between α-A and α-B); One of these is His-15 whose side-chain points towards the centre of the cavity. The role of the other two conserved residues in loop 1, Leu-16 and Phe-17, and of the additional N-terminal α-helix (α-A), not present in the other proteins, could then be explained by the need to keep His-15 in the correct position in order to serve as proximal ligand for the heme moiety. These two residues, in fact, point towards an hydrophobic cluster constituted by the side chains of Leu-11 (α-A); Leu-25, Leu-28, Leu-29 (α-B); Phe-53 (β-3); Phe-109, Phe-111 (β-7) and Tyr-116 (α-C). This cluster not only contributes in maintain the correct relative orientation of the α-helices with respect to the β-barrel in the N-terminal domain, but also, as already said, keeps loop 1 in position (Figure 4.5, B).

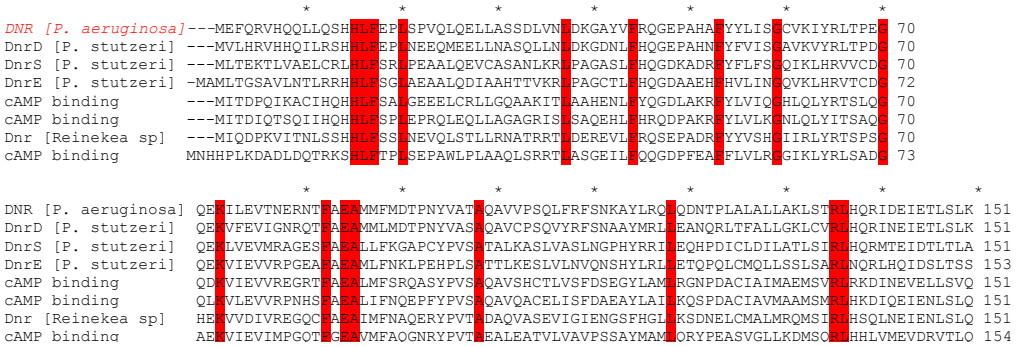

Figure 4.4 *Sequence alignment of the DNR subgroup Strictly conserved residues are boxed in red.*

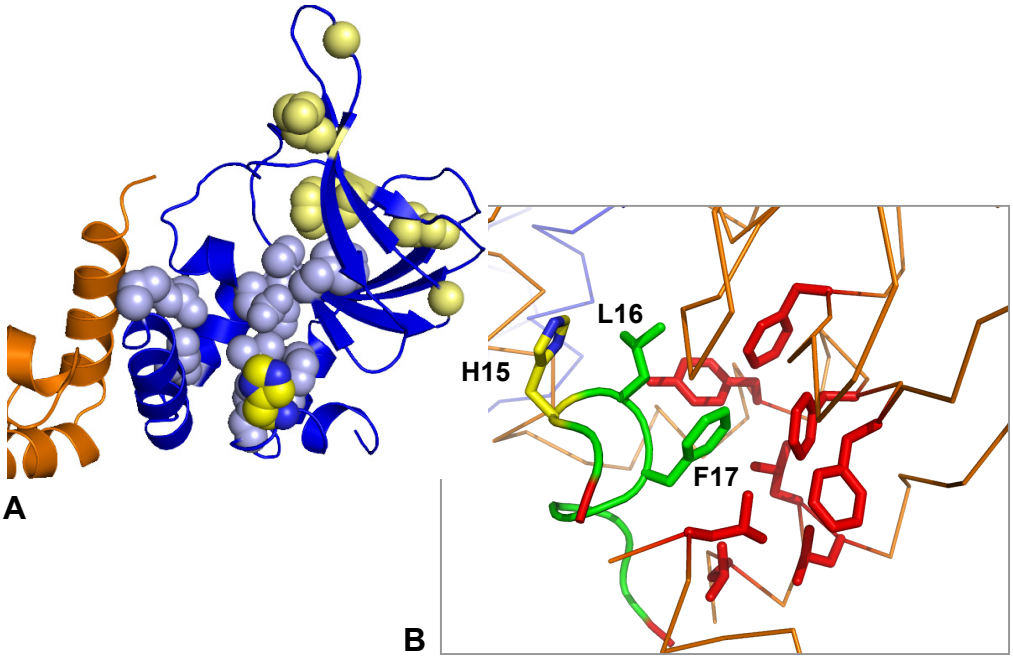

Figure 4.5 *A) conserved residues among the DNR subgroup of regulators. Residues that cluster around the cavity are shown as light grey spheres, the other as yellow spheres B) Hydrophobic cluster constituted by the side chains of Leu-11 (α-A); Leu-25, Leu-28, Leu-29 (α-B); Phe-53 (β-3); Phe-109, Phe-111 (β-7) and Tyr-116 (α-C) is coloured in red. Leu-16 and Phe-17 (green) keep loop 1 (green) in the correct position in order to allow the side chain of His-15 (yellow) to point towards the centre of the cavity.*

Moreover, in the three different ΔDNR monomers present in the asymmetric unit, electron density for residues of loop 1 is always clearly visible, indicating a well defined orientation of this loop; on the other hand while electron density for residues with numbering less than 10 is visible only if crystal contacts are formed, suggesting that these first residues are flexible and that they do not have a specific role in the structure.

All these observations converge in indicating that the observed cavity is the binding site for a putative cofactor, probably a heme.

4.3 Why the heme as cofactor in DNR?

The transcription factors belonging to the CRP-FNR superfamily of regulators, as already discussed, can be activated by a great number of effector molecules, both directly or by means of a cofactor. Among the redox-sensors regulators the only characterized cofactors are iron-sulfur clusters (i.e. FNR, and ANR which are general oxygen sensors in *E.coli* and *P.aeruginosa* respectively; see introduction) and heme (CooA, a CO sensing regulator).
In DNR we can exclude the possible formation of an iron-sulfur cluster on the basis of the sequence, in fact there is only one cysteine residue in the sensing domain. Thus we are keen to think that heme might be the possible cofactor.
Indeed a heme moiety for NO sensing is plausible, if we think that many well characterized heme proteins can bind NO both *in vivo* and *in vitro*, and that also CooA which physiologically binds CO, and whose structure will be analysed in more detail below, is able to bind NO (Reynolds *et al.,* 2000).
Well characterised heme proteins which physiologically bind NO are the guanylate cyclases (sGCs), which are redox sensors of nitrosative stress and have developed high specificity towards NO by increasing the affinity for this molecule. These eukaryotic heme sensor proteins can selectively bind NO in the presence of a large excess of oxygen. Recent discoveries place sGC in the H-NOX (heme nitric oxide and/or oxygen binding domain) family that includes bacterial proteins (Gilles-Gonzalez *et al*., 2005). The peculiar features of this family is that some H-NOX proteins tightly bind O_2 whereas others, such as sGC, show no measurable affinity for O_2. The molecular basis for this ligand selectivity has been established. A distal pocket tyrosine is pre requisite for O_2 binding and is crucial to distinguish kinetically between NO and O_2. In the absence of this tyrosine, the O_2 dissociation rate is so fast that the O_2 complex is never formed, whereas the rate of NO dissociation remains low, thus providing discrimination (Iyer *et al.,* 2003; Karow *et al*., 2004; Boon *et al.*, 2005). Another example of discrimination comes from the NO sensor in C*lostridium botulinum* involved in the chemotaxis machinery regulation. Again the NO-binding heme domain is similar to that of human soluble guanylyl cyclase (sGC) and shows a femto-molar sensitivity towards NO (Nioche *et al.*, 2004), due to its heme moiety organization. Finally the NO-scavanger cytochrome c' (cyt c') from *Alcaligenes xylosoxidans* can discriminate between NO and other typical heme ligands. The crystallographic data of cyt c', in fact, show that carbon monoxide (CO) and NO can bind to opposite sides of heme, causing different responses of the protein through conformational changes (Andrew *et al.*, 2001).
These considerations contribute to indicate that in DNR the heme is the best candidate over the other possible cofactors for NO-sensing.

If we now assume that DNR needs a heme in order to sense NO, then the hydrophobic cleft that we observe in ΔDNR structure could be the putative heme binding site. This assumption could also explain why we were able to obtain crystals only from the truncated protein and not from the full length. In fact, considering DNR as an *apo*-heme-protein, then in ΔDNR the absence of the cofactor is stabilized by the *hook* conformation that buries the exposed hydrophobic residues.

The presence of a putative binding site for a heme moiety in the structure of ΔDNR is consistent with the biochemical characterization of both the full length and the truncated DNR proteins, that is described in the result section and discussed below.

4.4 Biochemical and functional characterization of the recombinant DNR and DNR-N152stop

General characterization – Far UV circular dichroism spectra of purified DNR and ΔDNR *apo* and on the heme-*b* reconstituted proteins indicate that they are folded. No difference in the thermal stability of DNR wt is observed, the calculated thermal stability of 55°C for both *apo* and reconstituted DNR being in agreement with that reported for the homologous protein CRP from *E. coli* (Blaszczyk and Wasylewski 2003; Rinaldo *et al.,* 2005). On the other hand, reconstituted ΔDNR appears to display a lower stability with respect to the *apo*-protein, as qualitatively reflected by a decreased cooperativity in the thermal melting profiles. Although a quantitative analysis is complicated by precipitation events, this behaviour suggests a decrease in ΔH upon denaturation.
These results may be consistent with the hypothesis that when the heme binds in the cavity (coordinated to His-15) the C-terminal residues forming the *hook* are displaced and this results in the loss of the domain swapping interaction and in a decrease in the cooperativity of the ΔDNR dimer during denaturation (Figure 3.10, results).
HPLC analysis confirmed that both the proteins are dimers in solution. For DNR wt higher aggregation states (tetramer and esamer) are populated if NaCl concentration in the protein buffer is under 150 mM, while ΔDNR is always dimeric even at very low salt concentration. These results suggests that the HTH domain could be responsible for the propensity of these class of regulators to aggregate in solution, which as been reported as limiting in the crystallization process (Wisén *et al.,* 2004; Tomita *et al.,* 2003).

Cofactor and binding site(s): the hydrophobic cleft - To obtain some insight on the DNR structural organization and on the presence of an hypothetical heme binding site, an ANS (8-anilino-1-naphthalenesulfonic acid) titration was performed on DNR wild type (Rinaldo *et al.*, 2005) and on ΔDNR; moreover due to the high similarity with CRP from *E. coli*, parallel experiments were carried out using CRP.
When ANS binds to a protein in a hydrophobic pocket, its fluorescence intensity increases dramatically with a concomitant blue shift of the maximum emission wavelength from 530 nm to less than 500 nm. Such changes are taken as characteristic of the formation of a protein-ANS complex (Stryer, 1965). ANS titration on CRP indicates that the protein binds 1 molecule of ANS per monomer with a K_D= 600 μM and a maximum emission wavelength for the CRP-ANS complex at 480 nm. In the presence of 200 μM cAMP, the dissociation constant of CRP-ANS is roughly unchanged (about 500 μM) but the number of binding sites is reduced from 2 to about 1.2/dimer, suggesting that at least one cAMP binding site is involved in the ANS binding (Heyduk and Lee, 1989).
ANS experiments on DNR wild type and ΔDNR indicate that both proteins bind 1 molecule of ANS per dimer with a K_D = 6.2 μM and 6.9 μM respectively, suggesting that they have a different hydrophobic pocket as compared to CRP. This conclusion is consistent with the maximum emission wavelength of the ANS-DNR and ANS-CRP complexes, which is 460 nm for the ANS bound to DNR proteins, while the CRP-ANS complex peaks at 480 nm. This difference, though small, may suggest a decrease of solvent accessibility to the hydrophobic cleft of DNR where ANS is bound.
This consideration is consistent with kinetic studies on apomyoglobin, where the formation of intermediates during the folding process (with lower solvent accessibility to the hydrophobic pocket then the unfolded state) results in ANS fluorescence enhancement and a shift towards lower wavelengths of the maximum fluorescence peak (Sirangelo *et al.*, 1998). The higher affinity for ANS of DNR compared to CRP and the different stoichiometry indicate that DNR presents a different structural organization of the effector domain also in solution.
To further characterize the hydrophobic pocket of DNR, titrations with heme as well as different ligands were carried out.
Heme titration experiments *in vitro* indicate that both the mutant and the wild type proteins bind 1 heme per dimer, according to the finding that the heme-reconstituted protein is stable as a dimer. CRP was again used as a negative control, to exclude that the observed changes in the spectroscopic properties of DNR could be originated by aspecific binding. The fact that the CRP protein, which shares the same domain organization, is not able to bind the heme *in vitro* suggests that the observed binding site in the structure is a characteristic feature of the DNR protein. This finding indicates that the sensor N-terminal domain is involved in heme binding, confirming a possible role of the heme in the sensing activity of DNR.

The displacement of ANS bound to DNR proteins observed for the wild type but not for ΔDNR suggests a role of the HTH motif in the release of the ANS upon heme binding and also that heme and ANS do not compete for the same binding site. This observation suggests that the HTH domain conformation is affected by the presence of the heme.
To assign a role in NO sensing to the heme-DNR complexes, a NO-bound derivative was obtained after reduction of the heme with dithionite. Interestingly, the NO-bound derivative shows a peak at 398 nm which is indicative of a five-coordinate state of the heme iron and thus absence of the "proximal" bond with the protein. Reduced heme protein saturated with NO can be either six-coordinate or five-coordinate (with breakage of the bond with the proximal histidine) (Table II shows the absorbtion maximum of the six-coordinate and five-coordinate states) The five-coordinate form of the heme-NO complex is reported to be typical of the heme-based sensor domain of the soluble guanylyl cyclase enzyme (sGC). Upon NO binding, conformational changes occur and the guanylyl cyclase activity is enhanced (Koesling, 1999). A five-coordinate nitrosyl-Fe(II) heme, revealed by electronic absorption and EPR spectroscopy, is also reported in the case of reductive nitrosylation of CooA; the Soret peak of ferric CooA shifts from 423 to 398 nm upon reaction with NO (Aono, 2003).

Table 4.2

Absorbance peaks of NO-bound derivative of heme proteins.

Fe(II)-NO	Coordination	Soret	Visible	reference
6-coordinated	His	420	548, 579	*Antonini and Brunori, 1971*
5-coordinated	-	398	537, 572	*Koesling, 1999*

This evidence has suggested that DNR can sense NO by binding to the heme iron and forming a five-coordinate derivative with associated rupture of the proximal histidine-iron bond and conformational rearrangement that triggers DNA binding.

The biochemical characterization of DNR in solution fits very well with what observed in the structure of ΔDNR and with the hypothesis that DNR is a heme binding protein. It is straightforward then to compare the structural features of ΔDNR with CooA, the only known structure of a CRP-FNR regulator that binds the heme.

4.5 Comparison of DNR-N152stop with CooA

CooA from *Rhodospirillum rubrum* in a highly reducing environment senses the presence of CO by means of a heme cofactor and responds inducing the transcription of operons that encode proteins involved in the oxidation of CO to CO_2 and reduction of protons to H_2 (Aono *et al.,* 1996; Roberts *et al*., 2005).
As the other CRP-FNR like transcription factors, CooA is a dimer and binds the two hemes in a very peculiar manner. In each subunit the proximal ligand of the iron atom is a histidine residue while the distal coordination is provided by the N-terminal proline of the other monomer (Figure 4.5, A) (Lanzillotta *et al.,* 2000).

Comparing the heme position - The clefts in which the two hemes are accommodated are formed upon dimerization of the two chains of the protein, and are constituted by the sensor domain of one monomer and the dimerization helix of the other monomer, as it is shown in Figure 4.5, A.
We already excluded that DNR could bind the heme in the same way as it is observed in CooA, because the N-terminal of DNR is not a proline residue.
Now, by comparing the two structures, we can conclude that if DNR is a heme protein, the heme binds differently with respect to CooA. In fact, the two hydrophobic clefts in ΔDNR and the heme binding sites in CooA are positioned on the opposite side of the two sensing domains (Figure 4.5, B)

Comparing the heme clefts volumes – Although the position of the heme in CooA is different from the hydrophobic cleft in ΔDNR, it is possible to compare the relative volumes of these cavities to understand whether or not a heme could fit in the cleft that we observe in ΔDNR.
The volumes have been calculated using CASTp server (Dundas *et al.,* 2006). The hook residues of ΔDNR have been removed from the structure before the calculation.
The volumes of the cavities for monomer A and B in ΔDNR are of 830 $Å^3$ and 610 $Å^3$ respectively, while for CooA the two clefts have a volume of 580 $Å^3$ and 540 $Å^3$ (Figure 4.6).

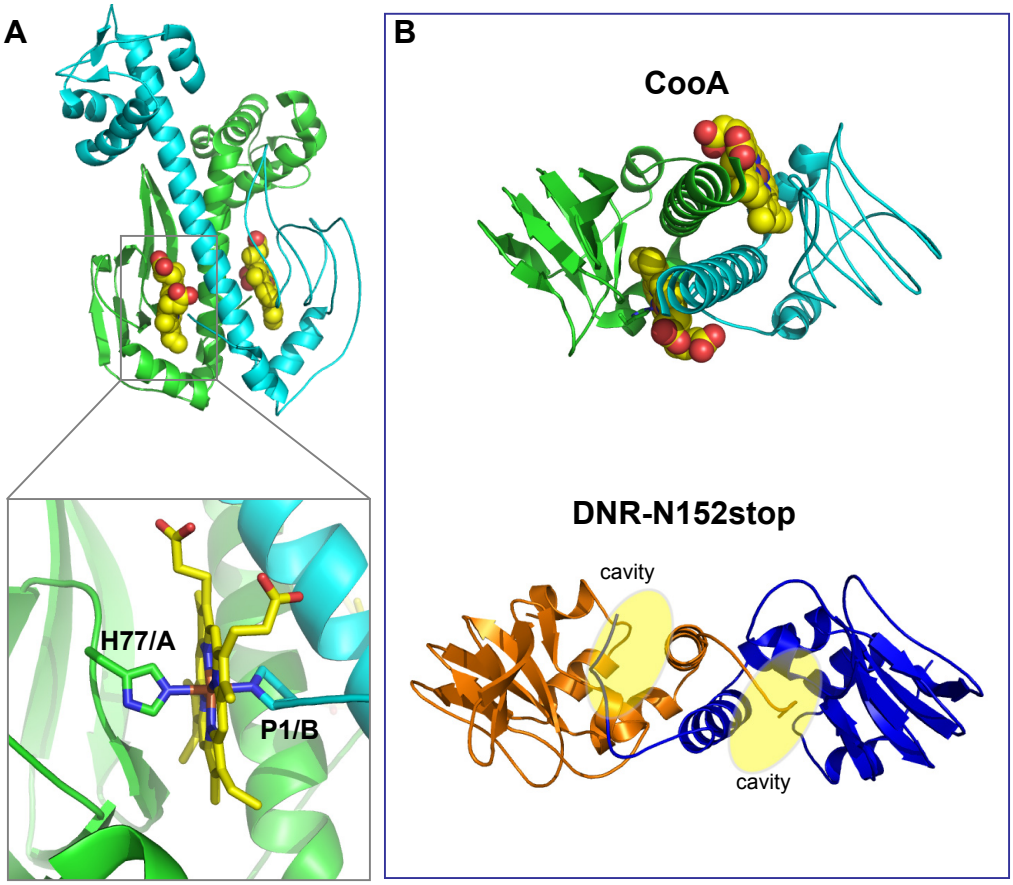

Figure 4.5 *Comparing CooA with ΔDNR. A) CooA dimer. The two monomers are coloured in green and cyan. Close view of the heme ligands His-77 from monomer A and Pro-1 from monomer B. B) Top view of both CooA (the HTH domains have been removed to allow a better view over the heme binding sites) and ΔDNR. In ΔDNR the hydrophobic cavities (highlighted in yellow) are in the opposite position with respect to the sensing domain.*

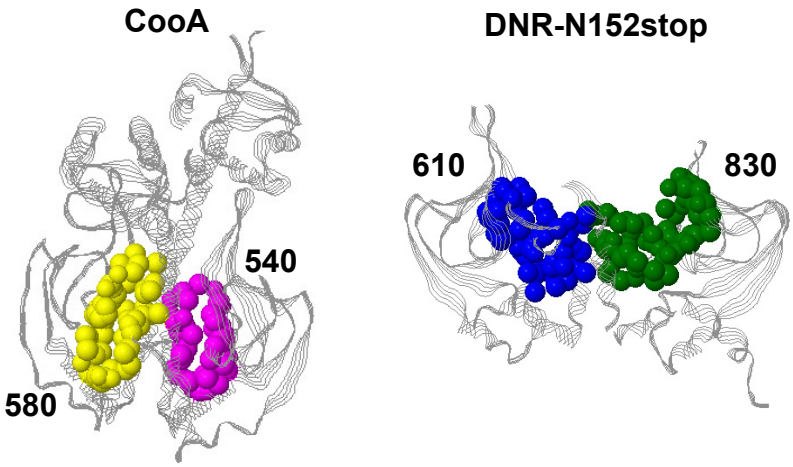

Figure 4.6 *Cavities detected by CASTp server (Dundas et al., 2006) and calculated relative volumes (Å^3) for CooA and ΔDNR. The hook residues were removed before calculation.*

The big difference in the calculated volumes of the cavity in ΔDNR can be explained considering that the volume of the pocket is deeply influenced by small changes in the relative orientation of the sensing domain and of mobile loops, especially the *flap*, with respect to the dimerization helix α-D. In fact the cavity is located at the junction between the N-terminal domain and the dimerization helix of the structure which has been observed to be flexible in ΔDNR structure. Indeed superimposition of the two subunits of the dimer results in a rms deviation of 1.16 Å., and a great variability is observed especially in the flap zone (β-hairpin; β-3 / loop-5 / β-4). The flexibility of the flap is explained considering that, lacking the HTH domain, these residues are totally exposed to the solvent. In fact electron density in this zone was of difficult interpretation or, in some case, absent (residues 68 to 71, subunit A) confirming mobility (Figure 4.7).
These relative differences among the two subunits can be explained if we think to the structure of ΔDNR as that of an *apo*-form. In this case it is clear that residues that cluster around the putative heme binding site, especially if belonging to flexible loops, reorient the side chains in order to minimize the solvent exposure of the cavity surface. Furthermore the need to bury hydrophobic residues of the side wall of the cleft is probably the origin of the *hook* formation.

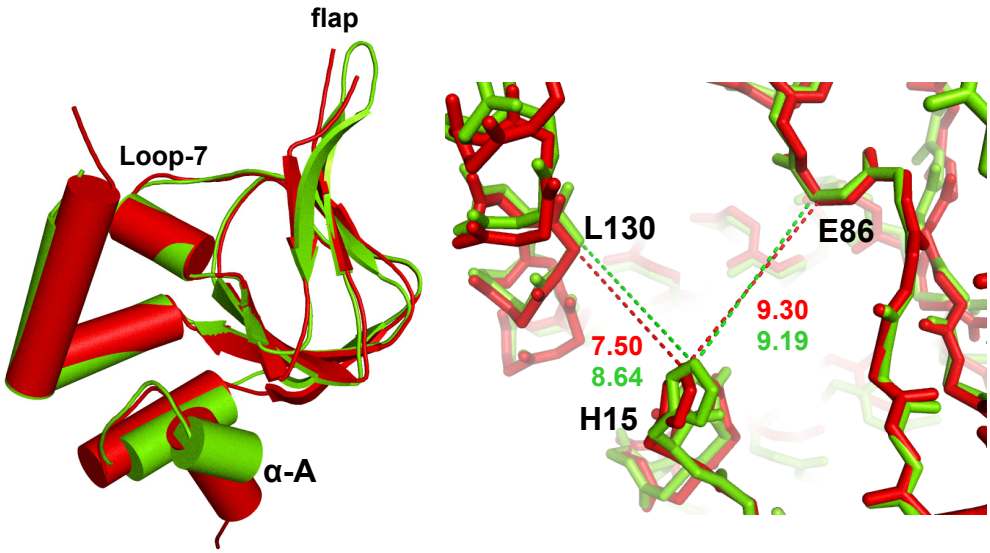

Figure 4.7 *superimposition of backbone atoms of different ΔDNR monomers. Subunit A and B are shown in red and green respectively. The C-terminal residues have been excluded from calculation starting from Leu-138. A) whole structure. B) relative distances in Å between the far-N of His-15 and Cαs of Leu-130 and Glu-86*

ΔCooA is correctly folded - It might be argued that the unfolding of the C-terminal, residues resulting in the hook, is due to the lack of the HTH domain in the mutant protein. Nevertheless it is surprising and intriguing that these residues can find enough space to dock in the sensor domain cavity, unless this space is due to the lack of a cofactor. Furthermore recently Kuchinskas and coworker (2006) have solved the structure of a CooA mutant lacking the DNA binding domain exactly as ΔDNR and the mutant structure of truncated CooA (ΔCooA) superimposes with the full length CooA (Lanzilotta *et al.,* 2000) with a rms deviation of only 0.7 Å. In this case the dimerization helix does not unfold and is forms the complete dimer interface as expected. Comparison between ΔCooA and ΔDNR structures (Figure 4.8) strengthen the hypothesis that the hook conformation observed in ΔDNR is a consequence of the presence of the hydrophobic cavity, which is physiological, and not vice versa.

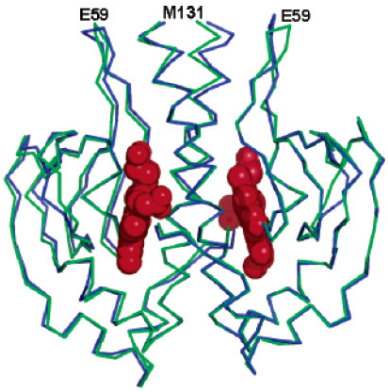

Figure 4.8 *ΔcooA superimposed on CooA wt. (taken from: Kuchinskas et al., 2006)*

Over and above these consideration, the crude information that can be extracted from the structural comparison of ΔDNR and CooA is the following: the hydrophobic cleft in the sensor domain of DNR has a volume which is compatible with heme binding.

4.6: Docking the heme in the cavity and Modelling the HTH domain

The position of conserved hydrophobic residues and of His-15, the spectroscopic properties of the heme reconstituted proteins and the calculated volume of the deep cavity observed in ΔDNR, strongly suggest a role of this cleft in heme binding.
To further strengthen this hypothesis, a heme-*b* was manually docked in the structure by assuming His-15 as the heme proximal ligand and fixing to 1,85 Å the distance between the iron atom and the far-nitrogen of the imidazole ring. the plane of the heme was kept perpendicular to the direction of the iron-nitrogen coordination. Our docking suggests that the heme is held in place by both hydrophobic and electrostatic interactions that are mainly created by the conserved similar residues. One of the propionate groups of the heme interacts with Lys-133 and the other with Asn-82, which are either conserved or substituted with residues that are capable of forming H-bonds (Figure 4.4). One of the vinyl groups is equidistant (<3Å) from Leu-16 and Leu-130, while the other is near the methyl group of Ala-129. Four side chains (Leu-16, Glu-86, Lys-133 and Glu-76) had to be shifted from the original position to fit the heme in the cavity or to avoid unfavourable electrostatic contacts, and alternative allowed rotamers, compatible with the presence of the heme, were selected.

Based on these consideration we can conclude that in our model the chemical environment is consistent with heme-binding (Figure 4.9 and also 3.22, results).

To confirm the presence of the cavity where the heme moiety was docked into, we modeled the missing DNA binding domain extrapolating its position on the basis of the α-D helices direction in ΔDNR. Thus the DNR full length model was completed by adding a polyalanine HTH domain extracted from the 2gau structure (pdb code). The resulting chimera, in which the sensing domain and the dimerization helix belong to ΔDNR while the HTH motif is an homology model, was constructed in order to inspect the possible orientation of the missing C-terminal domain with respect to the α-D helix. This is important to understand if the unusual wider angle formed by α-D with the sensing domain is compatible with DNA binding activity. In this model the distance of the two recognition helices is 28 Å, as found in CRP structure (1g6n; Passner *et al.,* 2000), and they share the same direction expected

in the ON-like conformation (Eiting *et al.,* 2005; Joyce *et al.,* 2006). Each HTH motif is able to contact the flap (Figure 4.9, D and Figure 3.23 in results). Of course this model is only qualitatively useful but it confirms that the relative position of α-D with respect to the N-terminal domain in ΔDNR is physiologically possible and is not solely determined by to the lack of the C-terminal domain.

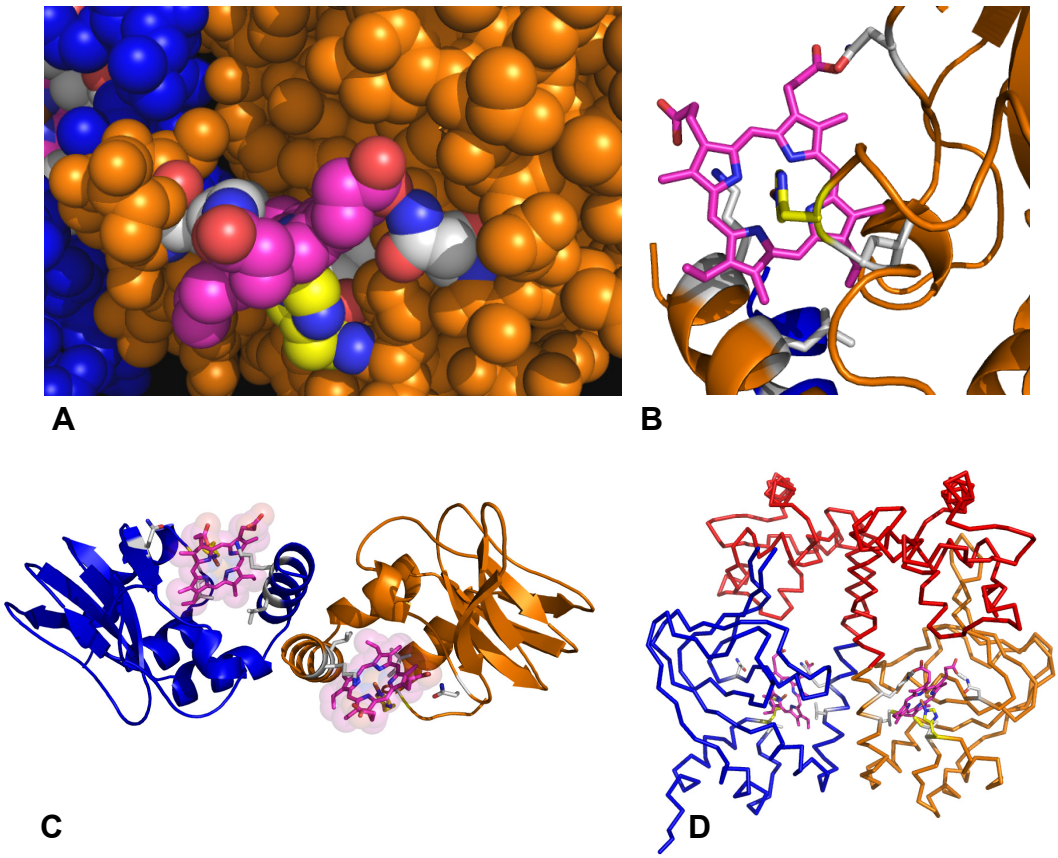

Figure 4.9 *Manual docking of heme-b in the hydrophobic cavity of ΔDNR. The C-terminal residues of the hook have been removed to accommodate the heme.*
The two monomers of ΔDNR are coloured in blue and orange, heme in purple, His-15 in yellow, Lue-130, Leu-16, Lys-133 and Asn-82 are in light grey. A) top view, sphere representation. B) Bottom view. C) Top view of the dimer. D) Ribbon representation of the DNR chimera: the modelled HTH domains are shown in red.

4.7 Minimal Dimer interface and signalling helix

The physiological dimer interface interactions in ΔDNR are unexpectedly formed by a core of only four leucine residues (Leu-131 and Leu-134 in each subunit) because of the unfolding of the last fifteen C-terminal residues that are involved the *hook* formation. The hook without doubt contributes to dimer formation by making additional hydrophobic interaction, but the unfolding of the last four turns of α-D is striking and it is tempting to attribute to the second half of the dimerization helix a major role in the allosteric mechanism of DNR activation.

Recently Anantharaman and co-workers (2006) have reported about a common functional theme in diverse signalling proteins identified as the *signalling helix* (S-helix). They found a conserved helical segment of about 40 residues (which they divide in repeating heptades - *abcdefg* - of residues) linking different domains in a wide range of signalling proteins. S-helix feature might also occur between two sensory domains and occasionally link a DNA-binding HTH domain to a sensory domain. They suggest that it functions as a switch that, upon occurrence of specific conformational changes due to binding of ligand or other sensory inputs, is able to transmit the signal from an upstream linked domain to the downstream linked domain.

Using a multiple alignment of 1000 distinct S-helix representatives, detected in their searches from across the three superkingdoms of Life, they construct a comprehensive multiple alignment and a sequence logo quantifying the conservation at each position of the heptade. The S-helix is typified by a strongly conserved ‘ERT’ signature seen in the central heptad unit in positions corresponding to ‘c’, ‘d’ and ‘e’ (Figure 4.9, A) and two periodic series of positions ‘a’ and ‘d’ dominated by conserved hydrophobic residues, which form the principal interface for dimerization through hydrophobic interactions.

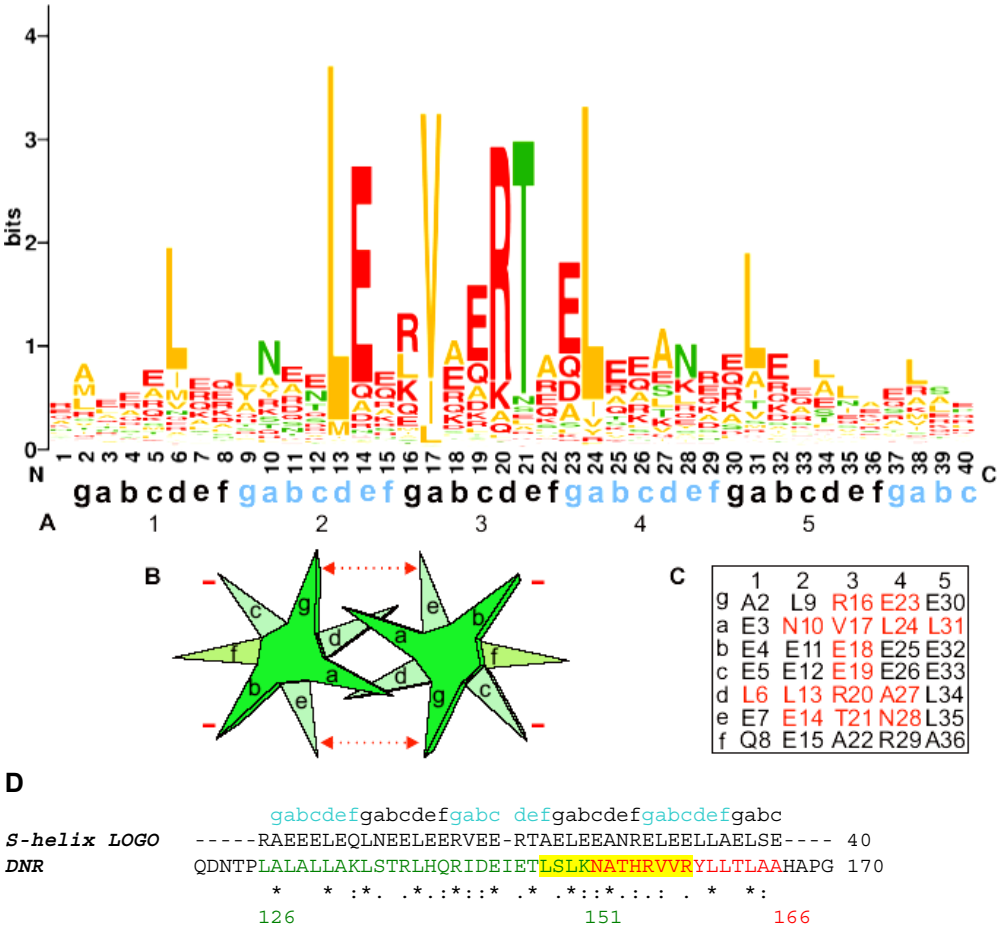

Figure 4.9 *Sequence logo and interaction models for the S-helix. A) The sequence logo generated by comprehensive multiple alignment. B) the heptad interaction between two parallel helices. The dotted red arrow indicates the 'g'-'e' interaction. The red negative sign indicates that most prevalent residues at the b and c positions are negatively charged. C) The most prevalent residue of each position on the S-helix is shown as a table with the rows showing the positions in each heptad, and the columns showing the five heptads. The residues in red indicate the highly conserved positions. D) DNR vs S-helix Logo alignment. Residues present in ΔDNR are coloured in green. α-E residues are coloured red. The hinge region is highlighted yellow. (figure A,B and C are taken from; Anantharaman et al., 2006)*

Sequence alignment of DNR with the logo of S-helix results in 70% of similarity in the zone from Leu-126 to Ala-166 (figure 4.9, D), thus the putative S-helix in DNR would be formed by the second half of the dimerization helix α-D and all the first helix of the HTH domain α-E (the hinge region) which are the key residues involved in the allosteric conformational changes discussed above. This findings suggest that the role of α-D is not limited to dimerization, but is also crucial in transmitting the conformational change from the sensing domain to the DNA binding domain during activation.

4.8 Conclusions and future perspectives

Understanding the mechanism of NO sensing in pathogens is a hot topic in biomedical research. I have solved the 3D structure of ΔDNR from *P. aeruginosa*. This is the first structure of an NO sensing domain of a bacterial regulator and the first protein belonging to the CRP-FNR superfamily of transcription factors and is fundamental to shed new light and provide insights into the effector-mediated allosteric switch and the chemistry of NO sensing of these transcription factors, that is still poorly understood.
On the basis of the biochemical characterisation of DNR wild type and of ΔDNR proteins, and of the DNA binding activity obtained by Dr. Rinaldo in our group (Rinaldo *et al.,* manuscript in preparation), we are firmly convinced that DNR is a heme binding protein. In fact, DNR and ΔDNR are able to bind heme-b *in vitro* with micro-molar affinity and a stoichiometry of 1 heme per monomer and the heme reconstituted proteins can form a NO bound derivative. The recombinant *apo*-form of DNR expressed in *E. coli* is unable to bind DNA, while recombinant DNR is able to bind the *nirS* promoter only when heme is present in the growth medium.
We observed a deep hydrophobic cavity, structurally different from the binding sites of other CRP-FNR proteins. This cleft is located at the junction between the sensor domain and the dimerization helix, and is likely to be the heme binding site in ΔDNR. Docking of a heme-*b* in this cavity results in a model consistent with heme binding, with the iron atom coordinated with the far-nitrogen of His-15.

To confirm these results, crystallization of DNR wild type in complex with the heme is still in progress.
To further investigate the nature of the axial ligand and the NO binding properties of the heme, MCD and EPR experiments are now in progress in collaboration with A. Thomson and M. Cheesman (Norwich, UK).
Site directed mutagenesis is being carried out to confirm the role of the residues that cluster around the cavity and, on the basis of the model, are involved in heme

binding. In particular we are mutating His-15, the putative proximal ligand, into alanine as well as the other conserved residues which cluster around the cavity. The chimera structure, reporting the hypothetical position of the HTH domain, will be useful to design constitutively active mutants (Ala-144 in CRP is structurally aligned with Val-158 in DNR, mutation of this valine to larger residues, as discussed above, should result in constitutively active protein) to be used both in crystallization trials and in finding optimal conditions for *in vitro* DNA binding assays.

MATERIALS AND METHODS

Protocols used for the common molecular biology and biochemistry techniques, if not indicated, are described in Molecular cloning: a laboratory manual (Sambrook *et al.*, 1989). Cloning, expression and purification of DNR from *P. aeruginosa* is described Rinaldo *at al.* (2005).

5.1 Cloning, expression and purification of DNR-HIS from *P. aeruginosa*

Cloning - The following oligos (5'-GGAATTCCATATGGAATTCCAGCGCGTCCACC AGC-3', 5'-CCGCTCGAGTCACTCGAAGCACTCCAGGCGTTCGC-3') were used to clone the *dnr* gene into the pET28b vector in frame with a 5'-sequence encoding for a hisidine tag (his-tag); extra NdeI-XhoI restriction sites at the 5' and 3' ends, respectively, were also introduced.
The *dnr* gene was linked to the his-tag motif through a sequence encoding a thrombin site, useful to remove the tag from the purified protein.
The pET-DNRHIS vector was transformed into BL21(DE3) *Escherichia coli* strain; the expression conditions reported below were followed for both vectors.

Expression in E. coli - Expression of the protein was obtained at 37°C in Luria Bertani (LB) medium containing 30μg/ml kanamicin. Aerobic cultures (0,75 l in 2 l flasks) were shaken at 250 rpm. DNRHIS protein expression was induced with 1 mM IPTG (isopropyl *β*-d-thiogalactoside) when OD_{600} was 0,4 (Rinaldo at al., 2005). Cells were then grown for 15 hours.

Purification of DNR - on a Q-Sepharose Fast Flow (Amersham) column; the protein was eluted with a 35-500 mM NaCl gradient in the same buffer. The fractions containing the protein were pooled together and applied on a Heparin Sepharose 6 Fast Flow (Amersham) column after dialysis against buffer A. The protein was eluted with 100 mM NaCl, concentrated and applied on a Superdex 75 gel filtration column (Amersham) equilibrated in 20 mM Tris-HCl pH 7.2, 2 mM EDTA and 150 mM NaCl (Rinaldo at al., 2005). After the first purification, 2-ME was removed from all the purification steps, due to the fact that no changes in protein yield and solubility were observed.
Fractions containing DNR were pooled, frozen in liquid nitrogen and stored at -70 °C. In all the purification steps DNR protein was detected through SDS-PAGE and western blot analysis. Polyclonal antibodies were obtained in rabbit from the

recombinant protein purified from *E. coli* (Davids Biotechnologie, Germany).
The extinction coefficient at 280 nm was determined by the BCA assay (Sigma) to be 14.8 mM^{-1} cm^{-1} (per monomer).

Purification of DNRHIS - Cells were resuspended in 50 mM Tris-HCl buffer (pH 8.0), 50 mM NaCl, 2 mM EDTA, 2 mM 2-ME (β-mercaptoethanol) and 1 mM PMSF (Phenylmethylsulfonyl fluoride) and sonicated. The cell extract was centrifuged 30' at 12000 rpm to remove any insoluble material. The soluble fraction was dialyzed against 20 mM Tris-HCl pH 7.2, 300 mM NaCl; the sample was then applied on a HiTrap™ Chelating HP column (Amersham) containing nickel sulfate salt and equilibrated with 20 mM Tris-HCl pH 7.2, 300 mM NaCl; the protein eluted with 300mM imidazole, in the same buffer. To remove the his-tag from the purified protein, the sample was loaded on a FPLC column (Superdex 75 16/30) and eluted with 20 mM Tris-HCl pH 7.2, 300 mM NaCl. Proteolytic digestion was carried out with 20 units of thrombin (Amersham) per mg of taged-protein, at RT for 15 hours. The sample was then applied a second time on a HiTrap™ Chelating HP column (Amersham) loaded with nickel sulfate and equilibrated with 20 mM Tris-HCl pH 7.2, 150 mM NaCl. Under these experimental conditions, the thrombin enzyme was recovered in the flowthrough, while the his-tag free protein and the his-tag tails eluted in presence of 60 and 300 mM imidazole, respectively.
The DNR protein was again loaded on a FPLC column (Superdex 75 16/30) and eluted with 20 mM Tris-HCl pH 7.2, 150 mM NaCl, frozen with liquid nitrogen and stored at -70°C.
Detection of DNR protein in all the purification steps was obtained through SDS-PAGE and western blot analysis, using anti his-tag polyclonal antibodies from rabbit (Santa Cruz Biotechnology, Inc.) for DNR-HIS and polyclonal antibodies obtained in rabbit from the recombinant DNR protein purified from *E. coli* (Davids Biotechnologie, Germany) for digested DNR. The extinction coefficient at 280 nm for DNR after digestion was determined by the BCA assay (Sigma) to be: 14.8 mM^{-1} cm^{-1} (per monomer).

5.2 Mutagenesis; DNR-N152stop

Site-directed mutant N152STOP was obtained on the pET-DNRHIS template, using a QuikChange site-directed mutagenesis kit (Stratagene). The mutation was verified by sequencing.
Expression of the mutant protein was obtained at 25°C in Luria Bertani (LB) medium containing 30μg/ml kanamicin. Cultures (0,75 l in 2 l flasks) were shaken at 160 rpm. protein expression was induced with 1 mM IPTG (isopropyl *β*-d-thiogalactoside)

when OD_{600} was 0,4. Cells were then grown for 15 hours and purification of was carried out as reported for the wild type his-tag containing protein.

Expression and purification of N152stop-HIS Se-Methionine derivative – Cells were grown in 5ml of Luria Bertani (LB) medium containing 30μg/ml kanamicin overnight at 37°C. 1ml of the overnight culture was diluted in 0.5L of M9 minimal medium (DIFCO) supplemented with 2mM $MgSO_4$ and 0.4% w/v glucose. Cells were grown at 25°C to 0.3 OD_{600}. At this point a feed back inhibition amino-acid mix is added (50mg of lysine, threonine and phenylalanine; 25mg of leucine, isoleucine, valine and seleno-methionine, SIGMA, dissolved in sterile water and filtered-sterilized immediately before use) to block the endogenous synthesis of methionine. After 15 minutes expression is induced as usual with 0.1mM IPTG. Cells were then grown for 15 hours.
Purification was performed as described for the tagged proteins except for the addition of 5mM β-mercaptoethanol in all used buffers. Seleno-methionine incorporation was assayed by LC-ESI Mass Spectrometry (with kind support of Prof. E. Schininà, Dipartimento di Scienze Biochimiche - University of Rome "La Sapienza").

5.3 Biochemical characterization of DNR and DNR-N152stop

Aggregation state - The aggregation state was determined on a FPLC column (Superdex 75 16/30) and further confirmed by HPLC (G3000SWxl Tosoh Biosep), at different NaCl concentration, in 20 mM tris-HCl pH 7.2 buffer (Rinaldo at al., 2005). The molecular weight calibration curve was obtained using protein standards (BSA 67 kDa, ovalbumin 43 kDa, chymotrypsinogen 25 kDa and RNase A 13.7 kDa - Amersham).

ANS binding - ANS (8-anilino-1-naphthalenesulfonic acid, SIGMA) binding was carried out by titrating a DNR wild type solution either 2, 4 or 7 μM (monomer) or a DNR-N152stop solution either 1, 2, or 4 μM (monomer) in 50 mM Tris-HCl pH 7.2, 150 mM NaCl with a 1 mM ANS solution in water. The dissociation constant of ANS-DNR complex was calculated using the following relation (when ANS_{tot}>DNR_{tot}):

$$1/I = 1/n\ \Psi\ [DNR]_{tot} + (K/n[DNR]_{tot}\ \Psi)(1/[ANS]_{free})$$

where I is the observed fluorescence intensity (counts per second), K is the dissociation constant for a dye-site complex, n are the total number of sites on protein, and Ψ is the proportionality constant connecting the fluorescence intensity

to the concentration of the probe-site complex.
If $ANS_{tot}>DNR_{tot}$, the plot of 1/I vs. $1/[ANS]_{tot}$ will be linear for fixed protein concentration with a common abscissa intercept, for different protein concentration, of –1/K, as described in Horowitz and Criscimagna (1985).
The number of binding sites on protein was assaied by titrating an ANS solution (either 1, 2 or 4 μM) with excesses of DNR wild type or DNR-N152stop and was calculated using the following relation:

$$1/I = 1/\Psi\ [ANS]_0 + (K/\Psi n[ANS]_0)(1/[DNR]_0)$$

In this case, the plots of 1/I vs 1/[DNR], for different ANS concentrations should have a common abscissa intercept of -n/K, as described in Horowitz and Criscimagna (1985).
In all cases, the signal was corrected for the fluorescence emission signal of free ANS in the same buffer.
For the experiments in which ANS bound to DNR wild type or DNR-N152stop were displaced by heme, 1 µl aliquots of a 0.2 mM solution of hemin were added to 2 ml solutions of 35 µM ANS and either 2 or 5 µM DNR wild type and 1 or 4 µM DNR-N152stop protein.
All fluorescence emission spectra were recorded in a quartz cuvette (1 cm light path, Helma) between 400 and 600 nm on Fluoromax single photon counting spectrofluorometer (Jobin Yvon). The excitation wavelength was 350 nm.

Heme titration and reconstitution - Heme binding *in vitro* was assayed by titrating a 11 μM DNR wilde type (monomer) solution and a 22 μM DNR-N152stop (monomer) solution respectively with increasing amounts of a freshly prepared solution of 0.5 mM ferric hemin (Sigma) in 10 mM NaOH. Titrations were carried out in 20 mM Tris-HCl pH 7.2 and 100 mM NaCl.
The cAMP binding protein (CRP) from *E. coli* was also titrated (17.1 μM monomer solution) with heme as a negative control. CRP was expressed as described in Rinaldo *et. Al.* (2005). and was purified as described in Heyduk and Lee (1989).
For each heme/protein mixture a spectrum was recorded between 260 and 700 nm on a Hewlett Packard spectrophotometer. The difference between absorbance at 412 and 380 nm was plotted as a function of the mole fraction of heme.

The DNR wild type and DNR-N152stop apo-proteins were reconstituted with a 1.5 stoichiometric excess of hemin in 20 mM Tris-HCl pH 7.2 and 300 mM NaCl at 16°C. Excess of free hemin was removed by gel filtration on a Sephadex G-25 column (Amersham).
Spectra of the heme-reconstituted proteins were recorded on a Hewlett Packard spectrophotometer, using a 1 cm quartz cuvette (Helma). The reduced derivatives -

obtained by adding an excess of sodium dithionite - were incubated in anaerobiosis under a saturated atmosphere of CO gas or with 10 μl of a 2 mM nitric oxide (NO) solution (20 °C and pH 7,2) to obtain the corresponding derivatives.

Circular dichroism* (*CD) spectra- CD spectra were collected, using a JASCO CD spectrophotometer with a 0.1 cm quartz cuvette (Hellma), at 20°C between 200 and 250 nm; a 8 μM monomer solution in 20 mM Tris-HCl pH 7.2, 300 mM NaCl buffer was used for experiments regarding DNR wild type, while a 18 μM solution in the same buffer was use for DNR-N152stop. To obtain the metal-bound derivative, 0.02-1 mM of a metal solution ($CuCl_2$, $ZnCl_2$, $CaCl_2$, $MgCl_2$, $MnCl_2$, $CuSO_4$) was added, if indicated.
Equilibrium thermal denaturations were followed at 222 nm, between 20°C and 80°C, using the experimental conditions reported above. The data were analysed according to standard two-state equation (Fersht, 1999) for thermal unfolding:

$$\Delta G_{D\text{-}N(T2)} = \Delta H_{D\text{-}N(T1)} + \Delta C_p(T2\text{-}T1) - T2\,(\Delta S_{D\text{-}N(T1)} + \Delta C_p(T2/T1))$$

where ΔC_p was estimated from the size of the protein and from literature data (Myers *et al.*, 1995 and Privalov *et al.*, 1971). Variation of the value of ΔC_p does not affect the calculation of the free energy of unfolding. Three measurements were averaged to determine the T_m.

5.4 Crystallization and Data processing of DNR-N152stop

Native DNR-N152stop – DNR-N152stop was concentrated up to 3.3 mg/ml in 20 mM Tris/HCl pH 7.2, 150 mM NaCl after the PCT (Per Crystallization Test, Hampton Research) and initial crystallization trials were performed with the hanging drop technique, using reagents supplied by Hampton Research (Crystal Screen 1-2).
Crystals appeared in 4 different conditions at 21°C with drops made mixing equal volumes (1μl) of protein solution and reservoir solution and allowed to equilibrate against 0.5 ml of the same reservoir (vapour diffusion method; Ducruix and Giegè, 1992).
The best crystals were observed in 0.1 M HEPES pH 7.5, 8% v/v ethylen glycol, 10% w/v PEG 8000 solution (n.37 Crystal Screen 2, Hampton). Crystal obtained in these condition did not diffract further than 7 Å resolution, thus were used for micro-seeding (see appendix A for method description). After optimisation, the best crystals were grown in 3-4 days at 21°C in 17% w/v PEG 4000, 0.1 M sodium citrate pH 7.4, 0.2 M ammonium phosphate. The droplets were made using the hanging drop vapour diffusion method (Ducruix and Giegè, 1992) by mixing 1.5 μl of protein

solution (2.3 mg/ml in 20 mM Tris/HCl pH 7.2, 150 mM NaCl) and 1.5 µl of a solution of reservoir (0.5 ml) containing crystalline seeds (10^{-4} dilution) of DNR-N152stop.
Crystals were cryoprotected in 10% glycerol, 20% w/v PEG 4000, 0.1 M sodium citrate pH 7.4, 0.2 M ammonium phosphate.
Data were collected at 100K on single crystals at European Synchrotron Radiation Facilities (ESRF), Grenoble, France, beamline ID14-3 equipped with a MAR CCD 165mm detector camera, and diffracted up to 2.3 Å resolution. All data were processed and scaled using DENZO and SCALEPACK (Otwinowski, 1993), and crystals belong to the C2 space group (a=54.76 Å, b=105.77 Å, c=74.86 Å, β = 98.21°), with 3 monomers in the AU, a solvent content of 40.5%, mosaicity of 0.85, R_{merge}=0.041 and χ^2=0.939.

DNR-N152stop Selenomethionine derivative – Seleno-methionine derivative was expressed and purified as described above. Single crystals were obtained in 2 days with the sitting drop tecnique (Ducruix and Giegè, 1992) by mixing 1 µl of selenomethionine derivatized protein solution (3.3 mg/ml in 20 mM Tris/HCl pH 7.2, 150 mM NaCl, 2 mM β-mercaptoethanol) and 1 µl of a solution of reservoir (0.5ml) composed of: 16% w/v PEG 4000, 0.1M Tris/HCl pH 8.0, 75mM ammonium solfate, 3% v/v ethylen glycol. Cryoprotection of the crystals was performed by gently adsorbing small volumes of mother liquor from the droplet with a paper wick (Jena Bioscience) and replacing it with the cryoprotectant solution made of: 20% w/v PEG 4000, 0.1M Tris/HCl pH 8.0, 75mM ammonium solfate, 15% v/v ethylen glycol. MAD data were collected at 100K on single crystals at ESRF, Grenoble, France, beamline ID14-4 equipped with a ADSC Quantum4 CCD detector, the radiation wavelength was set to 0.9795, 0.9797 and 0.9724 Å. The crystal, at the peak wavelength, diffracted at 3.1 Å resolution. Only the first 180 frames from the peak data set were used for SAD phasing, due to sever radiation damage. Data were processed and scaled using DENZO and SCALEPACK (Otwinowski, 1993), crystals belong the $P2_1$ space group (*a* = 57.05 Å, *b* = 167.73 Å, *c* = 59.10 Å, β = 116.93°) with 6 monomers in the AU, a solvent content of 48.8%, mosaicity of 0.5, R_{merge}=0.086 and χ^2=0.992

5.5 DNR-N152stop Structure solution and refinement

The positions of heavy atom sites were found using SOLVE (Terwilliger and Berendzen, 1999) leading to a figure of merit *m* of 0.23. Solvent flattening was performed using RESOLVE (Terwilliger a, 1999). RESOLVE uses a statistical approach to combine experimental X-ray diffraction information with knowledge about the expected characteristics of an electron density map of a macromolecule. The figure of merit after RESOLVE improved significantly to 0.43. Further density

modification and phase extension to 2.8 Å resolution was performed using PIRATE (Cowtan, 2000). PIRATE performs statistical phase improvement by classifying the electron density map by sparseness/denseness and order/disorder and often gives better results than conventional methods based on solvent flatterning.
The maps obtained with this first set of phases allowed us to build a first partial model consisting of the three dimers in the AU. The monomer of this partial structure was used as search model for molecular replacement in the higher resolution (2.3 Å) native data-set. A high number of solutions, coming from both PHASER (McCoy *et al.,* 2005) and MOLREP (Vagin *et al.*, 1997), where cross-checked to extract a final reliable solution of three monomers in the AU. The molecular replacement step was complicated by the presence of the third molecule in the AU. Monomer C, in fact, forms the physiological dimer with a symmetry related molecule, having the dimerization coincident with the crystallographic two-fold rotation axis.
Building and refinement was carried out using COOT (Emsley & Cowtan, 2004) and REFMAC5 (Murshudov *et al*., 1997). Refinement with REFMAC5 was alternated with steps of density modification by solvent flatterning, histogram matching and NCS averaging in DM (Cowtan, 1994). In the last stage translation-libration-screw (TLS) refinement were carried out using REFMAC5 (Winn *et al.,* 2001), single monomers were chosen as TLS groups.
Final statistics are the following: Rfac = 0.276 Rfree = 0.313 FOM = 0.720
rms bonds = 0.012 rms angles = 1.846. Further refinement is needed.

5.6 Modelling

Heme docking - Heme-b coordinates were extracted from PDB using the tool *get momomer* in COOT (Emsley & Cowtan, 2004). Coordinates of DNR-N152stop and the heme were manually docked using COOT by assuming that the possible heme proximal ligand is His-15 and the two propionate groups of heme are involved in separate electrostatic interactions one with the amino group of Lys-133 and the other with the amino group of Asn-82. The side chains of the residues Leu-16, Glu-86 and Lys-133 had to be moved from the original position because of close contacts with the heme, as well as Glu-76 that was making unfavourable electrostatic contacts with one propionate group, in this case and alternative allowed rotamers were chosen. Careful visual inspection, to adjust geometry and orientation of the heme plane with respect to the histidine ligand, was done with the kind help of Dr. Veronica Morea (National Research Council, Molecular Biology and Pathology Institute of Rome) using INSIGHT II (Molecular Structure Inc.). Ten cycles of structure idealization were carried out in REFMAC and the His-Fe distance was refined to the value of 1.85 Å.

HTH domain - The C-terminal HTH domain was modelled using as template the 1.9 Å structure of an homologue transcription factor from *Porphyromonas gingivalis* with pdb code 2gau (Zhang *et al.,* 2006 to be published). A superimposition of the sensing domains was initially performed using SSM (Krissinel and Henrick, 2004) implemented in COOT (Emsley & Cowtan, 2004). The two dimerization helices were then manually superimposed. The C-terminal residues of DNR-N152stop structure were deleted leaving the conserved Arg-137 as new C-terminal of the model. Based on the structural alignment of the two dimerization helices the model was completed, from residue 138 to 227, by adding a polyalanine backbone taken from 2gau structure. The HTH-motif and the second half of the C-helix coming from the 2gau structure were then further modelled to bring the dimerization helices in a coiled-coil conformation, that is found in the other structures of CRP-FNR superfamily proteins, and with the backbone distance at the dimerization interface of 6 Å.

REFERENCES

Anantharaman, V., Balaji, S. and Aravind L. (2006) The signaling helix: a common functional theme in diverse signaling proteins, *Biology Direct* 2006, **1**:25

Andrew, C.R., Green, E.L., Lawson, D.M. and Eady, R.R. (2001) Resonance Raman studies of cytochrome *c′* support the binding of NO and CO opposite sides of the heme: implication for ligand discrimination in heme-based sensors. *Biochemistry* **10**, 4115-4122.

Antonini, E. and Brunori, M. (1971) Hemoglobin and Myoglobin in their Reactions with Ligands, North-Holland Publishing.

Aono, S. (2003) Biochemical and Biophysical properties of the CO-Sensing Transcriptional Activator CooA, *Acc. Chem. Res.* **36**, 825-831.

Aono, S., Nakajima, H., Saito, K. and Okada, M. (1996) A Novel Heme Protein That Acts as a Carbon Monoxide-Dependent Transcriptional Activator in *Rhodospirillum rubrum*, *Biochem. Biophys.Res. Commun.* **228**, 752-756.

Arai, H., Igarashi, Y. and Kodama, T. (1995) Expression of the nir and nor genes for denitrification of Pseudomonas aeruginosa requires a novel CRP/FNR-related transcriptional regulator, DNR, in addition to ANR, *FEBS Lett.* **371**, 73-76.

Arai, H., Kodama, T. and Igarashi, Y. (1997) Cascade regulation of the two CRP/FNR-related transcriptional regulators (ANR and DNR) and the denitrification enzymes in Pseudomonas aeruginosa, *Mol. Microbiol.* **25**, 1141-1148.

Arai H., Kodama, T. and Igarashi, Y. (1999) Effect of nitrogen oxides on expression of the nir and nor genes for denitrification in Pseudomonas aeruginosa, *FEMS Microbiol. Lett.* **170**,19-24.

Arai, H., Mizutani, M. and Igarashi, Y. (2003) Transcriptional regulation of the nos genes for nitrous oxide reductase in Pseudomonas aeruginosa, *Microbiology* **149**, 29-36.

Arai, H., Hayashi, M., Kuroi, A., Ishii, M. and Igarashi, Y. (2005) Transcriptional regulation of the flavohemoglobin gene for aerobic nitric oxide detoxification by the

second nitric oxide-responsive regulator of Pseudomonas aeruginosa, *J. Bacteriol.* **187**, 3960-3968.

Barraud, N., D. J. Hassett, S.-H. Hwang, S. A. Rice, S. Kjelleberg, and J. S. Webb. (2006). Involvement of nitric oxide in biofilm dispersal of *Pseudomonas aeruginosa*. *J. Bacteriol*. **188**, 7344-7353.

Bastian, N.R. and Hibbs, J.B. (1994) Assembly and regulation of NADPH oxidase and nitric oxide synthase, *Curr. Opin. Immunol*. **6**, 131-139.

Blaszczyk, U., Wasylewski, Z. (2003) Interaction of cAMP receptor protein from Escherichia coli with cAMP and DNA studied by differential scanning calorimetry, *J Protein Chem.* **22**, 285-93.

Blow, D. M., and Crick, F. H. C. (1959). *Acta Cryst*. **12**, 794-802.

Boon, E.M. and Marletta, M.A., (2005) Ligand discrimination in soluble guanylate cyclase and the H-NOX family of heme sensor proteins *Curr. Op. Chem. Biol.* **9**, 441–446.

Botsford J.L. and Harman J.G., (1992), Cyclic AMP in prokaryotes, *Microbiol. Rev.*, **56**, 100-122.

Brooun, A., Liu, S. and Lewis. K. **(**2000). A dose-response study of antibiotic resistance in *Pseudomonas aeruginosa* biofilms. *Antimicrob. Agents Chemother*. **44,** 640–646.

Brünger, A. T., Adams, P. D., Clore, G. M., DeLano, W. L., Gros, P., Grosse-Kunstleve, R. W., Jiang, J.-S., Kuszewski,J., Nilges, M., Pannu, N. S., Read, R. J., Rice, L. M., Simonson, T. and Warren, G. L. *Acta Cryst.* D **54**, 905-921.

Brunelli, L., Crow, J.P., and Beckman, J.S. (1995) The comparative toxicity of nitric oxide and peroxynitrite to *Escherichia coli*, *Arch. Biochem. Biophys.* **316**, 327-334.

Busby S., Ebright R.H., (1999) Transcription activation by catabolite activator protein (CAP), *J. Mol. Biol.*, **293**, 199-213.

Chu, S.Y., Tordova, M., Gilliland, G.L., Gorshkova, I., Shi, Y., Wang, S., Schwarz, F.P. (2001) The structure of the T127L/S128A mutant of cAMP receptor protein facilitates promoter site binding 1 *J.Biol.Chem*. : **276**, 11230-11236.

Corker, H. and Poole, R., (2003) Nitric oxide formation by Escherichia coli. Dependence on nitrite reductase, the NO-sensing regulator Fnr, and flavohemoglobin Hmp, *J Biol Chem.* **278** 31584-92.

Costerton, J. W., Stewart, P. S. and Greenberg, E. P. (1999), Bacterial biofilms: a common cause of persistent infections. *Science.* **284**, 1318–1322.

Cowtan, K. (2000) General quadratic functions in real and reciprocal space and their application to likelihood phasing, *Acta Cryst. D.* **55** (12) 1612-1619.

Cowtan, K. D. & Zhang, K. Y. (1999). *Prog.Biophys. Mol. Biol.* **72**, 245-270.

Cowtan, K. (1994). Joint CCP4 and ESF-EACBM Newsletters on Protein Crystallography. **31**, 34-38.

Cruz-Ramos, H., Crack, J., Wu, G., Hughes, M.N., Scott, C., Thomson, A.J., Green, J. and Poole, R.K. (2002) NO sensing by FNR: regulation of the Escherichia coli NO-detoxifying flavohaemoglobin, Hmp, *EMBO J.* **21**, 3235-3244.

Denninger J.W. and Marletta M.A, (1999) Guanylate cyclase and the NO/cGMP signaling pathway. *Biochim Biophys Acta*, **1411**:334-350.

Dodson, E. (2003) is it Jolly SAD?, *Acta Cryst. D* **59**, 1958-1965

Ducruix, A. and Giegè, R. (1992). Crystallization by vapour diffusion methods. In: Crystallization of Nucleic acids and proteins. Eds: A. Ducruix and R. Giegè. IRL Press (Oxford, U.K.). pp 82-89.

Dundas, J., Ouyang, Z., Tseng, J., Binkowski, A., Turpaz, Y. and Liang J. (2006) CASTp: computed atlas of surface topography of proteins with structural and topographical mapping of functionally annotated resiudes. *Nucleic Acid Research*, **34**:W116-W118.

Eiting, M., Hagelűken, G., Schubert, W.D., Heinz, D.W., (2005) The mutation G145S in PrfA, a key virulence regulator of *Listeria monocytogenes,* increases DNA-binding affinity by stabilizing the HTH motif, *Molecular Microbiology* **56,** 433-446.

Emsley, P. and Cowtan, K. (2004) Coot:model-building tools for molecular graphics, *Acta Cryst. D* **60** (12) 2184-2195.

Fersht, A. (1999) Structure & Mechanism in Protein Science: A Guide to Enzyme Catalysis & Protein Folding, W. H. Freeman & Company.

Fux, C. A., J. W. Costerton, P. S. Stewart, and P. Stoodley. (2005). Survival strategies of infectious biofilms. *Trends Microbiol*. 13, 34-40.

Galimand, M., Gamper, M., Zimmermenn, A. and Haas, D. (1991) Positive FNR-like control of anaerobic arginine degradation and nitrate respiration in Pseudomonas aeruginosa, *J. Bacteriol.* **173**, 1598-1606.

Gilles-Gonzalez, M.A and Gonzalez, G. (2005) Heme-based sensors: defining characteristics, recent developments, and regulatory hypotheses. *J Inorg Biochem*, **99**, 1-22.

Green, J., Scott, C. and Guest, J.R. (2001) Functional versatility in the CRP-FNR superfamily of transcription factor: FNR and FLP, *Adv. Microbiol. Rev.* **44**, 1-34.

Guest, J.R., Green, J., Irvine, A.S. and Spiro, S. (1996) The FNR modulon and FNR-regulated gene expression. In: Regulation of Gene Expression in *Escherichia coli* (Lin, E.C.C. and Lynch, A.S., Eds.), pp. 317-342. Chapman and Hall, New York.

Harman, J. G. (2001) Allosteric regulation of the cAMP receptor protein, *Biochimica et Biophysica Acta*, **1547**, 1-17.

Hassett, D.J., Cuppoletti, J., Trapnell, B., Lymar, S.V., Rowe, J.J., Yoon, S.S., Hilliard, G.M., Parvatiyar, K., Kamani, M.C., Wozniak, D.J., Hwang, S.H., McDermott, T.R. and Ochsner, U.A. (2002) Anaerobic metabolism and quorum sensing by Pseudomonas aeruginosa biofilms in chronically infected cystic fibrosis airways: rethinking antibiotic treatment strategies and drug targets, *Adv. Drug. Deliv. Rev.* **54**, 1425-1443.

Hunt, S. M., E. M. Werner, B. Huang, M. A. Hamilton, and P. S. Stewart. (2004). Hypothesis for the role of nutrient starvation in biofilm detachment. *Appl. Environ. Microbiol*. **70**, 7418–7425.

Hendrickson, W. A., and Lattman, E. E. (1970). *Acta Cryst.* B26, 136-143.

Hentzer, M. and Givskov, M. (2003) Pharmacological inhibition of quorum sensing for the tratment of chronic bacterial infections. *J. Clin. Invest.* **112**, 1300-1307.

Heyduk, T. and Lee, J.C. (1989) Escherichia coli cAMP receptor protein: evidence for three protein conformational states with different promoter binding affinities, *Biochemistry* **28**, 6914-24.

Horowitz, P.M. and Criscimagna, N.L. (1985) Differential binding of the fluorescent probe 8-anilinonaphthalene-2-sulfonic acid to rhodanese catalytic intermediates, *Biochemistry* **24**, 2587-93.

Huie, R.E. and Padmaja, S. (1993) The reaction of NO with superoxide, *Free Radic. Res. Commun*. **18**, 195-199.

Hunt, S. M., Werner, E. M., Huang, B., Hamilton, M. A. and Stewart. P. S., (2004). Hypothesis for the role of nutrient starvation in biofilm detachment. *Appl. Environ. Microbiol*. **70**, 7418–7425.

Iyer, L.M., Anantharaman V., Aravind, L. (2003) Ancient conserved domains shared by animal soluble guanylyl cyclases and bacterial signaling proteins. *BMC Genomics*, **4**, 5.

Jones, D.T. (1999) Protein secondary structure prediction based on position-specific scoring matrices. *J. Mol. Biol.* **292**, 195-202.

Joyce, M.G., Levy, C., Gàbor, K., Pop, M.S., Biehl, B.D., Doukov, T.I., Ryter, J.M., Mazon, O., Smidt, H., van der Heuvel, R.H.H., Ragsdale, S.W., van der Oost, J.,Leys, D., (2006) CprK Crystal Structure Revel Mechanism for Transcriptional Control of Halorespiration, *J. Biol. Chem.* **281,** 28318-28325.

Karow D.S., Pan D., Tran R., Pellicena P., Presley A., Mathies R.A. and Marletta M.A, (2004) Spectroscopic characterization of the soluble guanylate cyclase-like heme domains from Vibrio cholerae and Thermoanaerobacter tengcongensis. *Biochemistry*, **43**, 10203-10211.

Kiley, P.J. and Beinert, H. (1999) Oxygen sensing by the global regulator, FNR: the role of the iron-sulfur cluster, *FEMS Microbiol. Rev.* **22**, 341-352.

Kim, J., Adhya, S. and Garges S. (1992) Allosteric Changes in the cAMP Receptor Protein of Escherichia coli: Hinge Reorientation *PNAS*, **89**, 9700-9704.

Koesling, D. (1999) Studing the structure and the regulation of soluble guanylyl cyclase, *Methods* **19**, 485-493.

Kolb A., Busby S., Buc H., Garges S., Adhya S., (1993) Transcriptional regulation by cAMP and its receptor protein, *Annu. Rev. Biochem.*, **62**,. 749-795.

Körner, H., Sofia H.J. and Zumft, W.G. (2003) Phylogeny of the bacterial superfamily of Crp-Fnr transcription regulators: exploiting the metabolic spectrum by controlling alternative gene programs, *FEMS Microbiol. Rev.* **27**, 559-592.

Krissinel, E. and Henrick, K. (2004) Secondary-structure matching (SSM), a new tool for fast protein structure alignment in three dimensions, *Acta Cryst. D,* **60**, 2256-2268.

Kuchinskas, M, Li, H., Conrad, M., Roberts, G. and Poulos, T.L. (2006) The Role of the DNA-Binding Domains in CooA Activation *Biochemistry*, **45***,* 7148-7153.

Kwiatkowski, A.V. and Shapleigh, J.P. (1996) Requirement of nitric oxide for induction of genes whose products are involved in nitric oxide metabolism in Rhodobacter sphaeroides 2.4.3., *J. Biol. Chem.* **271**, 24382-8.

Lanzilotta, W. N., Schuller, D. J., Thorsteinsson, M. V., Kerby, R. L., Roberts, G. P., and Poulos, T. L. (2000) Structure of the CO sensing transcription activator CooA, *Nat. Struct. Biol.* **7**, 876-880.

Leslie, A. G. W. (1988). In Proceedings of the CCP4 Daresbury Study Weekend. Warrington: Daresbury Laboratory.

Mai-Prochnow, A., F. Evans, D. Dalisay-Saludes, S. Stelzer, S. Egan, S. James, J. S. Webb, and S. Kjelleberg. (2004). Biofilm development and cell death in the marine bacterium *Pseudoalteromonas tunicata*. *Appl. Environ. Microbiol.* **70**, 3232–3238.

Matthews, B. W. (1968). Solvent content of protein crystals. *J.Mol.Biol.* **33**, 491-497.

McKay, D.B. and Steitz, T.A. (1981) Structure of catabolite gene activator protein at 2.9 A resolution suggests binding to left-handed B-DNA, *Nature (London)* **290**, 744-749.

McCoy, A.J., Grosse-kunstleve, R.W.,Storoni, L.C. and Read, R.J., (2005) Likelihood-enhanced fast translation function, *Acta Cryst. D* **61**, 458-464.

Murshudov, G. N., Vagin, A. A. and Dodson, E. J. (1997). Refinement of macromolecular structures by the maximum-likelihood method. *Acta Crystallogr.D.Biol.Crystallogr.* **53**, 240-255.

Myers, J.K., Pace, C.N. and Scholtz, J.M. (1995) Denaturant m values and heat capacity changes: Relation to changes in accessible surface areas of protein unfolding, *Protein Sci* **4**, 2138-2148.

Nathan, C.F. and Hibbs, J.B. (1991) Role of nitric oxide synthesis in macrophage antimicrobial activity, *Curr. Opin. Immunol*. **3**, 65-70.

Nioche, P., Berka, V., Vipond, J., Minton, N., Tsai, A. and Raman, C. S. (2004) Femtomolar sensitivity of a NO sensor from *Clostridium botulinum, Science* **306**, 1550-1553.

Otwinowski, Z. (1993). Data collection and processing. *Proceedings of the CCP4 study weekend*, 56-62.

Packer, L. (1996) Nitric oxide, part B: Physiological and pathological process, *Method Enzymol* **269**.

Passner, J. M. and Steitz, T. A. (1997) The Structure of a CAP-DNA Complex Having Two Camp Molecules Bound to Each Monomer, *Proc.Nat.Acad.Sci.USA* **94**, 2843-7.

Passner, J. M. Schultz, S.C. and Steitz, T. A. (2000) Modeling the cAMP-induced Allosteric transition Using the Crystal Structure of CAP-cAMP at 2.1 Å Resolution, *J. Mol. Biol.* **304**, 847-59.

Poole, R. K. and Hughes, M. N., (2000) New functions for the ancient globin family: bacterial responses to nitric oxide and nitrosative stress, *Mol. Microbiol.* **36**, 775-783.

Privalov, P.L., Kechinashvili, N.N. and Atanossov, B.A. (1971) Thermodynamic analysis of thermal transitions in globular proteins. I. Calorimetric study of ribotrypsinogen, ribonuclease and myoglobin, *Biopolymer*s **10**,1865-1890.

Purevdorj-Gage, B., W. J. Costerton, and P. Stoodley. (2005). Phenotypic differentiation and seeding dispersal in non-mucoid and mucoid *Pseudomonas aeruginosa* biofilms. *Microbiology* .**151**, 1569–1576.

Ramachandran, G. N. and Raman, S. (1956). *Curr. Sci.* **25**, 348-351.

Reents, H., Gruner, I., Harmening, U., Böttger, L.H., Layer, G., Heathcote, P., Trautwein, A.X., Jahn, D. and Härtig, E (2006) *Bacillus subtilis* Fnr senses oxygen via a [4Fe-4S] cluster coordinated by three cysteine residues without change in the oligomeric state, *Mol. Microbio.* **60**, 1432-1435.

Reynolds, M.F., Parks, R.B., and Burstyn J.N. (2000) Electronic Absorption, EPR, and Resonance Raman Spectroscopy of CooA, a CO-sensing Transcription Activator from *R. rubrum*, Reveals a Five Coordinate NO-Heme. *Biochemistry*, **39**, 388-396.

Rinaldo, S., Giardina, G., Brunori, M., Cutruzzola, F. (2005) N-oxide sensing in Pseudomonas aeruginosa: expression and preliminary characterization of DNR, an FNR-CRP type transcriptional regulator, *Biochem. Soc. Trans.* **33**, 184-6.

Roberts., G.P., Kerby R.L., Youn, H. and Conrad M. (2005) CooA, paradigm for gas sensing regulatory proteins, *J Inorg. Biochem.* **99**, 280-92.

Romeo, T. (2006) When the Party Is Over: a Signal for Dispersal of *Pseudomonas aeruginosa* Biofilms *Journal of Bacteriology*, **188**, 7325-7327.

Rossmann, M. G. & Blow, D. M. (1962). Acta Cryst. **15**, 24-31.

Sambrook, J., Fritsch, E. F., and Maniatis, T. (1989) Molecular cloning: a laboratory manual, 2nd ed., Cold Spring Harbor Laboratory, Cold Spring Harbor, NY.

Sarti, P., Fiori, P.L., Forte, E., Rappeli, P., Teixeira, M., Mastronicola, D., Sanciu, G., Giuffre`, A. and Brunori, M. (2004) *Trichomonas vaginalis* degrades nitric oxide and expresses a flavorubredoxin-like protein: a new pathogenic mechanism?, *Cell. Mol. Life Sci.* **61**, 618–623.

Sauer, K., A. K. Camper, G. D. Ehrlich, J. W. Costerton, and D. G. Davies. (2002). *Pseudomonas aeruginosa* displays multiple phenotypes during development as a biofilm. *J. Bacteriol*. **184**, 1140–1154.

Schultz, S. C., Shields, G. C. and Steitz, T. A. (1991) Crystal structure of a CAP-DNA complex: the DNA is bent by 90 degrees, *Science* **253**, 1001-7.

Singh, P. K., A. L. Schaefer, M. R. Parsek, T. O. Moninger, M. J. Welsh, and E. P. Greenberg. (2000). Quorum-sensing signals indicate that cystic fibrosis lungs are infected with bacterial biofilms. *Nature* **407**, 762–764.

Spiro, S. (1994) The FNR family of transcriptional regulators. *Antonie van Leeuwenhoek* **66**, 23-36.

Sirangelo, I., Bismuto, E., Tavassi, S. and Irace, G. (1998) Apomyoglobin folding intermediates characterized by the hydrophobic fluorescent probe 8-anilino-1-naphthalene sulfonate, *Biochim. Biophys. Acta.* **1385**, 69-77.

Southey-Pillig, C. J., Davies, D. G. and Sauer, K. (2005) Characterization of temporal protein production in *Pseudomonas aeruginosa* biofilms. *J. Bacteriol.* **187**, 8114-8126.

Stryer, L. (1965) the interactoin of a naphtalene dye with apomyoglobin and apohemoglobin. A fluorescent probe of non-polar binding sites. *J. Mol. Biol.,* **13**, 482.495.

Terwilliger, T. C. and Berendzen, J. (1999). Automated MAD and MIR structure solution. *Acta Cryst. D* **55**(4):849-861.

Terwilliger, T. C. (2002). Automated structure solution, density modification and model building. *Acta Cryst. D.* **58**, 1937-1940.

Taylor, G., (2003) The phase problem, *Acta Cryst. D* **59**, 1881-1890.

Toda N. and Okamura T, (2003) The pharmacology of nitric oxide in the peripheral nervous system of blood vessels*. Pharmacol Rev* 2003, **55**, 271-324.

Tomita, T., Fushinobu, S. and Nishiyama, M. (2003) Crystal structure analysis of transcription regulator, Dnr from *Alcaligenes faecalis* S-6. *Biological Science,* 225.

Unden G., (1998) Transcriptional regulation and energetics of alternative respiratory pathways in facultatively anaerobic bacteria, *Biochim. Biophys. Acta*, **1365**, 220-224.

Vagin, A., Teplyakov, A. (1997) MOLREP: an automatedprogram for molecular replacement, *J. Appl. Cryst.* **30**, 1022-1025.

Van Spanning, R.J., Houben, E., Reijnders, W.N., Spiro, S., Westerhoff, H.V. and Saunders, N. (1999) Nitric oxide is a signal for NNR-mediated transcription activation in Paracoccus denitrificans, *J. Bacteriol*. **181**, 4129-4132.

Vollack, K.U. and Zumft, W.G. (2001) Nitric oxide signaling and transcriptional control of denitrification genes in *Pseudomonas stutzeri*, *J. Bacteriol.* **183**, 2516-26.

Waite, R. D., Papakonstantinopoulou, A., Littler, E. and Curtis, M. A. (2005) Transcriptome analysis of *Pseudomonas aeruginosa* growth: comparison of gene expression in planktonic cultures and developing and mature biofilms. *J. Bacteriol*. **187**, 6571-6576.

Wang, B.-C. (1985). *Methods Enzymol.* **115**, 90-112.

Webb, J. S., M. Givskov, and S. Kjelleberg. (2003). Bacterial biofilms: prokaryotic adventures in multicellularity. *Curr. Opin. Microbiol*. **6**, 578–585.

Webb, J. S., L. S. Thompson, S. James, T. Charlton, T. Tolker-Nielsen, B. Koch, M. Givskov, and S. Kjelleberg. (2003). Cell death in *Pseudomonas aeruginosa* biofilm development. *J. Bacteriol*. **185**, 4585–4592.

Wink, D. A. and Mitchell, J. B. (1998) Chemical biology of nitric oxide: Insights into regulatory, cytotoxic, and cytoprotective mechanisms of nitric oxide, *Free Radic. Biol. Med*. **25**, 434-456.

Winn, M. D., Isupov, M. N., and Murshudob, G. N. (2001) *Acta Crystallogr.Sect. D Biol. Crystallogr.* **57**, 122–133.

Wisén, S., Sjögren, T., Olin, B. and Mannervik, B. (2004) Purification, crystallizatoin and preliminary X-ray data of the transcription factor NtcA from the cyanobacterium *Anabaena* PCC 7120, *Acta Cryst. D,* **60**, 923-925.

Yoon, S. S., R. F. Hennigan, G. M. Hilliard, U. A. Ochsner, K. Parvatiyar, M. C. Kamani, H. L. Allen, T. R. DeKievit, P. R. Gardner, U. Schwab, J. J. Rowe, B. H. Iglewski, T. R. McDermott, R. P. Mason, D. J. Wozniak, R. E. Hancock, M. R. Parsek, T. L. Noah, R. C. Boucher, and D. J. Hassett. (2002). *Pseudomonas aeruginosa* anaerobic respiration in biofilms: relationships to cystic fibrosis pathogenesis. *Dev. Cell*. **3**, 593–603.

Yoon, S. S., Coakley, R., Lau, G. W., Lymar, S. V., Gaston, B., Karabulut, A. C., Hennigan, R. F, Hwang, S.-H., Buettner, G., Schurr, M. J., Mortensen, J. E., Burns, J. L., Speert, D., Boucher, R. C. and Hassett, D. J. (2006). Anaerobic killing of mucoid *Pseudomonas aeruginosa* by acidified nitrite derivatives under cystic fibrosis airway conditions. *J. Clin. Investig*. **116**, 436-446.

Yu, S and Lee, J. C. (2004) Role of Residue 138 in the Interdomain Hinge Region in Transmitting Allosteric Signals for DNA Binding in *Escherichia coli* cAMP Receptor Protein *Biochemistry*, **43***,* 4662-4669.

Zumft, W.G. (1997) Cell biology and molecular basis of denitrification, *Microbiol. Mol. Biol. Rev.* **61**, 533-616.

Zumft, W.G. (2002) Nitric oxide signaling and NO dependent transcriptional control in bacterial denitrification by members of the FNR-CRP regulator family, *J. Mol. Microbiol. Biotechnol.* **4**, 277-86.

Protein crystallization

Crystallization of macromolecules is very complex and poorly understood. A theoretical treatment of it, despite recent progress, is at present impossible. Protein crystallization is mainly a trial and error procedure in which the protein is slowly precipitated from its solution. As a general rule however, the purer protein, the better the chances to grow crystals. Growth of protein crystals starts from a supersaturated solution of the macromolecule, and evolves towards a thermodynamically stable state in which the protein is partitioned between a solid phase and the solution.

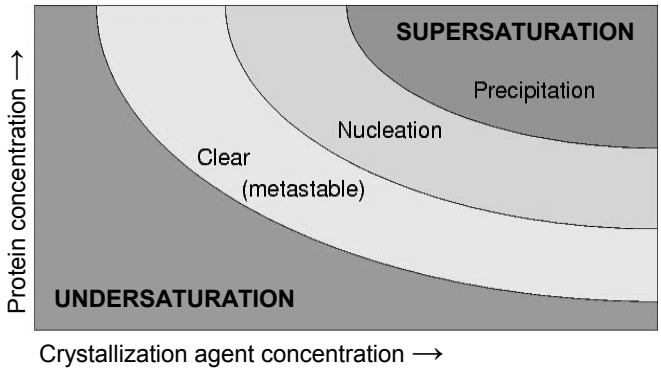

Figure 1
Phase Diagram showing zones for crystal nucleation, growth and precipitation.

Crystallization can be carried out by using different techniques, among them the crystallization in batch, the liquid-liquid diffusion methods, the crystallization under dialysis and the vapour diffusion technique. The vapour diffusion technique is the most used one and can performed by two different methods (Ducruix and Geigè, 1992) as shown in Figure 2.

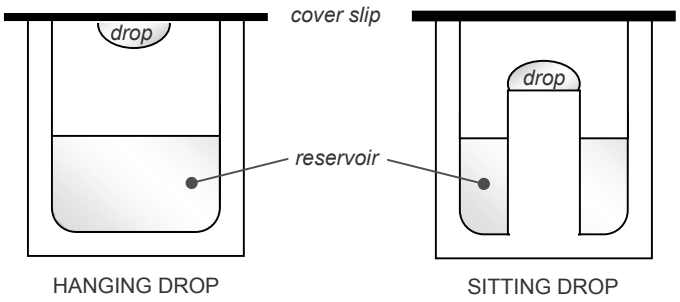

Figure 2 *Vapour diffusion crystallization techniques*

In the *Hanging Drop* method drops are prepared on a siliconized microscope glass cover slip by mixing 1 to 5 μl of protein solution with the same volume of precipitant solution. The slip is placed upside-down over a depression in a tray; the depression is partly filled with the required precipitant solution (reservoir solution). The chamber is sealed by applying oil or grease to the circumference of depression before the cover slip is put into place. The *Sitting Drop* is preferable if the protein solution has a low surface tension or if one wants to decrease the equilibrium rate between drop solution and reservoir solution.

Crystal macro and micro seeding – In micro-seeding very small crystals (seeds), obtained by breaking bigger crystals, are transfer to a drop that will support the growth of potentially larger and more perfect crystals. In marco-seeding one single crystal is transfer to a drop that will support its growth (Figure 3).
A seed can provide a template on which additional macromolecules can assemble and under the proper conditions, grow to form a large single crystal. Using seeding can avoid problems associated with the formation of too many nuclei during nucleation. Seeds can grow into larger crystals in the metastable region of the solubility curve, which is a region of lower, relative supersaturation.

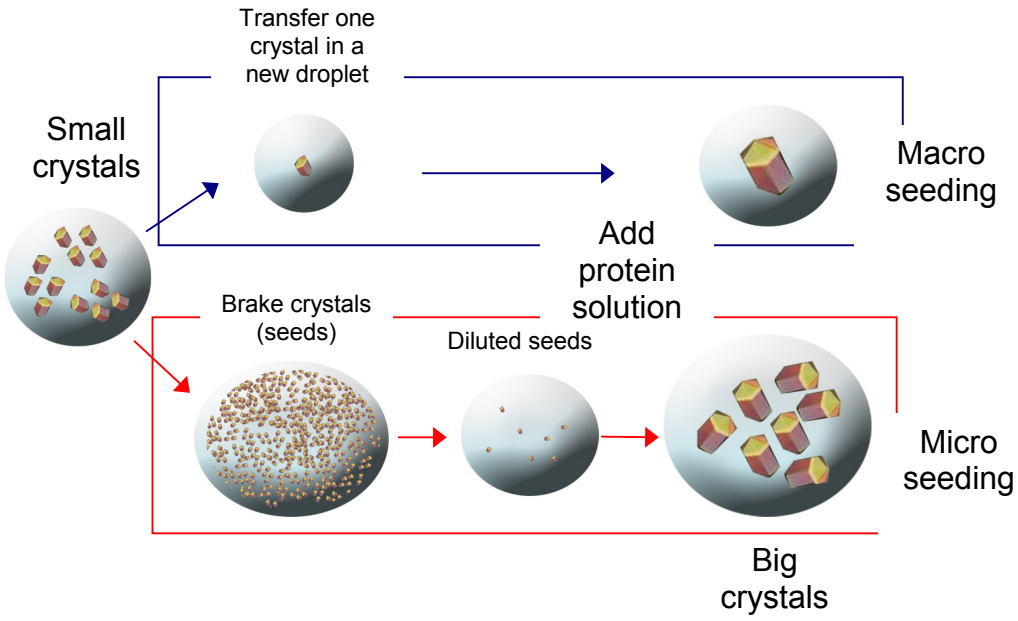

Figure 3 *macro (top)and micro (bottom) seeding procedures to obtain bigger crystals from small non diffracting crystals*

Basic mathematical concepts in Crystallography

Fourier series – a Fourier series is a sum of simple periodic functions (*Fourier terms*) that describes or approximates a complicated periodic function.

$$f(x) = \sum_h F_h \, e^{2\pi i(hx)}$$

Constructing a Fourier series - that is, determining the proper F, h and α values to approximate the complex periodic function – is called *Fourier synthesis.* Decomposing a complicated periodic function into its components is the *Fourier analysis.*

Fourier transform (FT) – Fourier demonstrated that for any function f(x), there exists another function F(h) such that

$$F(h) = \int_S f(x) \, e^{2\pi i(hx)} \, dx$$

Where F(h) is called the *Fourier Transform (**FT**)* of f(x). The units of the variable *h* are reciprocal of the units of *x.* The Fourier transform is reversible, this means that you can go from F(h) to f(x) by *back transforming (**FT**$^{-1}$)*

$$f(x) = \int_S F(h) \, e^{-2\pi i(hx)} \, dh$$

Structure factors and electron density function – when X rays hit the crystal they are diffracted by the atoms electrons. This diffracted beams will interphere and only the ones that meet the Bragg's law (see below) will be recorded. We call each diffracted beam *reflection* (because its as if the diffracted beam was reflected by a mirror parallel to the planes hkl, see below). Each reflection is a complicated wave, the sum of diffracting contribution from all atoms in the unit cell, and is described by a Fourier series whose terms are the atomic *scattering factors* of single atoms (f_j). This Fourier series is called *structure factor* $\boldsymbol{F_{hkl}}$.

$$F_{hkl} = \sum_j f_j \, e^{2\pi i(hxj+kyj+lzj)}$$

We can also think at F_{hkl} as the sum of contributions of electron density from each volume element in the unit cell (V), so being ρ(x, y, z) the average value of the volume element centred in (x, y, z) and integrating over the entire unit cell we can write

$$F_{hkl} = \int_V \rho(x, y, z) \, e^{\,2\pi i\,(hx+ky+lz)} \, dV$$

We can see then that F_{hkl} is the Fourier Transform of the electron density ρ(x, y, z) on the set of real lattice planes (hkl). Back transforming and considering that the reflections (structure factors F_{hkl}) are a set of discrete entities we have

$$\rho(x, y, z) = 1/V \sum_{hkl} F_{hkl} e^{-2\pi i (hx+ky+lz)}$$

Calculated structure factors (F_c or F_{calc}) - for a real experiment become more complicated and more refining parameters must be added

$$F_c = G \sum_j n_j f_j e^{2\pi i (hxj+kyj+lzj)} e^{-\mathbf{Bj} (\sin\theta / \lambda)^2}$$

Where:

G Overall ***Scale factor*** to put all F_cs on a convenient numerical scale

n_j ***Occupancy*** of the atom j

f_j ***Scattering factior*** of the atom j – depending on the nature of the atom and determining the amplitude of the contribution to F_c. The contribution falls off at higher diffraction angles, i.e. at higher esolution.

(xj, yj, zj) ***Coordinates*** in real space of the atom j - determining the phase of the contribution to F_c

Bj ***Temperature factor*** or ***B-factor*** accounting for vibration of the atom j around its rest position. In the simplest case, isotropic vibration, is equal to $\boldsymbol{8\pi^2 \langle u_j^2 \rangle}$ where $\langle u_j^2 \rangle$ is the mean-square displacement of the atom j. notice that the contribution of the B-factor to F_c depends on the angle of the reflection θ.

Conditions that produce diffraction, Bragg's law – In the crystal lattice three indices ***hkl*** identify a particular set of equivalent parallel planes. ***h*** gives the number of parts in which the edge a of the unit cell is cut by that specific set of planes, similarly ***k*** and ***l*** determine the number of parts in which the edges b and c are cut by the set of planes Figure 1, A. W.L. Bragg showed that a set of parallel planes with index hkl and interplanar spacing d_{hkl} produce a diffracted beam when X rays of wavelength λ impinge upon the planes at an angle θ and are reflected at the same angle, only if θ meets the following condition

$$\mathbf{2\, d_{hkl} \sin\theta = \mathit{n}\, \lambda}$$ where *n* is an integer.

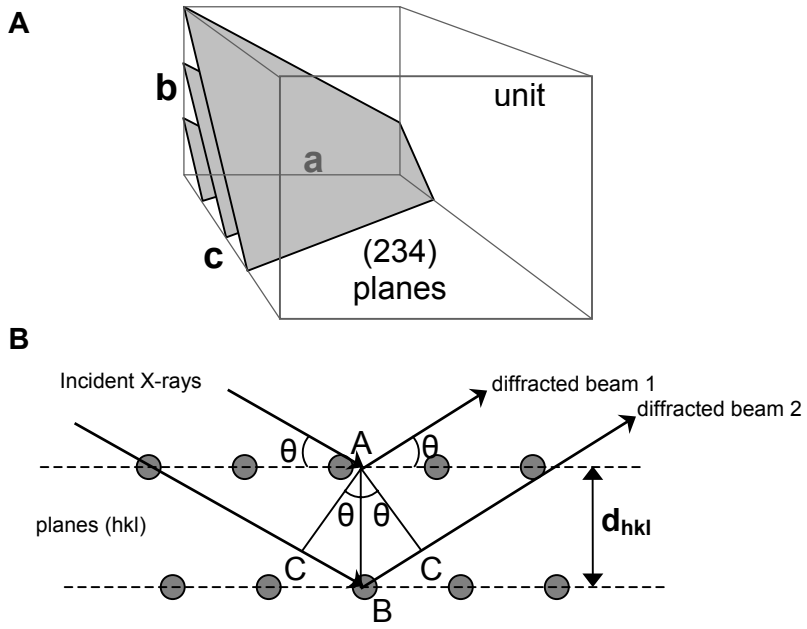

***Figure 1**. A) Parallel planes with indices (234). B) Geometric construction for Bragg's law. BC=ABsinθ=d_{hkl}sinθ*

Bragg's law is simply stating that, in order to interphere positively, emerging diffracted beams from the crystal must have a difference in *path length* equal to an integer number of *wavelengths.* The geometric construction in Figure 1-B, in which the dots represent two parallel planes of lattice points, helps to immediately relate the diffraction angle 2θ (angle between the incident X rays and the diffracted beams) with the indices hkl and certain interplanar distance d_{hkl} . The difference in *path length* for diffracted beam1 and 2 is equal to *2BC* that is $2d_{hkl}sin\theta$, imposing it to be equal to $n\lambda$ we get the Bragg's law.

The Phase problem

In the diffraction experiment (Figure. 2), we measure the intensities of waves scattered from planes (denoted by hkl) in the crystal. The amplitude of the wave $|F_{hkl}|$ is proportional to the square root of the intensity measured on the detector. To calculate the electron density at a position (x,y,z) in the unit cell of a crystal requires us to perform the following summation over all the hkl planes, which in words we can express as: electron density at (x,y,z) = the sum of contributions to the point (x,y,z) of waves scattered from plane (h,k,l) whose amplitude depends on the number of electrons in the plane, added with the correct relative phase relationship or, mathematically;

$$\rho(x,y,z) = 1/V \sum_{hkl} \left| F_{hkl} \right| e^{i\boldsymbol{\alpha hkl}} e^{-2\pi i(hx+ky+lz)}$$

where V is the volume of the unit cell and $\boldsymbol{\alpha_{hkl}}$ is the phase associated with the structure-factor amplitude $|F_{hkl}|$. We can measure the amplitudes, but the phases are lost in the experiment. *This is the phase problem*.

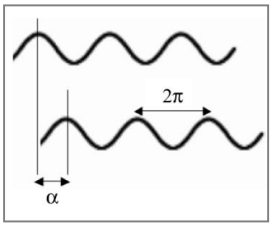

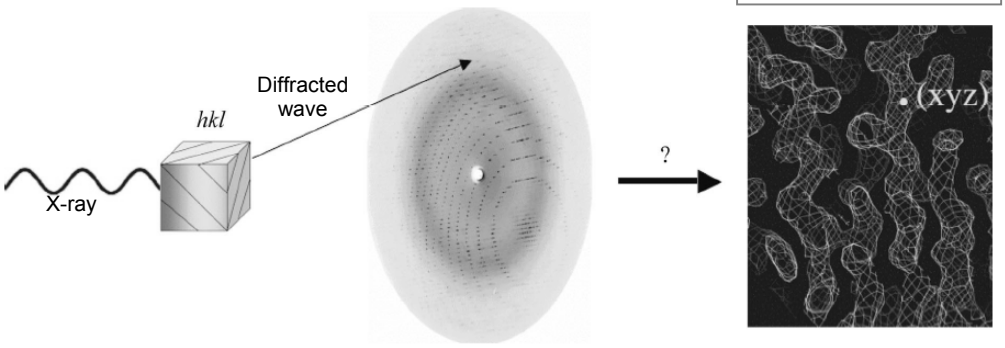

Figure 2 *The diffraction experiment*

The importance of phases in producing the correct structure is illustrated in Figures 3 and 4. In Figure 3 three electron-density waves are added in a unit cell, which shows the dramatically different electron density resulting from adding the third wave with a different phase angle. In Figure 4, from Kevin Cowtan's Book of Fourier (http://www.ysbl.york.ac.uk/~cowtan/fourier/fourier.html), the importance of phases in carrying structural information is beautifully illustrated. The calculation of an electron-density map using amplitudes from the diffraction of a duck and phases from the diffraction of a cat results in a cat: a warning of model-bias problems in molecular replacement!

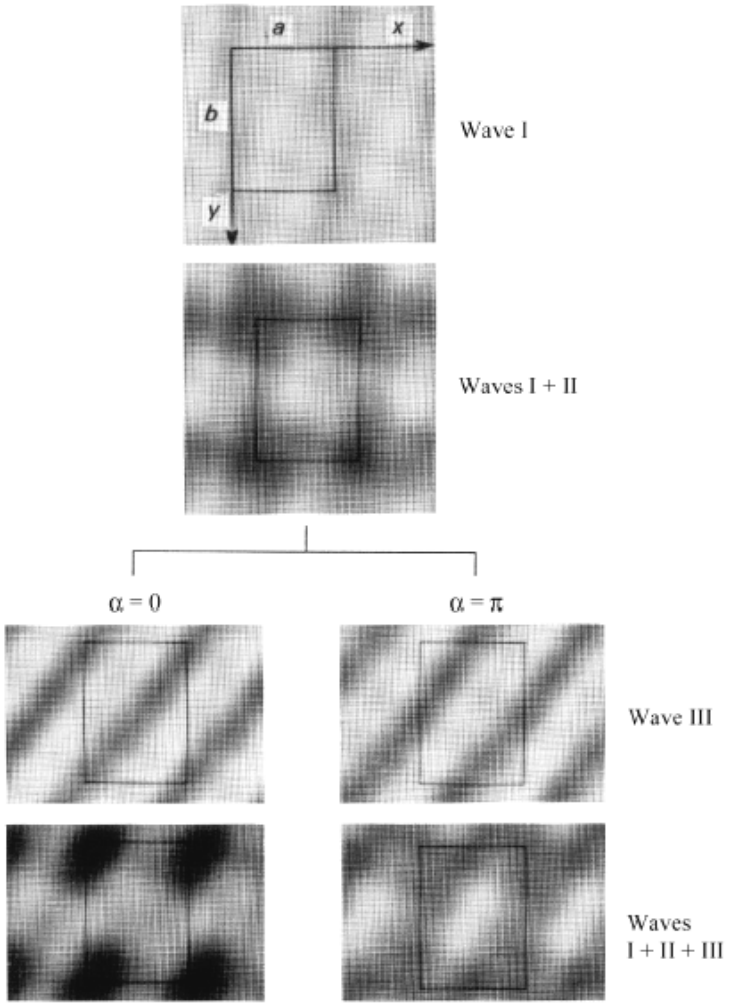

***Figure 3**. The result of adding three waves, where the third wave is added with two different phase angles.*

There is no formal relationship between the amplitudes and phases; the only relationship is via the molecular structure or electron density. Therefore, if we can assume some prior knowledge of the electron density or structure, this can lead to values for the phases. This is the basis for all phasing methods (Table 1).

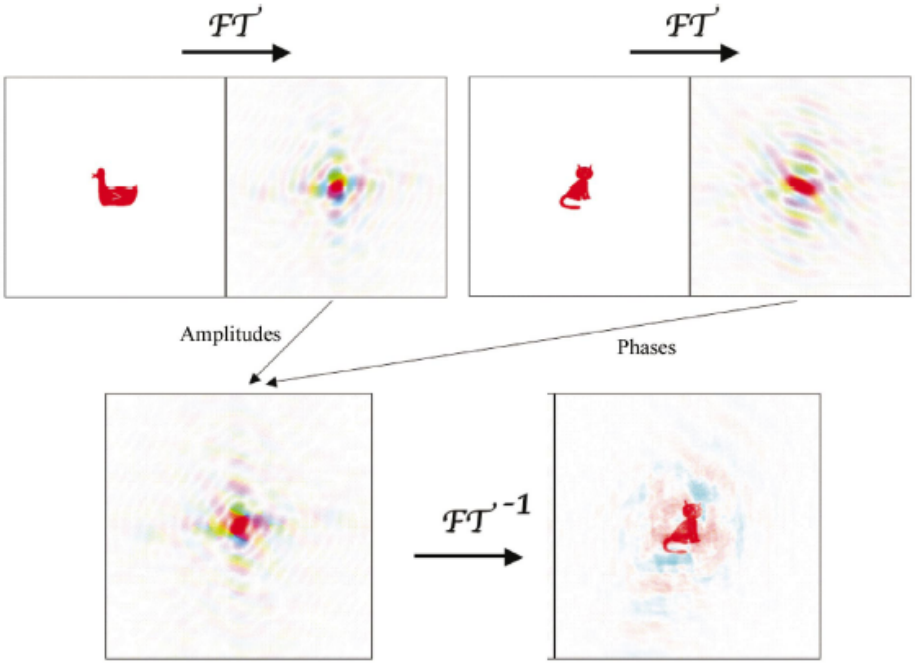

Figure 4. *The importance of phases in carrying information. Top, the diffraction pattern, or Fourier transform (FT), of a duck and of a cat. Bottom left, a diffraction pattern derived by combining the amplitudes from the duck diffraction pattern with the phases from the cat diffraction pattern. Bottom right, the image that would give rise to this hybrid diffraction pattern. In the diffraction pattern, different colours show different phases and the brightness of the colour indicates the amplitude. Reproduced courtesy of Kevin Cowtan.*

Table 1. *Phasing methods*

Method	**Prior knowledge**
Direct methods	ρ ≥ 0, discrete atoms
Molecular replacement	Homology model
Isomorphous replacement	Heavy-atom substructure
Anomalous scattering	Anomalous atom substructure
Density modification	Solvent flattening
(phase improvement)	Histogram matching
	Non-crystallographic symmetry averaging
	Partial structure
	Phase extension

For brevity we will not talk of the direct methods because the cannot be applied to macromoleculs. Before going into details of the other methods we need to introduce a few more concepts.

Structure factors as complex vectors – Crystallographers represent each structure factor (F_{hkl}) as a complex vector, that is, a vector (not a point) in the complex plane. The length of this vector represents the amplitude and the phase is represented by the angle α that the vector makes with the positive real-number axis. Thus the two fundamental properties of each F_{hkl} are immediately deducible from this geometrical representation (Argand diagram).

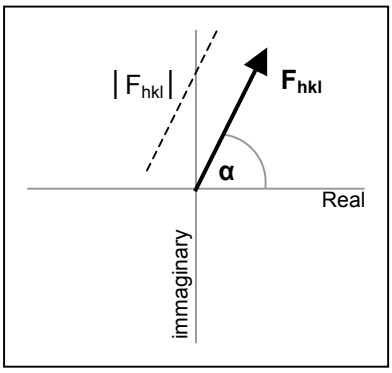

The Patterson function: P(u,v,w) – The Patterson function is a Fourier series that differs from ρ(x,y,z) used to compute structure factors because is independent from phases. The amplitude of each term is the square of the corresponding structure factor, which is proportional to the measured reflection intensity. Thus we can construct this series directly from intensity measurements, even though we have no phase information.

Patterson function: $P(u,v,w) = 1/V \Sigma \left| F^2_{hkl} \right| \exp[-2\pi i(hu+kv+lz)]$

Phasing methods

Molecular replacement (MR) - When a homology model is available, molecular replacement can be successful, using methods first described by Michael Rossmann and David Blow (Rossmann *et al.*, 1962). As a rule of thumb, a sequence identity >25% is normally required and an r.m.s. deviation of < 2.0 Å between the Cα atoms of the model and the final new structure, although there are exceptions to this. Patterson methods (see below) are usually used to obtain first the orientation of the model in the new unit cell and then the translation of the correctly oriented model relative to the origin of the new unit cell (Figure 5).

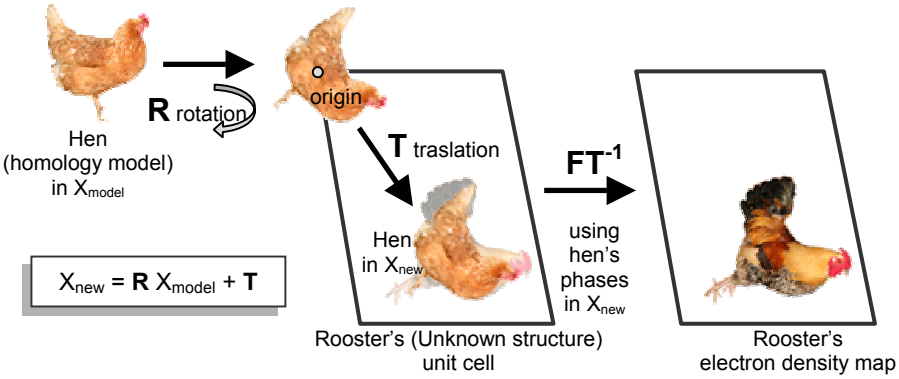

Figure 5 *The process of molecular replacement. Calculating Rooster's phases using a Hen as homology model.*

Isomorphous replacement - By soaking protein crystals in heavy-atom solutions or by cocrystallization techniques it is possible to create isomorphous heavy-atom derivatives (same unit cell, same orientation of protein in cell as in the native crystal) which give rise to measurable intensity changes that can be used to deduce the positions of the heavy atoms. In the case of a single isomorphous replacement (SIR) experiment, the contribution of the heavy-atom replacement to the structure factor amplitude and phases is best illustrated on an Argand diagram (Figure 6, A).

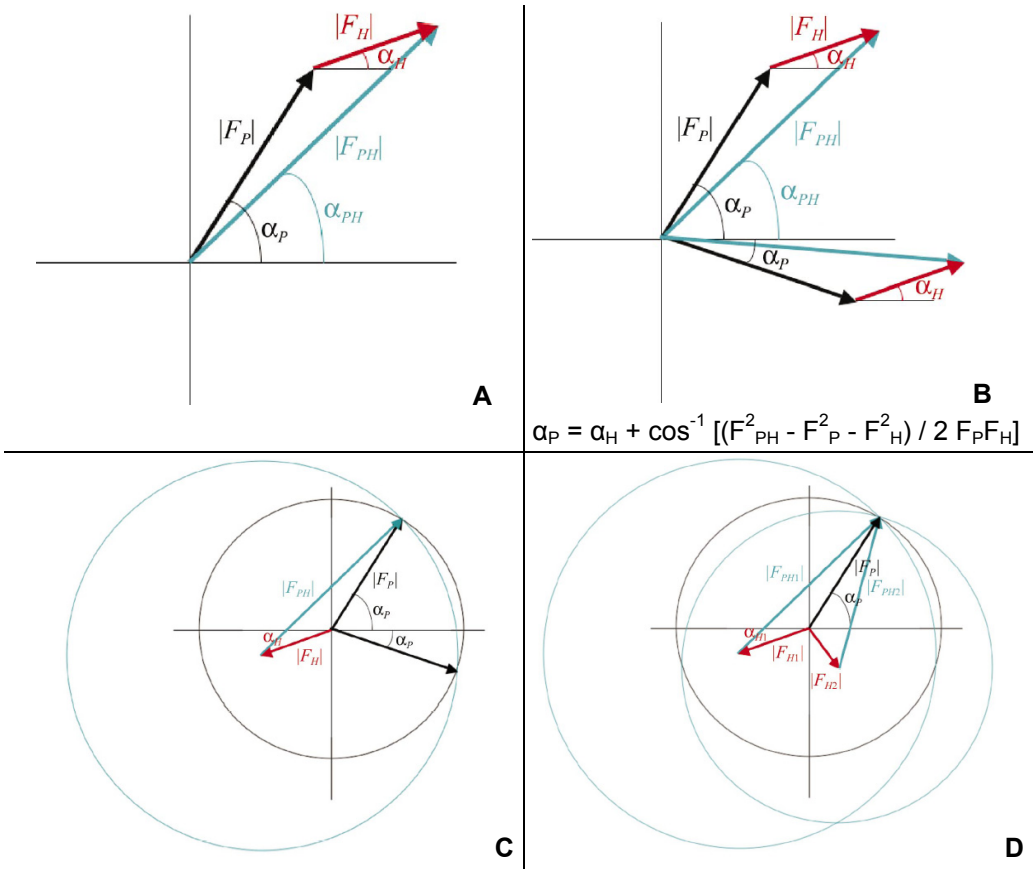

Figure 6 *A) Argand digram for SIR. $|F_P|$ is the amplitude of a reflection for the native crystal and $|F_{PH}|$ for the derivative crystal. B) Estimation of native protein phase for SIR. C) Harker construction for SIR. D) Harker diagram for MIR with two HA derivatives*

The amplitudes of a reflection are measured for the native crystal, $|F_P|$, and for the derivative crystal, $|F_{PH}|$. The isomorphous difference, $|F_H| = |F_{PH}| - |F_P|$, can be used as an estimate of the heavy-atom structure factor amplitude to determine the heavy-atom positions using Patterson or direct methods. Once located, the heavy-atom parameters (xyz positions, occupancies and Debye-Waller thermal factors B) can be refined and used to calculate a more accurate $|F_H|$ and its corresponding phase α_H. The native protein phase, α_P, can be estimated using the cosine rule (Figure 6, B), leading to two possible solutions symmetrically distributed about the heavy-atom phase. This phase ambiguity is better illustrated in the Harker construction (Figure 6, C). The two possible phase values occur where the circles intersect. The problem then arises as to which phase to choose.
This requires a consideration of phase probabilities.

Phase probability - In reality, there are errors associated with the measurements of the structure factors and in the heavy atom positions and their occupancies such that the vector triangle seldom closes. David Blow and Francis Crick introduced the concept of lack of closure ($\varepsilon = |F_{PH(obs)}| - |F_{PH(calc)}|$) and its use in defining a phase probability (Blow & Crick, 1959) (Figure 6). Making the assumption that all the errors reside in $F_{PH}(calc)$ and that errors follow a Gaussian distribution, the probability of a phase having a certain value is then;

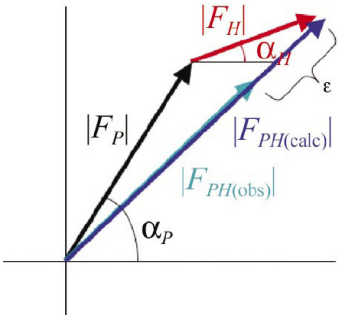

Figure 7 *the lack of closure ε*

$$P(\alpha_P) \propto \exp(-\varepsilon^2/2E^2) \qquad \text{where } E = \langle [F_{PH(obs)} - F_{PH(calc)}]^2 \rangle$$

Most phasing programs calculate such a probability from 0 to 360 to produce a phase probability distribution whose shape can be represented by four coefficients of a polynominal, the so-called Hendrickson-Lattman coefficients HLA, HLB, HLC and HLD (Hendrickson & Lattman, 1970). Blow and Crick also showed that an electron density map calculated with a weighted amplitude representing the centroid of the phase distribution gives the least error. Figure 8 shows the phase probability distribution for one reflection from an SIR experiment. The centroid of the distribution is denoted by F_{best}, whose amplitude is the native amplitude $|F_P|$ weighted by the *figure of merit*, m, which represents the cosine of the phase error.

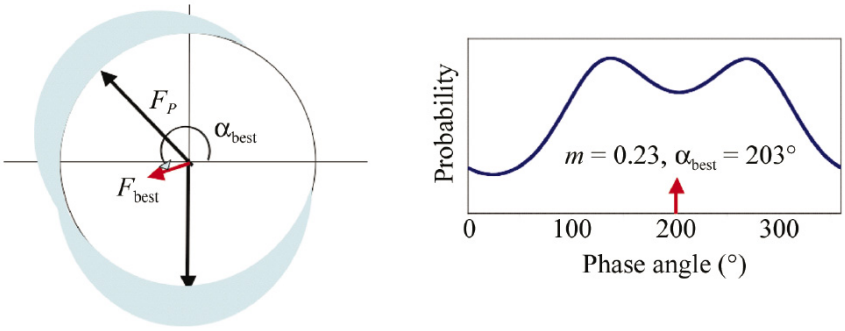

Figure 8*. Phase probability for one reflection in a SIR experiment. F_{best} is the centroid of the distribution. The map calculated with $|F_{best}|\exp(i\alpha_{best})$ [or $m|F_P|\exp(i\alpha_{best})$, where m is the figure of merit, $(\cos \Delta\alpha)$] has least error.*
m = 0.23 implies a 76° error.

The use of more than one heavy atom derivative in multiple isomorphous replacement (MIR) can break the phase ambiguity, as shown in Figure 6-D. The phase probability is obtained by multiplying the individual phase probabilities, as shown in Figure 9 for the same reflection as in Figure 8, but this time three heavy-atom derivatives have resulted in a sharp unimodal distribution with a concomitantly high figure of merit.

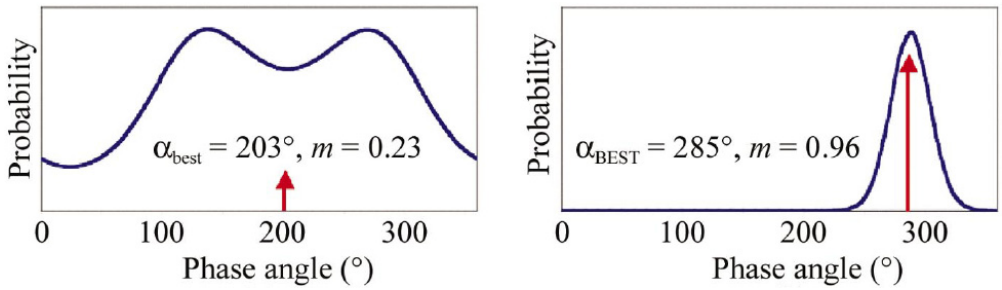

Figure 9 *Phase probability for one reflection in a MIR experiment. A. One derivative. B Three derivatives.*

Anomalous scattering - The atomic scattering factor has three components: a normal scattering term that is dependent on the Bragg angle and two terms that are not dependent on scattering angle, but on wavelength. These latter two terms represent the anomalous scattering that occurs at the absorption edge when the X-ray photon energy is sufficient to promote an electron from an inner shell. The *dispersive term (f')*reduces the normal scattering factor, whereas the *absorption term (f")*is 90° advanced in phase. This leads to a breakdown in Friedel's law ($|F_{hkl}| = |F_{-h-k-l}|$ and $\alpha_{hkl} = -\alpha_{-h-k-l}$), giving rise to anomalous differences that can be used to locate the anomalous scatterers. Figure 10-A shows the variation in anomalous scattering at the K edge of selenium and Figure 10-B the breakdown of Friedel's law.

The anomalous or *Bijvoet difference* can be used in the same way as the isomorphous difference in Patterson or direct methods to locate the anomalous scatterers. Phases for the native structure factors can then be derived in a similar way to the SIR or MIR case.

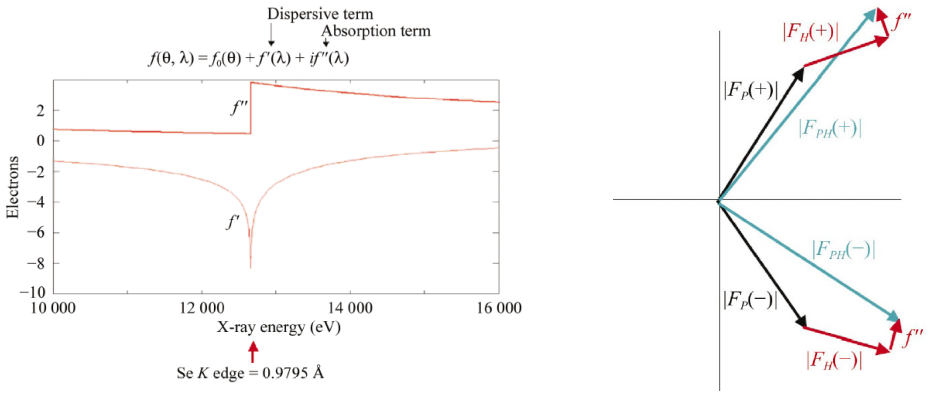

Figure 10 *Anomalous scattering. A) Variation in anomalous scattering at the K edge of selenium. B) Breakdown of Friedel's law $f_j(\theta, \lambda) = f_j(\theta) + f'(\lambda) + if''(\lambda)$. $F_{hkl} \neq F_{-h-k-l}$. $\Delta F^{\pm} = |F_{PH}(+)| - |F_{PH}(-)|$ is the Bijvoet difference.*

Anomalous Diffraction (MAD) - The use of the multiwavelength anomalous diffraction (MAD) method overcomes the non-isomorphism problems. Data are collected at several wavelengths, typically three, in order to maximize the absorption and dispersive effects. Typically, wavelengths are chosen at the absorption, f", peak (λ1), at the point of inflection on the absorption curve (λ2), where the dispersive term (which is the derivative of the f" curve) has its minimum, and at a remote wavelength (λ3 and/or λ4). Figure 11 shows a typical absorption curve for an anomalous scatterer, together with the phase and Harker diagrams. The changes in structure-factor amplitudes arising from anomalous scattering are generally small and require accurate measurement of intensities. The actual shape of the absorption curve must be determined experimentally by a fluorescence scan on the crystal at the synchrotron, as the environment of the anomalous scatterers can affect the details of the absorption. There is a need for excellent optics for accurate wavelength setting with minimum wavelength dispersion. Generally, all data are collected from a single frozen crystal with high redundancy in order to increase the statistical significance of the measurements and data are collected with as high a completeness as possible. Note that the signal size increases with resolution owing to the fall-off of normal scattering (f_j) with resolution.

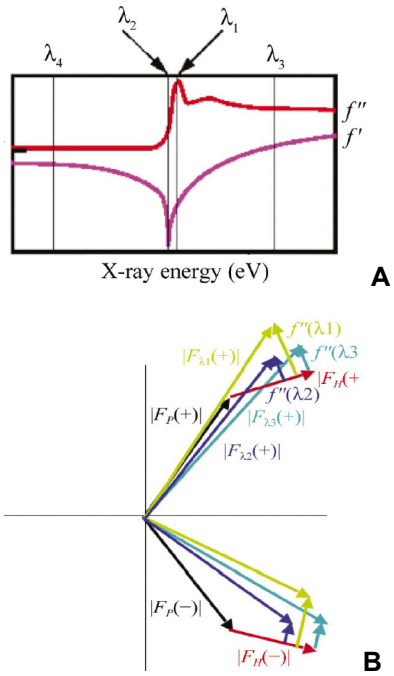

Figure 11. *MAD phasing.*
A) *Typical absorption curve for an anomalous scatterer.*
B) *Phase diagram, $|F_P|$ is not measured, so one of the λs is chosen as the native.*
C) *Harker construction.*

Single Anomalous Diffraction (SAD) - It is not formally possible to evaluate a protein phase exactly if there are only two experimental measurements, e.g. when the data are restricted to one wavelength (SAD) with only a single anomalous difference available or in the SIR case when only the native and one derivative data set is measured. Even assuming that the measured protein amplitudes, F_{PH}+ and F_{PH}-, and the calculated amplitude and phase contributions of the anomalous partial structure, F_H and α_H, are error-free, there is a twofold ambiguity in the estimation of the protein phase (Ramachandran & Raman, 1956). The two possible phase values of the protein structure factor, F_P, are symmetrically oriented around (α_H – 90°) as shown in figure 11.

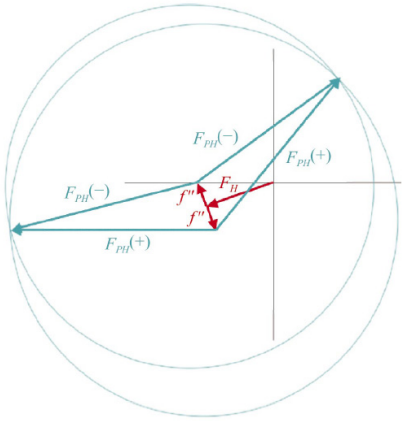

Figure 12*. Harker construction for SAD. $\Delta F^{\pm}$ is used to find the substructure, followed by phasing and phase improvement to break the phase ambiguity.*

for anomalous differences we can write the following equation (Dodson, 2003)

$$\Delta F^{\pm} = \left| F^{+} \right| - \left| F^{-} \right| \approx 2F_{H}'' \sin(\alpha_{P} - \alpha_{H})$$

Thus, in principle, the positions of anomalous scatterers can be found from the Bijvoet differences for single-wavelength data. However, once initial pahes are calculated we still have to brake the phase ambiguity, the most powerful approach to improving the phase distributions and break the choose the right phase is the use of density-modification procedures.

Phase improvement - It is rare that experimentally determined phases are sufficiently accurate to give a completely interpretable electron density map. Experimental phases are often only the starting point for phase improvement using a variety of methods of density modification, which are also based on some prior knowledge of structure. *Solvent flattening, histogram matching* and *non-crystallographic (NCS)averaging* are the main techniques used to modify electron density and improve phases.

Solvent flattening Removes negative electron density and sets the value of electron density in the solvent regions to a typical value of 0.33 $eÅ^{-3}$, in contrast to a typical protein electron density of 0.43 $eÅ^{-3}$. Automatic methods are used to define the protein-solvent boundary. Developed by Wang (1985) and then extended into reciprocal space by Leslie (1988).

Histogram matching Alters the values of electron-density points to concur with an expected distribution of electron-density values.

NCS averaging Imposes equivalence on electron density values when more than one copy of a molecule in present in the asymmetric unit

These methods are encoded into programs such as DM (Cowtan & Zhang, 1999), RESOLVE (Terwilliger, 2002) and CNS (Brünger *et al.*, 1998). Density-modification techniques will not turn a bad map into a good one, but they will certainly improve promising maps that show some interpretable features.
Density modification is often a cyclic procedure, involving back-transformation of the modified electron density map to give modified phases, recombination of these phases with the experimental phases (so as not to throw away experimental reality) and calculation of a new map which is then modified and so the cycle continues until convergence.

Such methods can also be used to provide phases beyond the resolution for which experimental phases information is available, assuming higher resolution native data have been collected. In such cases, the modified map is back-transformed to a slightly higher resolution on each cycle to provide new phases for higher resolution reflections. The process is illustrated in Figure 13.

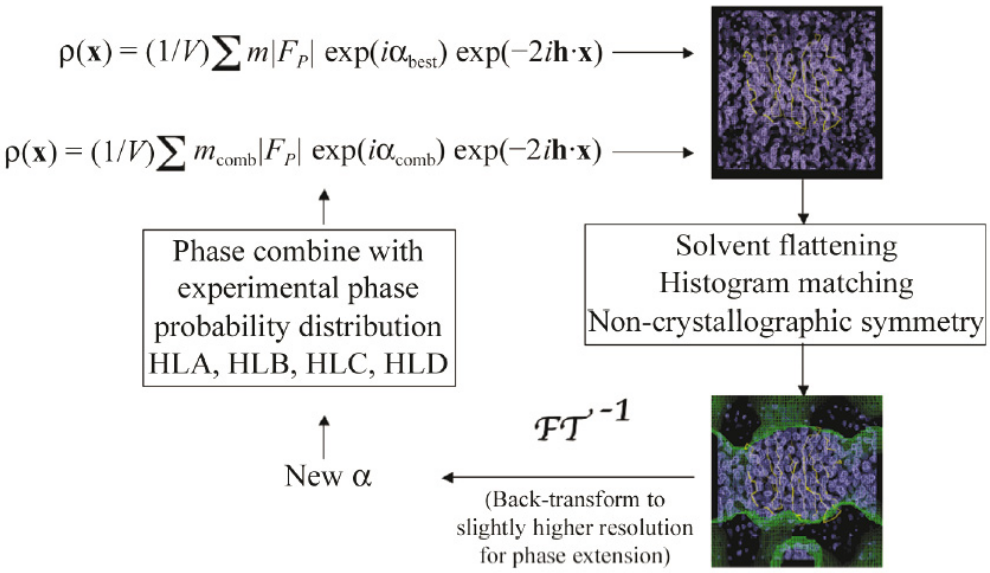

***Figure 13**. Phase improvement by density modification*

The phase problem in crystallography is reviewed in Tayor (2003), many pictures in this appendix are taken from this paper.

ATTACHMENTS

Rinaldo S., Giardina G., Brunori M., Cutruzzolà F. (2005) N-oxide sensing in *Pseudomonas aeruginosa*: expression and preliminary characterization of DNR, an FNR-CRP type transcriptional regulator, *Biochem Soc Trans.* **33**,188-190.

Rinaldo S., Giardina G., Brunori M., Cutruzzolà F. (2006) N-oxides sensing and denitrification: the DNR transcription factors, *Biochem Soc Trans,* **34**, 185-187

188 Biochemical Society Transactions (2005) Volume 33, part 1

N-oxides sensing in *Pseudomonas aeruginosa*: expression and preliminary characterization of DNR, an FNR–CRP type transcriptional regulator

S. Rinaldo, G. Giardina, M. Brunori and F. Cutruzzolà[1]
Department of Biochemical Sciences 'A. Rossi Fanelli', University of Rome La Sapienza, P.le A. Moro 5, 00185 Rome, Italy

Abstract

In denitrifying bacteria, the concentration of NO is maintained low by a tight control of the expression and activity of nitrite and NO reductases. Regulation involves redox-linked transcription factors, such as those belonging to the CRP-FNR superfamily, which act as oxygen and N-oxide sensors. Given that few members of this superfamily have been characterized in detail, we have cloned, expressed and purified the dissimilative nitrate respiration regulator from *Pseudomonas aeruginosa*. To gain insights on the structural properties of the dissimilative nitrate respiration regulator, we have also determined the aggregation state of the purified protein and its ability to bind hydrophobic compounds such as 8-anilino-1-naphthalenesulphonic acid.

Introduction

In denitrifying bacteria, the concentration of extracellular NO is maintained low (nanomolar) by a tight control of the expression and activity of nitrite and NO reductases. Regulation involves redox-linked transcription factors, such as those belonging to the CRP-FNR (where CRP stands for cAMP receptor protein and FNR stands for fumarate and nitrate reductase regulator) superfamily [1], structurally related to the CRP from *Escherichia coli* [2]. FNR belongs to this superfamily, which contains an Fe-S cluster bound to a set of conserved cysteines and the fnr-like proteins (ANR, FnrA, FnrP), active under low-oxygen tension [1]. Other modulatory proteins, such as those of the dnr subtype [3–5], lack the conserved cysteine cluster and regulate both the nitrite reductase (*nirS*) and nitric oxide reductase (*norCB*) gene expressions. The NO dependence of the transcriptional activity of promoters regulated by these proteins has suggested, by genetic approach, that these factors may act as NO sensors *in vivo* [6,7].

Given that no structural information and little biochemical data are available on the dnr-type class of regulators, we have cloned, expressed and purified the DNR (dissimilative nitrate respiration regulator) protein from *Pseudomonas aeruginosa*. In this species, the *dnr* gene is located upstream of the *nir* and *nor* gene clusters, and it was shown to be able to transactivate *in vivo* the *nirS*, *norCB* and *nos* (nitrous oxide reductase) promoters in response to nitrite [8,9]. DNR is 227 amino acids long; primary structural analysis and molecular modelling suggest the presence of three domains. The signal sensing domain is located at the N-terminus, followed by a long dimerization helix, and at the C-terminus a helix–turn–helix domain was found which was involved in the recognition of the DNA target sequence, the FNR box (TTGATN$_4$ATCAA), conserved both in the FNR target promoter and in the *nir–nor* promoters [10].

To gain insights on the structural properties of DNR, we have also determined the aggregation state of the purified protein and its ability to bind hydrophobic compounds such as ANS (8-anilinonaphthalene-1-sulphonic acid).

Key words: anaerobiosis, denitrification, nitric oxide, *Pseudomonas aeruginosa*, sensor, transcriptional regulation.

Abbreviations used: ANS, 8-anilinonaphthalene-1-sulphonic acid; CRP, cAMP receptor protein; DNR, dissimilative nitrate respiration regulator; FNR, fumarate and nitrate reductase regulator; IPTG, isopropyl β-D-thiogalactoside; 2-ME, 2-mercaptoethanol.

[1]To whom correspondence should be addressed (email francesca.cutruzzola@uniroma1.it).

Materials and methods

Cloning

The *dnr* gene was amplified from *P. aeruginosa* PAO1 strain genomic DNA. The purified PCR product, verified by sequencing, was ligated into a pET28b vector (Novagen) to yield the pET-DNR plasmid and transformed into BL21-(DE3) *E. coli* strain for expression.

Expression and purification

Expression of the protein was obtained at 25 and 37°C in Luria–Bertani medium containing 30 μg/ml kanamycin. Expression was induced with 1 mM IPTG (isopropyl β-D-thiogalactoside) and cells were grown for 15 h after induction. Cells were resuspended in 50 mM Tris buffer (pH 8.0), 50 mM NaCl, 2 mM EDTA, 2 mM 2-ME (2-mercaptoethanol) and 1 mM PMSF and sonicated. The cell extract, after centrifugation, was dialysed against 20 mM Tris (pH 7.2), 2 mM EDTA and 2 mM 2-ME (buffer A) and applied on a Q-Sepharose Fast Flow (Amersham Biosciences, Cologno, Monzese, Italy) column; the protein was eluted with a 35–500 mM NaCl gradient in buffer A. The purification was then carried out on a Heparin Sepharose 6 Fast Flow (Amersham Biosciences) column in buffer A (eluted with 100 mM NaCl)

and on a Superdex 75 gel filtration column (Amersham Biosciences) in buffer A with 150 mM NaCl. The molar absorption coefficient at 280 nm was determined by the Bradford assay to be 10.5 $mM^{-1} \cdot cm^{-1}$ (per monomer).

The aggregation state was determined by gel filtration on a Superdex 75 column (Amersham Biosciences) and further confirmed by HPLC (G3000SWxl, Tosoh Biosep) at different NaCl concentrations.

CRP was expressed and purified from an overproducing *E. coli* strain transformed with a cloned CRP gene (a gift from J.C. Lee, University of Texas, U.S.A.) [11].

ANS binding

ANS binding was carried out by titrating a DNR solution either 2 or 5 μM (monomer) in 50 mM Tris (pH 7.5), 150 mM NaCl and 0.5 mM 2-ME with a 1 mM ANS solution in water. The dissociation constant of the ANS–DNR complex was calculated using the following relation (when $ANS_{tot} > DNR_{tot}$):

$$1/I = 1/n\psi\,[DNR]_{tot} + (K/n[DNR]_{tot}\psi)(1/[ANS]_{free})$$

where I is the observed fluorescence intensity, K is the dissociation constant for a dye–site complex, n are the total number of sites on protein and ψ is the proportionality constant connecting the fluorescence intensity to the concentration of the probe–site complex.

If $ANS_{tot} > DNR_{tot}$, the plot of $1/I$ versus $1/[ANS]_{tot}$ will be linear for a fixed protein concentration with a common abscissa intercept of $-1/K$, for different protein concentrations [12].

All fluorescence emission spectra were recorded in a cuvette (1 cm light path) between 400 and 600 nm on a Fluoromax single photon counting spectrofluorimeter (Jobin Yvon). The excitation wavelength was 350 nm.

Results and discussion

Protein expression and purification

The *dnr* gene was isolated from *P. aeruginosa* genomic DNA by PCR and inserted in the expression vector pET28b. High levels of protein expression were obtained at 37°C in BL21 (DE3) *E. coli* strain; after induction with 1 mM IPTG, the protein was found to be mainly in the soluble fraction of the total cell extract (Figure 1A). A slight increase in the solubility was observed when the growth temperature was lowered to 25°C. A purification procedure was devised, which yielded a protein, pure to the homogeneity, in high yields (15 mg/l; Figure 1A).

General characterization

The molecular mass of the recombinant protein was 26054.16 Da (by MS). Determination of the N-terminal sequence has confirmed that the recombinant protein is correctly maturated in *E. coli*. The far-UV CD spectrum suggests that the purified protein is folded in solution (results are not shown).

Figure 1 | (A) Expression and purification of the DNR protein and (B) aggregation state of the purified protein

(**A**) Lane 1: SDS/PAGE of the soluble fraction of the cell extract from *E. coli* BL21(DE3) cells containing the pET-DNR plasmid after induction with 1 mM IPTG. Lane 2: SDS/PAGE of the purified DNR protein. Lane M: molecular mass markers 10–180 kDa (MBI Fermentas, Munich, Germany). (**B**) DNR in 20 mM Tris buffer (pH 7.2) and 150 mM NaCl was run on a gel filtration Superdex 75 column in comparison with molecular mass markers. The elution profile of the DNR sample (trace b) is superimposed on that of the markers (trace a, from left to right: BSA 67 kDa, ovalbumin 43 kDa, chymotrypsinogen 25 kDa and RNase A 13.7 kDa).

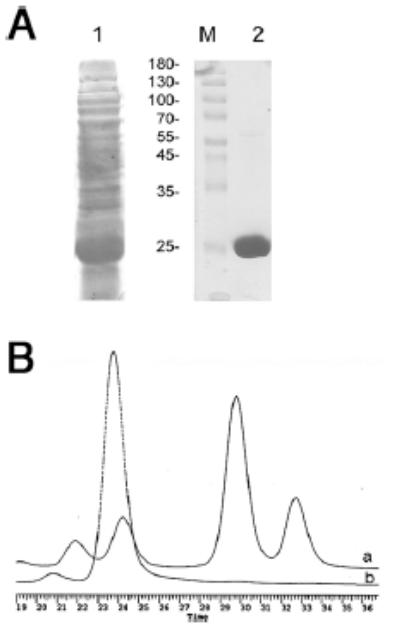

DNR is mainly a dimer in solution, as determined by gel filtration of the purified protein in 20 mM Tris buffer of pH 7.2 and 150 mM NaCl (Figure 1B). Higher aggregation states are populated at low salt concentration and thus all binding experiments have been carried out in the presence of 150 mM NaCl.

Binding of ANS

As reported for the *E. coli* CRP [11], titrations with ANS were performed to get some insights of the DNR structural organization. The emission of ANS increases when the molecule is bound in a non-polar environment with a shift in the wavelength for a maximum emission of approx. 530 to 500 nm.

Figure 2 | Binding of ANS

Protein concentrations: ●, 5 μM and ▼, 2 μM. The dissociation constant for the ANS–DNR complex was obtained from the abscissa intercept as described in the Materials and methods section. Inset: fluorescence emission spectra of the DNR–ANS complex at different ANS concentrations (2–50 μM range).

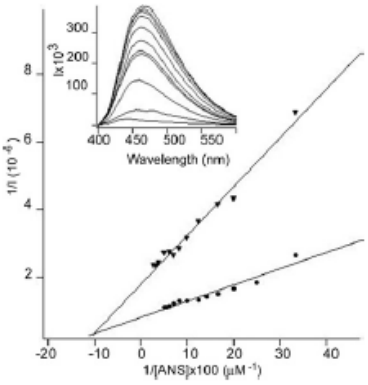

DNR (2–5 μM) was titrated with increasing amounts of ANS (2–50 μM) (Figure 2). The maximum fluorescence emission for the ANS bound to DNR was 460 nm, whereas it was 480 nm with CRP [11]. This difference in the position of the emission peak of ANS suggests that in DNR the hydrophobic cleft where ANS is bound is less solvent accessible, as reported for other proteins [13]. The data were analysed as in [12], and a dissociation constant for ANS of 7 μM (±0.8) was calculated. These results show that DNR binds ANS with higher affinity than CRP ($K_d = 600\ \mu$M) [11].

Experiments on the *in vitro* DNA binding activity and the *in vivo* activation of gene expression by the recombinant DNR are being carried out. A major task will be the determination of the structure of DNR by crystallography; crystallization experiments are in progress.

Funds from the Ministero Istruzione, Università e Ricerca of Italy (COFIN 2003) and from the European Union COST Action 856 are gratefully acknowledged.

References

1 Korner, H., Sofia, H.J. and Zumft, W.G. (2003) FEMS Microbiol. Rev. **27**, 559–592
2 McKay, D.B. and Steitz, T.A. (1981) Nature (London) **290**, 744–749
3 Vollack, K.U., Hartig, E., Korner, H. and Zumft, W.G. (1999) Mol. Microbiol. **31**, 1681–1694
4 Arai, H., Igarashi, Y. and Kodama, T. (1995) FEBS Lett. **371**, 73–76
5 Van Spanning, R.J.M., De Boer, A.P.N., Reijenders, W.N.M., Spiro, S., Westerhoff, H.V., Stouthamer, A.H. and Van der Host, J. (1995) FEBS Lett. **360**, 151–154
6 Van Spanning, R.J.M., Houben, E., Reijenders, W.N.M., Spiro, S., Westerhoff, H.V. and Saunders, N. (1999) J. Bacteriol. **181**, 4129–4132
7 Hasegawa, N., Arai, H. and Igarashi, Y. (1998) FEMS Microbiol. Lett. **166**, 213–217
8 Arai, H., Kodama, T. and Igarashi, Y. (1997) Mol. Microbiol. **25**, 1141–1148
9 Arai, H., Mizutani, M. and Igarashi, Y. (2003) Microbiology **149**, 29–36
10 Green, J., Scott, C. and Guest, J.R. (2001) Adv. Microbiol. Physiol. **44**, 1–34
11 Heyduk, T. and Lee, J.C. (1989) Biochemistry **28**, 6914–6924
12 Horowitz, P.M. and Criscimagna, N.L. (1985) Biochemistry **24**, 2587–2593
13 Strangelo, L., Bismuto, E., Tavassi, S. and Irace, G. (1998) Biochim. Biophys. Acta **1385**, 69–77

Received 5 September 2004

The 11th Nitrogen Cycle Meeting 2005

N oxides sensing and denitrification: the DNR transcription factors

S. Rinaldo,[1] G. Giardina, M. Brunori and F. Cutruzzolà

Department of Biochemical Sciences 'A. Rossi Fanelli' and Istituto di Biologia e Patologia Molecolari – CNR, University of Rome La Sapienza, P. le A. Moro 5, 00185 Rome, Italy

Abstract

All denitrifiers can keep the steady-state concentrations of nitrite and nitric oxide (NO) below cytotoxic levels controlling the expression of denitrification gene clusters by redox signalling through transcriptional regulators belonging to the CRP (cAMP receptor protein)/FNR (fumarate and nitrate reductase regulator) superfamily.

Nitric oxide (NO)-responsive regulators belong to three different subgroups of the CRP (cAMP receptor protein)/FNR (fumarate and nitrate reductase regulator) superfamily [FNR, DNR (dissimilative nitrate respiration regulator) and NnrR] and can control N oxide homoeostasis both under anaerobic and aerobic conditions. The FNR-type share a cysteine-rich motif involved in the formation of an iron–sulphur cluster as a redox centre, which is not present in the other two subgroups.

Most of the regulators involved in the regulation of denitrification, belonging either to the DNR and NnrR subgroups, regulate nitrite reductase (*nir*), NO reductase (*nor*) and nitrous oxide reductase (*nos*) gene expression. The NO dependence of the transcriptional activity of promoters regulated by these transcription factors has suggested that these factors may act as NO sensors *in vivo*. To date, no structural information and little biochemical data are available on this class of regulators.

In order to gain insights into the molecular and structural basis of the NO-dependent regulation, we have recently expressed in *Escherichia coli* and partially characterized the DNR protein from *Pseudomonas aeruginosa*.

NO-responsive elements belonging to the CRP/FNR superfamily of transcription factors

The expression of the denitrification gene clusters is tightly controlled by redox signalling through a cascade of oxygen-responsive regulators activating the N oxides-responsive ones. These regulators control the NO homoeostasis maintaining the steady-state concentration of nitrite and NO below cytotoxic levels; as a consequence, free NO concentration is in the nanomolar range.

Key words: dissimilative nitrate respiration regulator (DNR), denitrification, cAMP receptor protein/fumarate and nitrate reductase regulator superfamily (CRP/FNR superfamily), nitric oxide, *Pseudomonas aeruginosa*, transcriptional regulation.

Abbreviations used: ANR, anaerobic regulation of arginine deaminase and nitrate reduction; CRP, cAMP receptor protein; DNR, dissimilative nitrate respiration regulator; FNR, fumarate and nitrate reductase regulator.

*To whom correspondence should be addressed (email serena.rinaldo@uniroma1.it).

The denitrification pathway is transcriptionally regulated by redox-linked transcription factors mostly belonging to the CRP/FNR superfamily [1], structurally related to the CRP protein from *E. coli* [2]. The CRP/FNR proteins are constant in size with approx. 230–250 amino acid residues, the first 150–170 residues corresponding to the effector domain [1]. These regulators respond to both extracellular and intracellular signals by binding the allosteric effector either directly (as for cAMP in CRP from *E. coli*) or through a prosthetic group (as for the iron–sulphur cluster of FNR from *E. coli*) [3]. All members of this superfamily bind DNA with a C-terminal helix–turn–helix domain which interacts with the major groove of target DNA sequence, the FNR box (TTGATN$_4$ATCAA) [1].

Multiple members of these regulators, belonging to different subgroups, can either coexist in the same host or regulate the same metabolic pathway in different organisms [1]. This is the case for the regulators of denitrification and in general for NO-responsive components which belong to three different subgroups of the CRP/FNR superfamily (FNR, DNR and NnrR) and can control N oxide homoeostasis both under anaerobic and aerobic conditions [1]. To date, no structural information and limited biochemical data are available on the last two subgroups involved in the regulation of denitrification, while the first one is well characterized. In *E. coli*, as an example, nitrosative stress induces expression of the flavohaemoglobin protein, encoded by the *hmp* gene, which acts as a NO scavenger. The *hmp* gene expression requires the FNR protein which is a repressor under normal conditions; in the presence of NO, the $[4Fe\text{-}4S]^{2+}$ cluster is converted into the $[2Fe\text{-}2S]^{2+}$ state inducing monomer formation in the FNR protein [4]. The FNR form modified by NO binds the *hmp* promoter with lower affinity, inducing flavohaemoglobin expression.

The DNR-type of transcription regulators

All members of the DNR subgroup share the same motif (E-SR amino acid residues) involved in recognition of the binding site on DNA, while most members of the NnrR

Figure 1 | Multiple alignment of DNR protein sequences from *Ps. aeruginosa* (DNR) and *Ps. stutzeri* (DnrD, DnrS and DnrE)

Amino acid one-letter codes are used. Dashes represent insertions and deletions; numbers at the beginning of each sequence indicate absolute sequence numbering. Invariant positions are boxed in black; alignment columns displaying amino acid with the same physicochemical properties are boxed in white with the conserved residues shown in boldface.

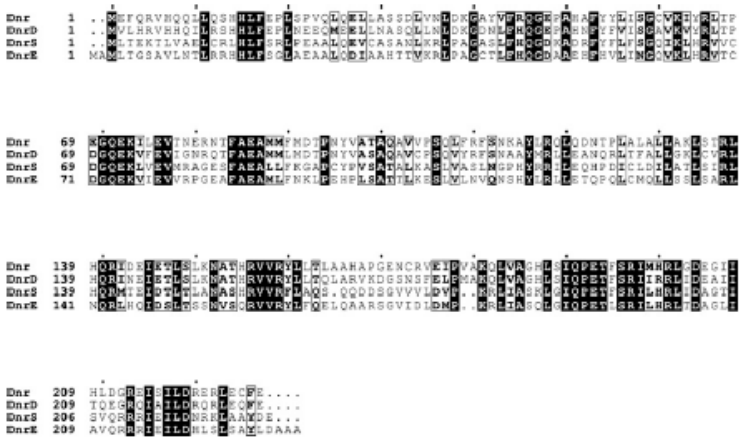

subgroup contain a histidine instead of a glutamate residue. Both groups of regulators (DNR and NnrR) do not contain enough cysteine residues for iron–sulphur clusters formation contrary to FNR, suggesting a different mechanism of N oxide(s) sensing.

Members of both NnrR and DNR subgroups are found in facultatively anaerobic bacteria; the transcriptional regulation is exerted in the presence of N oxide(s) and under low oxygen tension. In *Rhodobacter sphaeroides* and in *Paracoccus denitrificans* for example, it was shown, by genetic approach, that the transcriptional regulators designated respectively as NnrR (belonging to the NnrR-type) and Nnr (belonging to the DNR subgroup) can both activate the expression of the nitrite and NO reductase genes in response to NO [5,6].

The members of DNR-type class of regulators found in the *Pseudomonas* spp. [7,8] share a high sequence identity (Figure 1) but may not fulfil an identical physiological role. This is not surprising given that Pseudomonads are well known for their metabolic flexibility which reflects the capability of the different species to survive as free living organisms in soil, water and animals, where they are often responsible for diseases.

In *Pseudomonas stutzeri*, there are at least three regulators (DnrD, DnrS and DnrE) involved in the NO sensing (DnrD), activation of the nitrate pathway (DnrE) and possibly in redox sensing (DnrS) under anaerobic conditions [1].

The DnrD transcription factor induces the expression of *nirSTB*, *norCB* and *nosZ* operons (encoding nitrite, NO and nitrous oxide reductases respectively) in the presence of NO but not nitrite (the *nos* gene is activated also in presence of high concentration of nitrous oxide). The NO concentration required for the *nir-nor* operons activation is in the range of 5–50 n*M* [8]. DnrD overexpression itself is not sufficient for the transcription of the *nir-nor* operons, indicating that additional factors may be required [8].

NO sensing in *Ps. aeruginosa*

Ps. aeruginosa is one of the most important pathogens in lung chronic infections associated for example with cystic fibrosis, where it uses denitrification as the anaerobic energy producing pathway [9]. Low oxygen tensions and the presence of N oxides produced by the host defence mechanism induce high levels of expression of *nir-nor* operons [9]. Under anaerobic conditions, the denitrification pathway works both as a source of electrons and as NO scavenger given that the classical flavohaemoglobin-mediated detoxification pathway is not active [10].

The induction of denitrification by oxygen depletion requires ANR (anaerobic regulation of arginine deaminase and nitrate reduction), an FNR-like global regulator for anaerobic gene expression in *Ps. aeruginosa* [11]. ANR induces the expression of the DNR protein (dissimilative nitrate respiration regulator, belonging to DNR subtype), which activates, in the presence of N oxide(s), the *nirS*, *norCB* and *nosR* promoters [7,12,13]. Mutants without the *anr* or *dnr* genes are not able to induce *nirS* and *norCB* promoters under growth conditions where denitrification should be active [12]. *anr* defective strains are not able to activate the transcription

of the *dnr* gene but denitrification can be induced after transformation with a plasmid carrying the *dnr* gene [7]. DNR-mediated transcriptional activation of denitrification depends on endogenous NO concentration [13,14].

The sequence alignment shown in Figure 1 clearly indicates a higher degree of similarity of DNR from *Ps. aeruginosa* to DnrD, in agreement with the involvement of DNR in NO sensing. Given that only one DNR-type regulator is found in the *Ps. aeruginosa* genome, in this pathogen the role of DnrE and DnrS might be played by different factors.

In order to study the biochemical basis of the NO-dependent regulation of the DNR protein, after cloning the *dnr* gene from *Ps. aeruginosa*, we have purified to homogeneity the protein expressed in *E. coli* using the pET system [15]. The recombinant protein, produced in high yield (15 mg/l), is soluble and stable as a dimer [15].

To obtain some insight of the DNR structural organization, ANS (8-anilinonaphthalene-1-sulphonic acid) titrations were performed [15]. DNR has a hydrophobic pocket which is more accessible as compared with *E. coli* CRP ($K_{d\,DNR} = 7\ \mu M$ and $K_{d\,CRP} = 600\ \mu M$), suggesting that DNR may present a different structural organization of the effector domain. This hydrophobic cleft is a likely candidate for the binding of the cofactor(s) required for NO-mediated activation of the DNR protein.

DNA binding assays, crystallization and structure determination of DNR, now in progress, will shed more light on the structural determinants of the NO-dependent activation process.

Funds from the Ministero Istruzione, Università e Ricerca of Italy (COFIN 2003 – Structural dynamics of metalloproteins) and from the European Union COST Action 856 are gratefully acknowledged.

References

1 Komer, H., Sofia, H.J. and Zumft, W.G. (2003) FEMS Microbiol. Rev. **27**, 559–592
2 McKay, D.B. and Steitz, T.A. (1981) Nature (London) **290**, 744–749
3 Unden, G. and Schirawski, J. (1997) Mol. Microbiol. **25**, 205–210
4 Cruz-Ramos, H., Crack, J., Wu, G., Hughes, M.N., Scott, C., Thomson, A.J., Green, J. and Poole, R.K. (2002) EMBO J. **21**, 3235–3244
5 Kwiatkowski, A.V. and Shapleigh, J.P. (1996) J. Biol. Chem. **271**, 24382–24388
6 Van Spanning, R.J., Houben, E., Reijnders, W.N., Spiro, S., Westerhoff, H.V. and Saunders, N. (1999) J. Bacteriol. **181**, 4129–4132
7 Arai, H., Kodama, T. and Igarashi, Y. (1997) Mol. Microbiol. **25**, 1141–1148
8 Vollack, K.U. and Zumft, W.G. (2001) J. Bacteriol. **183**, 2516–2526
9 Hassett, D.J., Cuppoletti, J., Trapnell, B., Lymar, S.V., Rowe, J.J., Yoon, S.S., Hilliard, G.M., Parvatiyar, K., Kamani, M.C., Wozniak, D.J. et al. (2002) Adv. Drug Deliv. Rev. **54**, 1425–1443
10 Arai, H., Hayashi, M., Kuroi, A., Ishii, M. and Igarashi, Y. (2005) J. Bacteriol. **187**, 3960–3968
11 Galimand, M., Gamper, M., Zimmermann, A. and Haas, D. (1991) J. Bacteriol. **173**, 1598–1606
12 Arai, H., Igarashi, Y. and Kodama, T. (1995) FEBS Lett. **371**, 73–76
13 Arai, H., Mizutani, M. and Igarashi, Y. (2003) Microbiology **149**, 29–36
14 Arai, H., Kodama, T. and Igarashi, Y. (1999) FEMS Microbiol. Lett. **170**, 19–24
15 Rinaldo, S., Giardina, G., Brunori, M. and Cutruzzolà, F. (2005) Biochem. Soc. Trans. **33**, 184–186

Received 23 September 2005